# Mechanical Properties of Candidate Materials for Morphing Wings

by

**Michael Thomas Kikuta**

Thesis Submitted to the Faculty of the
Virginia Polytechnic Institute and State University
in partial fulfillment of the requirements for the degree of

Master of Science

in

Mechanical Engineering

Dr. Daniel J. Inman, Chair
Dr. Harry H. Robertshaw
Dr. Donald J. Leo

December 11, 2003

Blacksburg, Virginia

Keywords: Materials, Mechanical properties, Morphing wing, Skins

**Mechanical Properties of Candidate Materials for Morphing Wings**

by

**Michael Thomas Kikuta**

# Abstract

The research presented in this thesis investigates the mechanical properties of candidate materials that could be used as a skin for a morphing wing. A morphing wing is defined as a wing that changes shape. Although engineers have been designing different morphing wing configurations, there has been limited research investigating materials that could be used as a skin for a morphing wing. Specifically, after investigating the different morphing wing abilities engineers at Virginia Tech are designing, criteria were determined for candidate materials. A suitable skin material for a morphing wing will have to be elastic, flexible, have high recovery, resistant to different weather conditions, resistant to abrasions and chemicals, and have a hardness number high enough to handle the aerodynamic loads of the aircraft while in flight. Using some of the preceding criteria, different materials were selected that are readily available in the commercial market. The materials tested were a type of thermoplastic polyurethanes, copolyester elastomer, shape memory polymer, or woven materials that are made out of elastane yarns.

The first study determined the required forces to strain the material in a uniaxial direction. A test stand was designed with a gripping device to hold the material. By grounding one side of the material, the other side of the material was pulled using a winch. Using a force transducer and a string potentiometer the required forces and the amount the material was strained was recorded, respectively. Utilizing the same test stand, the amount the material recovered was also acquired. Also, by measuring how much the material necked the elongation ratio was calculated. The final test determined if the forces "relaxed" after being strained to a stationary position. It was found that each material performed differently, but some materials were definitely better suited for morphing wing material. The materials that were made out of thermoplastic polyurethanes, copolyester elastomer, and shape memory polymer required less force and were able to strain more, when compared to the woven materials.

The second study determined if the material could be strained in a biaxial direction. The reason for this was for a better understand how the material would perform if the material was strained to an extreme condition. A test stand was designed using the same principles and components as the uniaxial test stand. The only difference was additional sensors were required to measure the force and strain along the other axis. Although a recovery analysis was warranted for the biaxial experiments, most of the materials test failed while being strained a small amount. Also, the material strained a lot less before ripping, when compared to the straining capabilities when only being strained in the uniaxial direction. After conducting the experiments, the results were similar to the uniaxial experimental results. In terms of required forces to strain the material, the thermoplastic polyurethanes and the copolyester elastomer required less force, when compared to the woven materials. The only advantage of the woven materials was they did not break.

The final study determined how much the material deflected while being subjected to a pressure load before breaking. The test stand used an air compressor to supply a pressure load to the material, while a laser vibrometer measured how much the material deflected. A regulator was used to control the amount of pressure that was applied to the material. As the pressure load was increased, the material deflected more. The test stand also determined the maximum sustained pressure load the material could handle before breaking. After conducting all the experiments and analyzing the data, it was found woven materials are not suitable as a skin material. The reason air is allowed to pass through the woven material. Therefore, woven materials could not sustain the aerodynamic loads of an aircraft while in flight. The rest of the materials performed differently. Specifically if the material strained well and required less force while conducting the uniaxial and biaxial experiments, those materials could not sustain a high pressure load. Yet, the materials that did not strain well and required more force were able to handle a larger sustained pressure load.

# Acknowledgments

First off I would like to thank my committee, Dr. Daniel J Inman, Dr. Harry H. Robertshaw, and Dr. Donald J. Leo. Dr. Inman has supported my research, answered all my silly questions, and on numerous occasions provided me with non stop laughter with his comedy acts. Dr. Robertshaw provided me with his time, which allowed me to a better grasp of the morphing wing program at Virginia Tech. Dr. Leo thanks for answering all my questions concerning my research effort and for being a great controls professor.

Next, I would like to thank Dr. Dwight Viehland. Thanks for providing me with the documents you acquired concerning different materials that could be used as a skin material for a morphing wing. Also, thanks for all the personal relations work you did to acquire sample materials to test.

Thanks go out to the following companies that provided free sample materials. Speciality Extrusion by way of Thomas Yip provided sample materials of Tecoflex® and Arnitel®. Cornerstone Research Group by way of Ernie Havens provided the shape memory polymer samples. Ticona by way of Bob Imes provided samples of Riteflex®. H. Worshow and Sons by way of David Harrington and David Firth provided samples of Tru-Stretch® and Spandura®.

To the members of CIMSS, thank you all for your assistance. Without all your help I would have not have had all the ideas needed to complete my research. I would also like to thank my dear friend, Ms. Gigi Switz. Gigi, without all those talks and flying shoes I would have never had the motivation to finish writing this thesis. Now, I am wait for your dissertation, so for one time on one day, I will call you "Dr. Switz." To the VBC, wow what a group of friends, no words express my thanks for all your support and fun times.

Last, but certainly not least, I thank my parents, Mr. Miles Y. Kikuta and Mrs. Michele E. Kikuta. Without your lasting love and support and could have not come this far. By believing in

my abilities you have helped me conquer all the goals I have set, while still supporting the goals I have yet to achieve.

# Table of Contents

# List of Tables

# List of Figures

**Chapter 1 Introduction**



**Chapter 2 Material Selection**



**Chapter 3 Test Stands**

**Chapter 4 Test Results and Comparison of Materials**

# Nomenclature

$\delta$ is the total elongation of the member.

$\delta_w$ is the elongation of the material in the lateral direction.

$\delta_l$ is the elongation in the axial direction.

$l$ is the original material length in the axial direction.

$L$ is the original length of the member.

$w$ is the original material length in the lateral direction.

# Chapter 1

# Introduction

## 1.1 Thesis Overview

Revolutionary changes are occurring with aircraft wing designs. Specifically, engineers are designing an aircraft wing to change shape with morphing abilities. Conventional aircraft wings provide flight control by actuating the discrete control surface (flaps) on the wing. These conventional aircraft wings are able to change the effective chamber, allowing greater lift at lower speeds or allowing better efficiency at higher speeds. Studies have been done, proving a morphing wing can be as efficient as or even more efficient than conventional wing designs, providing more maneuverability and allowing the aircraft to be pertinent for multiple missions.

Great emphasis has been put on the designing of a morphing wing, in terms of the actuation and movement of the wing. There seems to be very few, if any at all, studies being conducted on plausible skin material for these morphing wings. Therefore, this report will discuss the investigation of candidate materials as a skin for a morphing wing.

This report will have a section that will present a background of current aircraft that utilize some form of morphing wing. This is followed by a section discussing the purpose and motivation of investigating candidate skin materials. Within the motivation section of the report, the difference between a conventional wing and a morphing wing will be presented. Also, the different wing configurations a morphing wing will be discussed. Based on these morphing wing shapes, Chapter 2 will discuss the criteria used to research plausible skin materials.

Chapter 2 will also provide a history and literature review of the different materials that were tested. Since analytical solutions take less time to get an insight of how a material will perform, this section will present a literature review of previous research, articles, websites, and books used to perform an analytical solution for some materials similar to those that were tested for this report.

Chapter 3 is dedicated to discussing the purpose of each test stand, the fabrication of the test stands, how the test stand works, and the procedure followed to operate the test stand. Three test stands were designed to gather the mechanical properties of the plausible skin materials. The uniaxial test stand allowed uniaxial loading conditions, allowing the determination of a force and strain relationship. Also, a recovery analysis could be completed after the material was deformed. The biaxial test stand would gather the same information as the uniaxial test stand, except the loading conditions would be placed on both sides of the material. Finally, a pressure-deflection test stand was conceived to determine if the material could handle the aerodynamic loads of an aircraft while in flight. After all the testing was completed, the analyses of the experiments were completed.

Chapter 4 will present the results of all the candidate materials tested. After discussing the results of each material separately, a matrix will be presented comparing the results for each material. Also, this matrix will help determine which material(s) have the ability to be a skin for a morphing wing.

The final chapter, Chapter 5, provides a conclusion for this thesis investigation. Within this chapter, a brief summary of thesis will be presented. A separate section will provide recommendations to improve the test stands that were designed. Next, there will be a discussion of other materials that should be investigated. Also, provided in the conclusion will be a section discussing the need for an analytical solution. Finally, there will be a section discussing future work that can be conducted.

## 1.2 Morphing Wing Background

This section will present a brief history and background of current aircraft that change the shape of their wing for different missions. Due to advancements in technologies, engineers have moved beyond traditional boundaries in terms of designing aircraft wings. These aircraft wings have the ability to morph into a particular shape depending on the mission.

In 1903 the Wright Brothers used their wing-warping control system on the 1903 Wright Flyer, which allowed the wing to warp. This provided the ability to control the aircraft better. Understanding the ability to twist the wing allowed greater maneuverability, the Air Force Research Laboratory, Boeing's Phantom Works, and NASA Dryden worked together creating program called the Active Aeroelastic Wing (AAW) program (Barr). Their collaborated research lead to the development of an F/A-18A that had the ability for the outer wing panels to twist up to five degrees. The first flight was on November 15, 2002 at Edwards Air Force Base in California.

Another participant investigating morphing wings is NASA's Langley Research Center (LaRC). LaRC researchers are investigating birds to understand how they maneuver. Birds have many more maneuvering capabilities than aircrafts. Birds have the ability to hover, fly backwards and sideways (Barry). Airplanes today might only have one of these abilities. Researchers at LaRC are investigating all the components vital for a morphing aircraft, which include the structures, flow physics, systems and multidisciplinary optimization, integration controls, acoustics, and materials (McBowan et al. 1999).

Currently there are four modern airplanes that take advantage of a morphing wing. The F-14 Tomcat and the B-1B Lancer wings are designed with a variable sweep, specifically using the "swingwing" technology. The wings are swept back for supersonic flight, allowing better efficiency and control when traveling at high speeds. The AFTI/F-111 Mission Adaptive Wing (MAW) and the F/A-18A Hornet with Active Aeroelastic Wing (AAW) are designed with a seemless camber. This design allows the aircraft "to maneuver more quickly, achieve better lift to drag ratios, and to have greater ranges in flight" (Arrisonet et al. 2003). Although the MAW wing design seemed to be successful, the program was canceled in the late 1980's.

Great accomplishments have been made with morphing wing design as discussed in the preceding paragraph. But one clear conclusion from those morphing wings is they only have the ability to change into two different specific shapes. Morphing wings in the future will be able to change into multiple shapes, allowing the aircraft to be versatile for an array of missions. Therefore, an investigation was conducted concerning the morphing wing designs currently being researched at Virginia Tech. This leads to the purpose and motivation section of the report. Understanding how the wing will maneuver and operate will help determine the material characteristics needed for a morphing wing.

## 1.3 Purpose and Motivation for an Elastic Skin Material

History has shown most aircraft are designed to serve one primary mission. A few examples are both the B-52 and the B-2 stealth bomber have a long wing span allowing optimal cruise for long range missions, but are not used as a fighter plane because of its inability to maneuver. On the other hand, the F-14 Tomcat and F-18 Hornet have a smaller wing span and are primarily used as a fighter/attack aircrafts because they have the ability to maneuver quicker. In most cases bomber planes are escorted by the smaller, lighter, and more maneuverable aircrafts such as the F-14 or F-18 aircrafts for protection. A new concept is for military aircraft to have both bomber and fighter characteristics, which would allow the aircraft to be used for an array of missions. Therefore, there is a need for a morphing wing.

Many engineers have been researching, designing, and testing different wing kinematics, to achieve a morphing wing. Today, most conventional aircraft wings change shape by the actuation of hinged flaps or pivots. Even the aircraft that were previously discussed that take advantage of some form of wing morphing use hinges or a pivot to change the shape of the wing. The flaps are made separately and are integrated into the wing. Since the flaps and the wing are separate components the skin material is rigid, usually a type of a thin sheet metal. For example, Figure 1.3-1 shows an F/A 18 with AAW.

**Figure 1.3-1.** Picture of an F/A-18 with AAW [NASA Dryden photo].

A morphing wing can be designed to change into many different wing configurations. A possible morphing ability is for the wing to have a variable sweep, as shown in Figure 2. When the wing is crescent backwards, left-hand side of Figure 1.3-2, it allows an aircraft to have greater maneuverability at higher speeds. While in the sweep position, right-hand side of Figure 1.3-2, in a cruise flight condition it should exhibit greater efficiency. According to van Dam (1987), analysis has been shown that a backward curvature of a wing improves the induced efficiency to a value greater than a flat untwisted wing of elliptical shape, which is considered optimal in classic wing theory design.

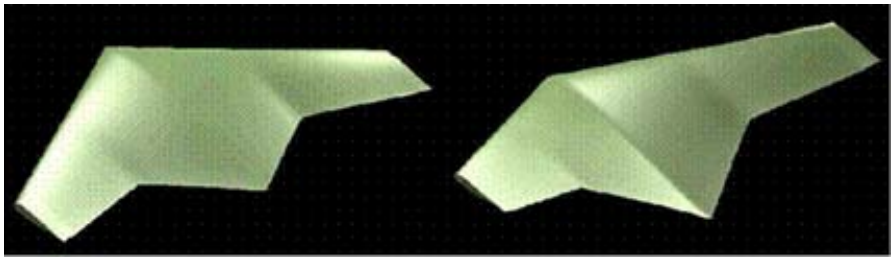

**Figure 1.3-2.** A morphing wing with different sweep characteristics. The wing design on the left is median wing design, while the wing design on the right is morphed in an extreme sweep position [Pettit].

Another ability of a morphing wing is for the wing to change to a dihedral position. This wing configuration is shown in Figure 1.3-3. "Arguments have been made that a longer wing span decreases induced drag, but a longer wingspan with a fixed wing area, increases the weight of the wing due to higher bending moments and a thinner, less efficient structure" (Kroo p. 587-

317). There is a trade-off for this morphing wing design, depending on the application of the aircraft. Although there might be arguments if this morphing wing ability is efficient, it is a morphing ability that is currently being researched by other engineers. Therefore, it is another morphing configuration to take into account when determining what type of skin material is needed.

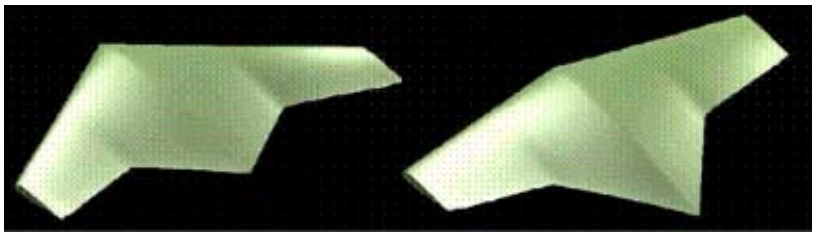

**Figure 1.3-3.** A morphing wing in the dihedral position. The wing position on the left is median wing design, while the wing design on the right is morphed to a dihedral position [Pettit].

The next morphing ability that was considered is changing the chamber. The shape of the camber can change depending on the application of flight, as shown in Figure 1.3-4. Changing the camber acts like flaps. A changing camber allows the wing to have minimal induced drag effects while in cruising mode, while also having the ability to increase lift at slower speeds. These non-planar wing designs have a component of induced velocity. Cone (1962) stated "The velocity can be beneficial in increasing the lift of the system for a given induced drag".

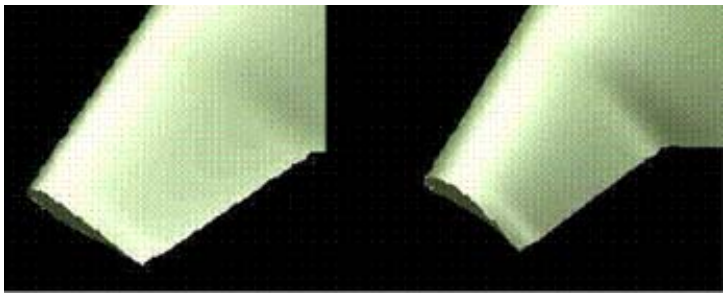

**Figure 1.3-4.** A morphing wing with different camber configurations. The camber design on the left is with a "normal" camber, while the wing design on the right has an extreme camber shape [Pettit].

A different morphing ability that can minimize drag is a reflex wing, as shown in Figure 1.3-5. Again depending on the application of the aircraft, a morphing reflex wing design can increase the efficiency of the aircraft.

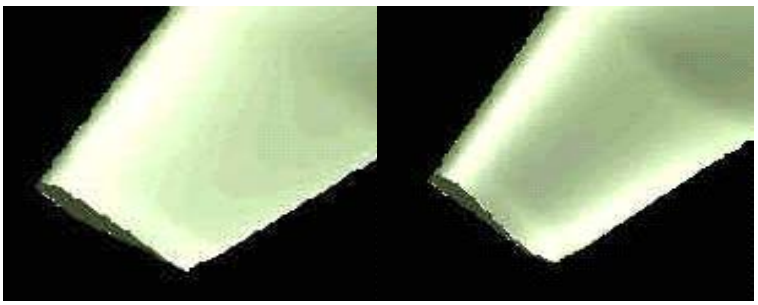

**Figure 1.3-5.** A morphing wing with different reflect configurations [Pettit].

The final morphing ability is a wing that can twist, as shown in Figure 1.3-6. This is the same capability that was previously discussed for the F/A-18A AAW that had the ability for the outer wing panels to twist up to five degrees. Flick (2002) stated with AAW, "the leading and trailing edge control surfaces are deflected, which causes a change in the aerodynamic pressure distribution on the wing's surface causing it to warp or twist. The surfaces are deflected such that the wing twists into a shape that helps the wing perform better than if it did not twist at all."

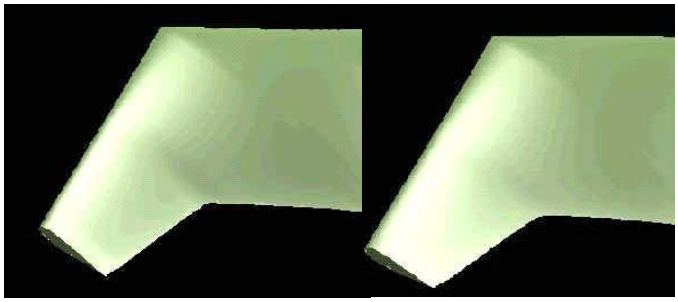

**Figure 1.3-6.** A picture showing a morphing wing twisting [Pettit].

## 1.4 Chapter Summary

At the beginning of this chapter, the outline of the entire report was presented. The outline presented a general path the report will follow as well as a general reason why each section or topic is important to discuss. The second section of this chapter presents current aircraft that using a form of morphing wing technology. Although advancements in aircraft wing design have been made, future morphing wing aircrafts will be suitable for a variety of missions. Therefore, the third section of this chapter went into detail concerning morphing wing abilities engineers are currently achieving. After discussing the different possible morphing configurations it is easy to understand a rigid skin material, such as a thin metal plate, is not suitable. A more plausible skin material will have to be flexible and elastic, while still having the toughness and abrasion resistance of metal. The following material characteristics were used to investigate possible skin materials: elastic, flexible, high recovery, resistant different weather conditions, resistant to abrasions and chemicals, and having a hardness number high enough to handle the aerodynamic loads of the aircraft while in flight.

# Chapter 2

# Material Selection

## 2.1 Introduction to Material Requirements

As discussed in Chapter 1, a morphing wing skin material cannot be a completely rigid material. Therefore an investigation was performed to discover what types of materials are currently available that could be used as a skin material for a morphing wing. After reviewing some of the different wing configurations of a morphing wing, criteria for skin materials were developed. A plausible skin material will have to be flexible and elastic so the material can be easily deformed, while still having the strength to carry the aerodynamic loads of the aircraft. Also the material has to have the abrasion resistance of metal so the material would not be damaged when subject to changing environments. After the material has been deformed to a different wing shape, the material should be able to recover its original size. Plastic deformation could occur where there is excess material after the wing is brought back to its original position. This excess material could cause more drag. If there is additional drag, the efficiency of the aircraft will decrease. The criteria provided a fundamental basis that was used to investigate plausible skin materials.

## 2.2 Material Overview

Engineering advancements in the area of polymers have allowed materials to be more durable, flexible, elastic, and have a higher recovery percentage. Due to these advancements, there are different materials that have the opportunity to be used as skin materials over different parts of a morphing wing. Specifically the material can be used around the area of the ribs, the location where the wing will be changing shape. A possible skin material would be made out of polyurethane. Polyurethane is a synthetic material, which allows it to be combined with other chemicals so different properties can be achieved depending on the application (Thermedics Polymer Products 2003). A material that has similar characteristics of polyurethane is copolyester. Copolyester is a type of material that is easy to process and has the characteristics of thermoset elastomers (Ticona 2003). Another plausible material are shape memory materials. Shape memory materials have a transition temperature above which the properties of the material change. The transition temperature is referred to as the glass transition temperature, $T_g$. Below the glass transition temperature the material is rigid, while above the glass transition temperature it acts like a flexible rubber. The final type of material that was investigated is stretchable woven materials, such as Spandex. These materials have elastic properties and have high recovery abilities.

### 2.2.1 Polyurethanes

One material studied is polyurethane, which was invented in the 1930's by Otis Bayer. According to Bunker corporation (2003) polyurethane was originally invented as an alternative to rubber because rubber became in short supply during world war two. After years of chemical engineering refinement, there are different versions of polyurethane for various applications in the commercial market. Polyurethane is popular because it has the ability to provide the elasticity of rubber, while having the advantages of toughness and durability of metal. Since polyurethane is a synthetic material, there are different chemical formulas which allow the material to have a different hardness. Figure 2.2-1 shows a Durometer range. Typically polyurethanes have a hardness range between Shore A 30-100 and Shore D 20-75.

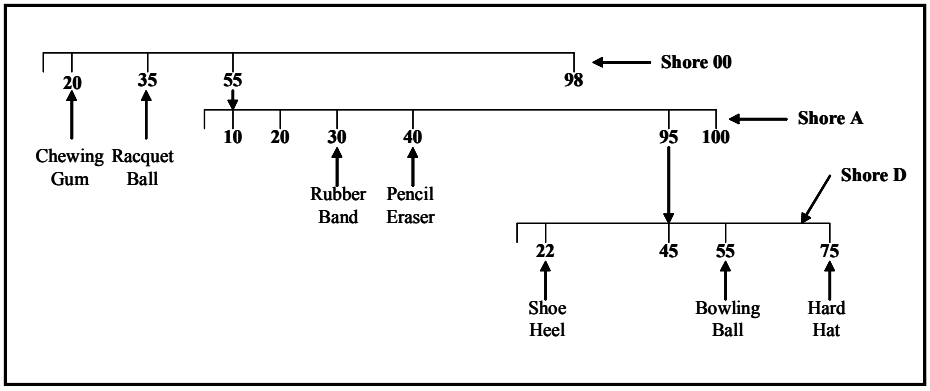


**Figure 2.2-1.** Durometer scale.

A couple of other advantages polyurethane has are the ability to withstand abrasions and the ability for polyurethane to handle pressure loads. Polyurethane is resistant to oils, solvents, fats, greases, and gasoline. Polyurethane can be designed to handle various loads, depending on the chemical formula. Since aircraft are subject to various weather conditions, the skin material has to have the ability to withstand different weather elements. Polyurethane is resistant to oxygen, ozone, and sunlight.

The elastic characteristic of polyurethane is due to entropy. The disordered polymer chains that make the polyurethane material allows the un-stretched to be in its natural state. When the material is stretched the polymer chains are in a state of order. Since the natural state of polyurethane is when the polymer chains are disorder, the material returns to its original state and size when it is allowed to un-stretch.

One family of materials being tested is Tecoflex®. Tecoflex® is a type of medical thermoplastic polyurethane's (TPU's) that is manufactured by Thermedics Polymer Products. According to Thermedics Polymer Products (2003), Tecoflex® materials are currently being used in the medical field, which are available with different characteristics. Some of these characteristics meet the criteria that are needed for a morphing wing skin material. The specific Tecoflex® materials that were tested are EG-80A, EG-93A, and EG-100A, where the material properties are listed in Appendix A.

### 2.2.2 Copolyester

There are two specific materials that were tested that fall under the copolyester category. One material is Arnitel® and the other is Riteflex®, specifically these materials are a type of thermoplastic. One reason why these materials were chosen to test is the availability of these materials. According to the manufacture of Riteflex® (Ticona 2003) they "combine the features of thermoset elastomers and the easy processing capabilities of plastics."

Riteflex® is manufactured by Ticona. The molecular structure of Riteflex allows the material to be formulated with different degrees of hardness through the relative proportion of the soft phase and hard phase (Ticona 2003). This is done by the alternating soft and hard polyether components the molecular structure level. The main design objective for Riteflex® is the ability to work well with applications that rubber and other elastomers cannot perform (Ticona 2003). These material characteristics are also similar to polyurethane. After reading the information provided on Ticona's website, Riteflex® seemed to meet many of the criteria that were determined that would make the material a good candidate for a skin material for a morphing wing. The two specific materials there were tested are Riteflex® 640 and Riteflex® 663.

The final copolyester material tested was Arnitel®. Arinitel® is a copolyester elastomer that is produced by DSM. DSM (2003) states that Arnitel® has many characteristics of a polyurethane, by "combining the advantages of engineering thermoplastics, being easy to process with excellent mechanical properties, at the same time with the flexibility of rubbers." Arnitel® has the same characteristics as polyurethanes like, strength, abrasion resistant, heat resistant, and chemically resistant.

### 2.2.3 Shape Memory Materials

Another family of material that was investigated was shape memory materials (SMM). Within the family of SMM there are different types, such as, shape memory polymer (SMP), shape memory alloy (SMA), and liquid crystalline elastomers (LCE). Lui et al. (2002) states SMM "are materials that can be deformed into a temporary and dormant shape under specific conditions of temperature and stress and will later, under thermal, electrical, or environmental

stimuli, relax to their original, stress-free conformation due to the elastic energy stored during the initial deformation." Although SMAs are introduced within the family of SMM, this report is not investigating them. The emphasis will be on the shape memory polymers, since a sample SMP was provided by Cornerstone Research Group. The identification number for the SMP from Cornerstone Research Group is JLR-055-24A. LCE have properties of mechanical anisotropy, soft elasticity, and a coupling between rubber-elasticity and liquid crystalline ordering (Lui 2002). Although liquid crystalline elastomers were discussed no samples were available to test. Yet, they seem to provide properties that met the criteria set for plausible skin materials for a morphing wing.

Shape memory polymers have similar characteristics of rubber, but since there is a chemical or physical cross-link in the polymer chains, the SMPs have superior "elasticity above a critical temperature controlled by its glass transition temperature ($T_g$)" (Chen, Zhu, and Gu p. 1504-1512). This phenomenon allows the shape of the material to change, depending on the temperature (Chen, Zhu, and Gu p. 1504-1512). Figure 2.2-2 shows a generic elastic modulus versus temperature plot for a shape memory polymer (Liang, Malafeew, and Rogers p 382, Hayashi et al. p 29, Lee, Kim, and Xu p 5782, Monkman p 490). SMPs made out of polyurethane take advantage of the glass transition temperature, since the mechanical properties of the material changes (Hayashi, Lin, and Tobushi p. 109-114). Below the glass transition temperature, the material acts like a rigid solid. During the transition state, the material has both solid and rubber characteristics. Once beyond the transition state the material is in a rubbery state, which allows deformation to occur. Most SMPs have flow state, which once the material is heated beyond this point the material looses its ability to recover. Specifically for the SMP provided by Cornerstone Research Group, the glass transition temperature is 85 degrees Celsius. A product engineer suggested the viable state to apply deformation is at 100 degrees Celsius. This is also the temperature to induce recovery of the material after being deformed.

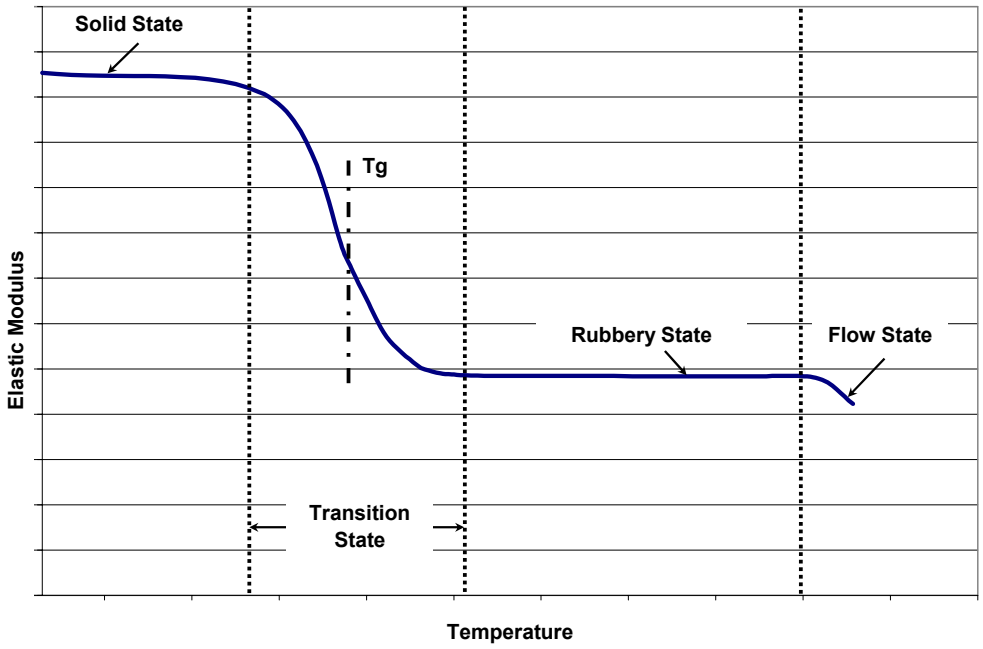


**Figure 2.2-2.** A plot showing the elastic modulus range versus temperature for an SMP.

Bhattacharyya (In Press) stated SMPs are a class of polyurethanes that have the ability to undergo significant deformations, since the thermomechaical input allow the material to change its elastic modulus. Polyurethane SMPs also have become popular because they have the ability to be injection molded, the ability for the SMPs to be colored since the original color is transparent, and finally the glass transition temperature can be designed for a specific application (Hayashi et al. p. 296-302). It is important to clarify that all polymers have a glass transition temperature, but not all polymers exhibit the shape memory effect.

### 2.2.4 Woven Materials

The final type of material that was investigated is made out of elastane fibers or yarns. These synthetic yarns are made out of segmented polyurethanes which consist of alternating polyurethane hard segments and polyether or polyester soft segments (Gaymans, Krijgsman, and Niesten p. 46-48). These elastane fibers are within the family of fibers that are commonly referred to as Spandex®. According to Fourné and GmbH (2001), these yarns are known for both their high elasticity and recoverability. Since these types of materials have the elasticity and recoverability effects that are suited for a skin material for a morphing wing, sample materials

were sought. The two available types of woven materials were Spandura® and Tru-Stretch®, which were provided by H. Warshow & Sons.

Spandura® is a product of Dupont, specifically in their Invista division. Spandura® is made out of a Cordura® and Lycra® blend. According to Seattle Fabrics (2003), a manufacture and supply company of Spandura®, Spandura® is a product that combines the durability of Cordura® nylon and the stretching ability of Lycra®. According to the Lyrca's website (2003), Lycra® is also shape retention, meaning Spandura recovers after being stretched. Cordura's website stated Cordura® is ten times more durable than cotton duck, three times more durable than standard polyester, and two times more durable than standard nylon as well as the durability allows it to be resistant to not only abrasions, but also to tears and scuffs.

Tru-Stretch® is made out of a Lycra® and Nylon® blend. It has the same material characteristics as Spandura®. The only difference between Tru-stretch® and Spandura® is Spandura® is elastic in all directions, while Tru-stretch® is only elastic in one direction. The reasons for the differences are the way the material was woven as well as the chemical formulation of the yarns. A visual representation is shown in Figure 2.2-3.

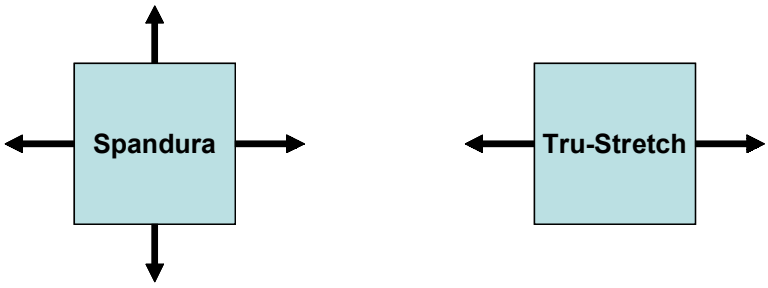


**Figure 2.2-3.** Visual representation on the elastic effect available for Spandura and Tru-Stretch.

## 2.3 Literature Review: Analytical Solutions

Although analytical solutions were not performed for this thesis, a literature review was completed. This section will present books, websites, equations, and theories that could be used to determine an analytical solution for materials that have similar rubber characteristics.

In terms of uniaxial or biaxial loading condition, the material could exhibit linear relationship between stress and strain or force and strain. These relationships are defined by Hooke's Law, which are readily available in many mechanics of materials books. Boresi, Schmidt, and Sidebottom (1993) and Ugural and Fenster (1981) discuss Hooke's Law.

For most of the materials that were tested, the force and strain curve results were non-linear. These results are due to the material being a non-linear elastic, a viscoelastic, or a viscoplastic material. To determine an analytical solution for these non-linear responses many have formulated constitutive equations based on the strain energy potentials. Most of theses models are based on the statistical mechanics of the material. Some of these models are the Mooney-Rivlin, Neo-Hookean, and Odgen Potential. Most of these models are found in books that are specifically written to discuss rubber theories. Two books that were reviewed that discussed rubber theories as well as the models are, *Theory and Practice of Engineering with Rubber* by Freakley and Payne, also *Rubber Engineering* which is a collection of information by Indian Rubber Institute. Another reference is ANSYS, which is a finite element modeling software. In the help section of ANSYS type in "hyperelasticity" this will lead to a quick overview of the strain energy potentials models it has available as well as the governing equations. These references could be used to determine an analytical solution that quantifies the relationship between stress and strain or force and strain as well as the ability for the material to recover.

There are two possible analytical expressions for determining the deflection of a material due to a pressure load. One analytical expression is given by Boresi et al, where they discuss the Prandtl Elastic-Membrane (soap-fim) Analogy. The other analytical expression is given by Maier-Schneider et al, where they determined an analytical solution for the deflection of a material undergoing a pressure load of square membranes.

## 2.4 Chapter Summary

An overview of the type of materials to test and the criteria that were used to choose these materials were presented. Some details concerning the requirements for a candidate material for a morphing wing has been presented. Specifically candidate materials must be elastic, flexible, have a high recovery, resistant to both weather conditions and chemicals,

resistant to abrasions, as well as have a hardness number high enough to handle the aerodynamic loads of the aircraft while in flight. Based on the characteristics, the second portion of the chapter gave a brief overview of the different materials that were tested.

# Chapter 3

# Test Stands

## 3.1 Overview of the Test Stands

This section will discuss the functions and the procedures for the uniaxial, biaxial, and pressure deflection test stands. The uniaxial test was able to determine the following mechanical characteristics, force versus strain, recovery strain, and elongation ratio. The elongation ratio was calculated after measuring the axial and lateral strain of the material while undergoing uniaxial deformation. The biaxial test stand was design to gather a force and strain relationship. The biaxial test stand allowed a better understanding of how the material would perform as a skin for a morphing wing. The pressure deflection test stand determined the maximum pressure load the material could sustain before breaking and the amount the material deformed under the pressure load. Specifically, the pressure-deflection test would determine if the material could handle the aerodynamic loads applied to an aircraft wing while in flight.

## 3.2 Uniaxial Deformation Test Stand

The test stand uses four components, a string potentiometer, a force transducer, a winch, and a fabricated gripping device. Utilizing these components together allowed the determination of the desired mechanical properties. Figure 3.2-1 shows a schematic of how each component was applied in the test stand to gather the appropriate data. Using a piece of material that has equal dimensions on each side, hence a square, one side of the material is gripped and grounded while leaving the opposite side of the material free to move. On the side of the material that is free to move, the material is also gripped. The gripper is then attached to a machined material that is tapped for a threaded rod. The threaded rod is then connected to the force sensor. The opposite side of the force sensor has a rod end eye socket. This allows it to be attached to the cable of the winch, which is grounded. The string pot is also grounded and attached to the gripping device to gather accurate displacement measurements. The string potentiometer and the force sensor are connected to display meters for appropriate readouts.

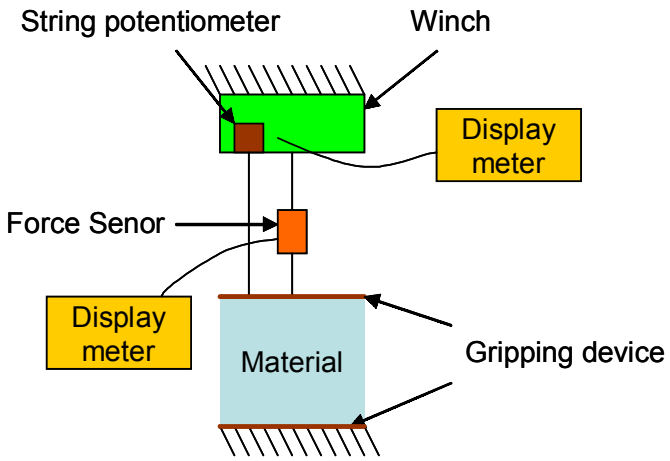


**Figure 3.2-1.** Schematic for uniaxial deformation.

Figure 3.2-2 shows a picture of a material being tested using the uniaxial test stand. The winch and the display meters are not shown in the picture. The force transducer is shown in the green oval, the string potentiometer is labeled with the blue arrow, the fabricated gripping devices are shown in the red arrows, the connector between the gripping device and the force transducer is shown with the black arrow, the rod end eye socket that connects the force transducer to the

winch is depicted by the magma arrow, and the electrical cords that are attached to display meters are represented by green arrows.

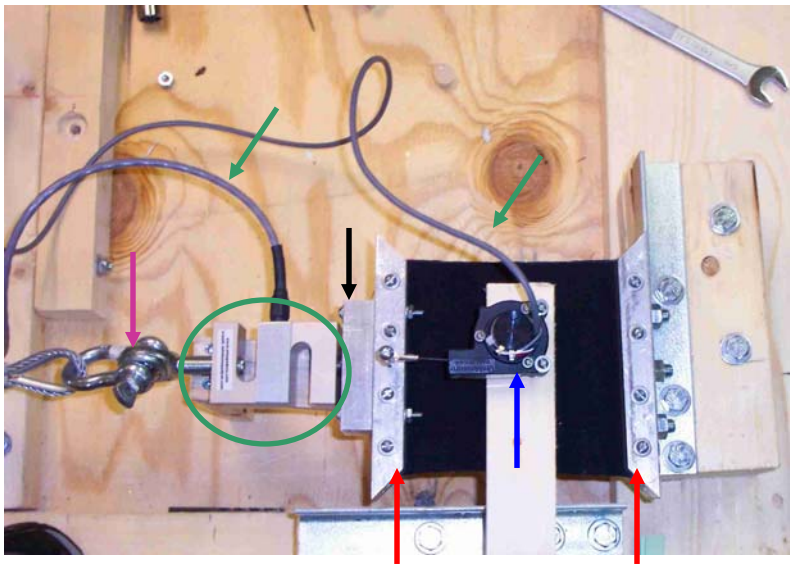

**Figure 3.2-2.** Picture of a material undergoing a uniaxial experiment.

### 3.2.1 Uniaxial Deformation Procedure

The following procedure was followed for the force and strain comparison experiment. Once everything was connected, the winch was rotated until there was no slack in the wire, which was connected to the force transducer. Then the force the gripping device and force transducer created due to gravity was recorded from the display meter, which would be subtracted when determining the force versus strain analysis was completed. The display meter output for the force transducer was in mV. Also, the initial voltage from the string potentiometer was recorded. The winch was then turned approximately $\pi/16$ and the outputs from the force transducer and string potentiometer were recorded. This was repeated until the material was strained to approximately 2.5 times its original length, if the material allowed such a deformation.

Another experiment used the following procedure. The material was initially strained and held stationary. Then the forces were recorded every 10 seconds. This would allow the determination if the material relaxed after being strained.

The test stand utilized two different force transducers. One force transducer was rated for 0-50 lbs and the other was rated for 0-250 lbs. Depending on the initial material characteristics, one of the two force transducers was utilized for the most accurate measurements. The output from the force transducer was in milivolts and the output from the string potentiometer was in volts. After all the data was collected, MATLAB was used to convert the voltages to pounds or inches, for the force transducer and string potentiometer, respectively.

## 3.3 Biaxial Deformation Test Stand

Since biaxial testing was also conducted, the same concept from the uniaxial stand was applied for biaxial test stand. Figure 3.3-1 shows the schematic for biaxial testing. The exact same components used for uniaxial testing were applied to biaxial testing. Therefore the biaxial test stand used two force transducers, two string potentiometers, two winches, and two display meters. This allowed the use of one test bed, but by adding the same components to the other axis, the test stand could be converted to perform a biaxial deformation analysis.

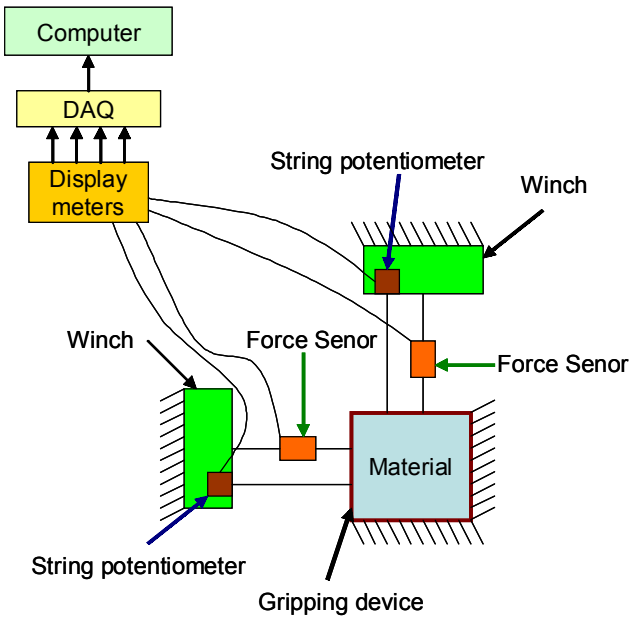


**Figure 3.3-1.** Schematic for biaxial deformation.

The relevant data that needed to be recorded were the voltage outputs from the string potentiometers and the force transducers. Since there were four outputs and recording the data by hand would be difficult, a data acquisition (DAQ) system was developed. Non-inverting amplifiers were designed for an ideal gain of 101 to amplify the voltages from the force transducers to amplify the signals from the force transducers which output between 0 and 30 mV. MATLAB and Simulink were used in conjunction with DSpace Control Desk to develop a user interface that allowed data to be collected from the DAQ system.

Figure 3.3-2 shows a picture of a material being tested using the biaxial test stand. The force transducers are shown in the green circle, the string potentiometers are labeled with the blue arrow, the fabricated gripping devices are shown with the red arrows, the connector between the gripping device and the force transducer are shown with the black arrows, the rod end eye hole that connects the force transducer to the winch is depicted using the magma arrows, and the electrical cords that are attached to display meters are represented by green arrows.

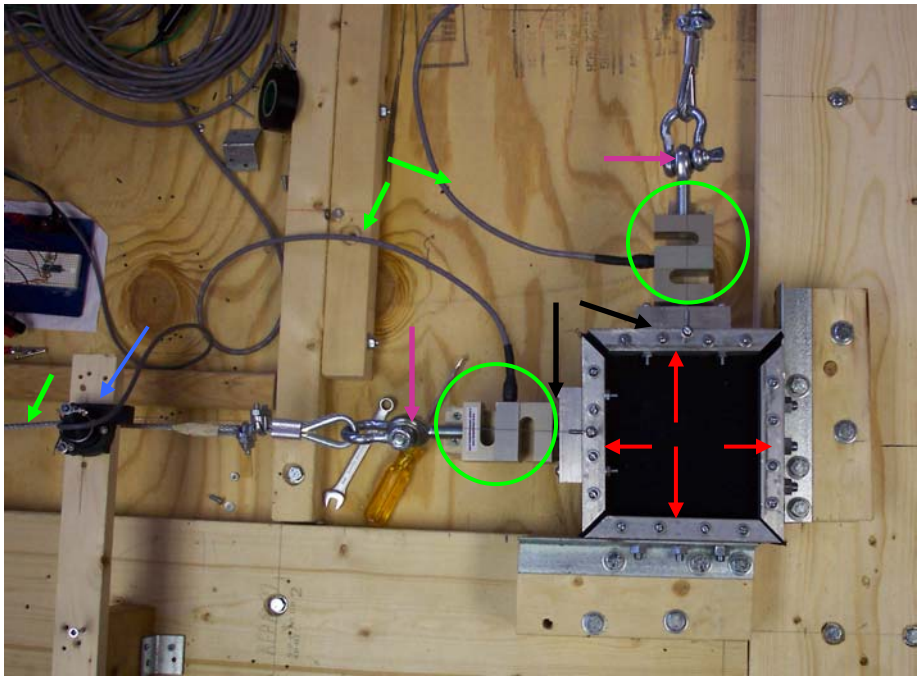

**Figure 3.3-2**. Picture of a material undergoing a biaxial experiment.

### 3.3.1 Biaxial Deformation Procedure

The following procedure was followed for the force versus stretch ratio experiment. Once the material was attached to the gripping device, the sensors were then connected. Then, the winches were rotated until there was no slack in the wires, which was connected to the force transducers. The user interface program that controlled the DAQ system was then started to record the initial forces that were produced by the gripping device and force transducer, which were created due to gravity. After approximately 10 seconds, both winches would be turned at approximately $\frac{1}{5}$ radians per second which would strain the material at approximately the same rate. The forces might not be the same in both directions, since some materials were not homogenous. For example, Tru-Stretch® is woven in such a manner that the force could be different along the different axis. The DAQ system recorded the output voltages produced both the string potentiometers and the force transducers.

Just like the uniaxial test stand, the biaxial test stand also was able to determine the required forces necessary to hold the material at a given strain. This was completed by starting the program and waiting approximately 10 seconds. Then the material was strained a displaced amount while the DAQ system kept recording the forces.

## 3.4 Uniaxial and Biaxial Test Stand Fabrication

This section will discuss the concept behind the design of the test stand component that dealt with gripping the material. The gripping device uses the concept of ordinary pliers. Pliers use teeth to grip anything that needs to be held stationary. Therefore understanding the material will have to be held, the fabricated gripping device was conceived. The teeth were designed not to have 90 degree angles, since the material could be damaged when the gripping device is bolted together. To accomplish this teeth configuration, there were two parts. One part was the "male" part, while the other was the "female" part, as shown in Figure 3.4-1. When the parts are mated together, it forms the gripping device.

**Figure 3.4-1.** CAD model showing the teeth designed to hold the material.

The gripping device was also designed to work with both the uniaxial and biaxial experiments. Since it was important to test sample materials where the boundary condition is originally square, the ends of the gripping devices were cut at 45 degree angles, as shown in Figure 3.4-2. Also there are four holes that are for bolts so the mated pieces can be held together.

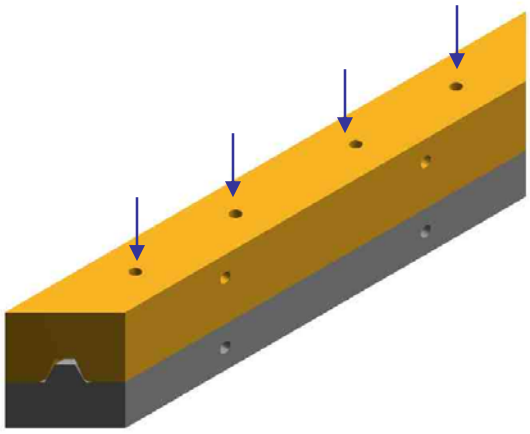

**Figure 3.4-2.** CAD model showing one side of the gripping device. The blue arrows show the location of the holes for the bolts.

Since the ends of each part was cut at a 45 degree angle, when the parts are put together it forms a perfect square. The holes that are shown by the blue arrow in Figure 3.4-3 are for the connection part for the force sensor, while the holes that are shown by the red arrow are for angle bars to ground the parts.

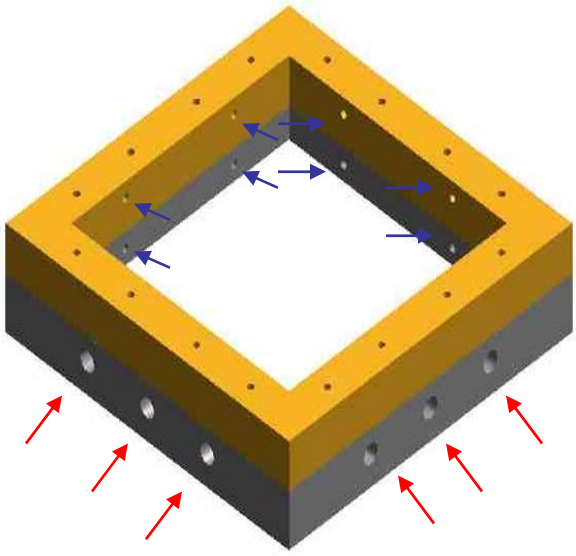

**Figure 3.4-3.** CAD model of the assembled gripper.

Figure 3.4-4 shows the connection part, which is shown in blue. This allows the force sensor to be connected to the mated grippers by a threaded rod. The reason for such a design was the force transducers were already threaded for rods.

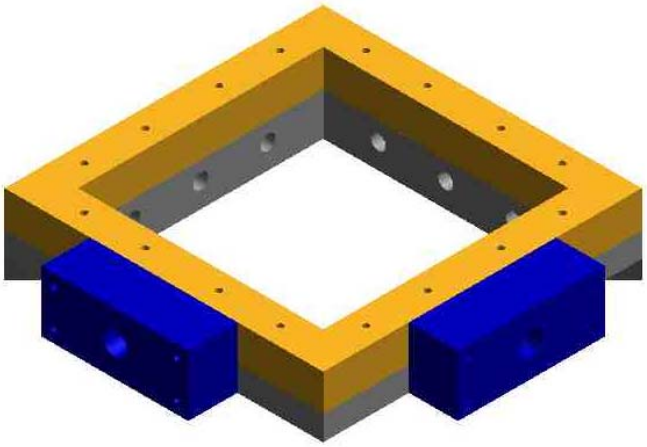

**Figure 3.4-4.** CAD model of the assembled model with the connecting parts.

The force transducers used for the experiments are manufactured by Omega. Depending on the material, either the force transducers rated for 50 pounds, model number LC101-50, were used or the transducers rated for 250 pounds, model number LC105-250, were used. The specifications for the force transducers are located in Appendix C. The string potentiometers are manufactured by Unimeasure, model number LX-PA-15, and the specifications are located in Appendix D.

As previously discussed the shape memory polymers (SMPs) have to be heated beyond the glass transition temperature to be viable. Therefore a housing unit was designed that would allow the material to be heated up by convection. The glass transition temperature for the SMP is 85 degrees Celsius. After talking with a product engineer from Cornerstone Research Group, they recommended the SMP should be heated to 100 degrees Celsius. Therefore, the glass transition temperature was a criterion used to design the housing unit. Two materials were chosen for the housing unit. One material was a thin sheet of aluminum that would encase all the sides except for the top of the housing unit. The top part of the housing unit was made out of a polycarbonate. There were two reasons for choosing polycarbonate for the top of the housing unit. The first reason is the polycarbonate allowed a visual inspection of the experiment since its actual color is clear and its formulated to handle temperatures well above the viable temperature of the SMP. The housing was designed with two holes. One hole was for an opening for a thermometer, and the other hole was for a heat gun, as shown in Figure 3.4-5.

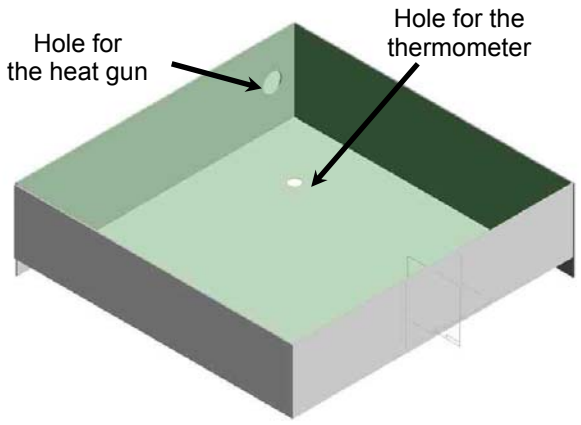


**Figure 3.4-5.** CAD model of the housing unit for the SMPs.

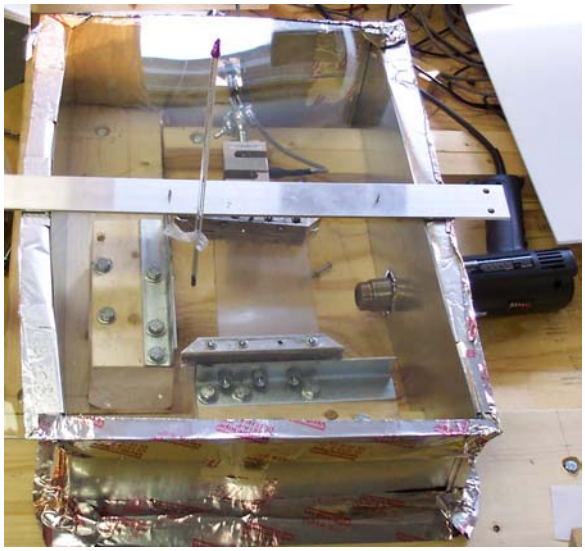

**Figure 3.4-6.** Picture of the housing unit used to encase the SMP during testing.

## 3.5 Pressure Deflection Test Stand

A successful skin material must have the ability to handle the aerodynamic loads which are applied to the wings while in flight. Therefore, the concept for a load deflection test stand was conceived. Mainer-Schneider, Maibach, and Obermeir (1995) stated "the load-deflection method is a well known method for the measurement of the elastic properties of thin films". Although the materials that were tested are not films, they were elastic and relatively thin.

The schematic shown in Figure 3.5-1 is a representation of how the test stand works for the pressure deflection experiments. An air compressor is connected to a regulator before entering the component that grips the material. The skin material gripper allowed the boundary conditions to be grounded on all the sides of the material. The regulator applied different pressures to the material. The controlling of different pressures is essential to determine the pressure load that would damage the material. A laser vibrometer will be used to determine the amount the material displaces. The laser vibrometer in conjunction with the regulator will allow the determination of how far the material displaces by the given pressure load. It is important to note that only one point on the surface of material was measured. The center of the material was the location used to measure the deflection of the material, since it was the location of the greatest

deflection. Using Simulink and DSpace Control Desk allowed the design of a data acquisition system that gathered the displacement data for a given pressure load.

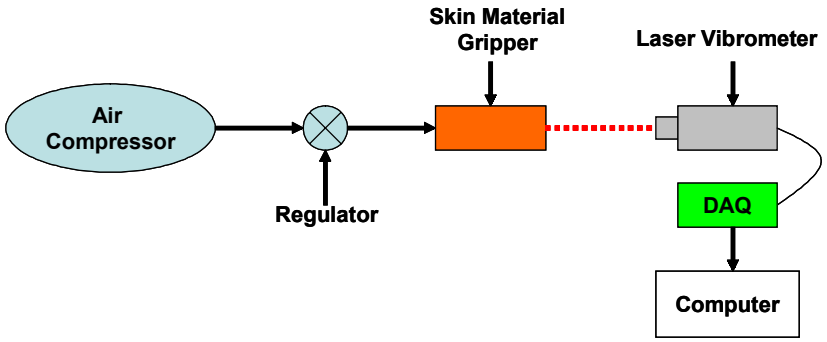


**Figure 3.5-1.** Schematic for the load-deflection test stand.

Figure 3.5-2 shows a picture of the test stand. Although the air compressor is not shown in the picture, all the other vital components necessary to complete test are shown. The regulator is shown in the green circle, the material gripper is shown in the blue oval, the laser vibrometer is shown in the red oval, and the green arrow shows where the hose for the air compressor mated with the regulator. The laser vibrometer is connected to the DSpace board to gather the displacement of the material at a given pressure.

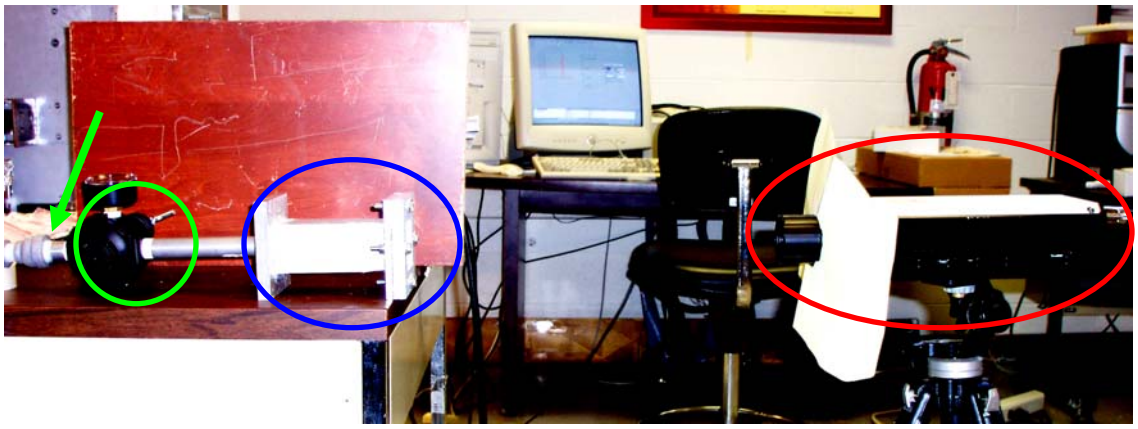

**Figure 3.5-2.** Picture of the test stand used for the pressure deflection experiments.

Once the material was placed in the gripping unit, a very small piece of copper tape is place at the center of the material, as shown in Figure 3.5-3. The small piece of copper tape

allows a reflected surface for the laser vibrometer to measure the displacement of the material, which is shown inside the blue circle of Figure 3.5-3.

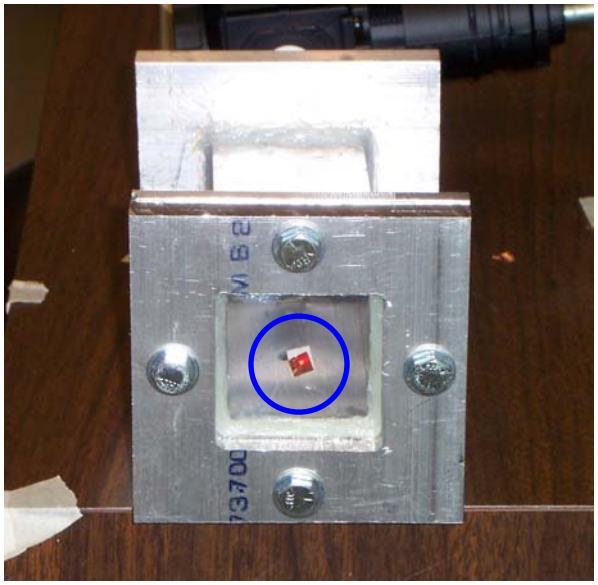

**Figure 3.5-3.** Picture showing the placement of the copper tape for the pressure deflection test stand.

### 3.5.1 Pressure Deflection Procedure

Once the material was placed in the test stand, the interface program created from dSpace Control Desk was started on the computer to start gathering data. Then the knob on the regulator was turned clockwise, which increased the pressure. For most materials, the incremented pressure amount was 5 psi, but other materials were incremented less. Once the pressure increased, the material was allowed to settle while still gathering the deflection data before increasing the pressure again. This procedure was repeated until the material broke.

### 3.5.2 Pressure Deflection Gripping Device

The skin gripper was fabricated with a male and female part, as shown in Figure 3.5-4. This will allow the boundary conditions along the edge of the material to be grounded, while allowing an easy test stand to assemble. Once the material is placed between the two parts, they are bolted together. Since the parts are bolted together, the system is closed by not allowing any pressure losses.

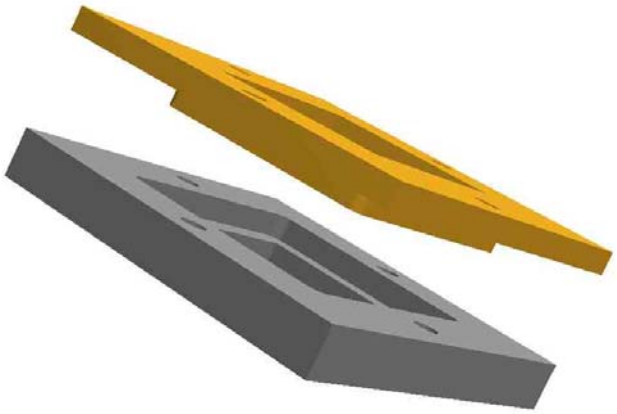

**Figure 3.5-4.** The gripper mechanism used to hold the skin material. The bronze color part is the male part, while the gray part is the female part.

## 3.6 Chapter Summary

This chapter presented the function, the components used, and the procedures followed for each test stand. The three test stands include a uniaxial, biaxial, and a pressure deflection test stand. The uniaxial test stand would allow the determination of the required forces needed to strain the material, the strains necessary to calculate the elongation ratio, how much the material could recover, and during the strain and hold experiment the determination of how much the forces dissipated after the material was strained. The biaxial test stand would find the results of how much for is required to strain the material, how much the material would recover, and determined if the forces dissipated once the material was strained to a stationary position. The final test stand, the pressure deflection test stand, found the maximum pressure load the material could sustain and how much the material deflected at a given pressure load.

# Chapter 4

# Test Results and Comparison of Materials

## 4.1 Chapter Overview

This chapter is presented in five separate parts. The first section will discuss the analysis and results of the uniaxial experiments for all the materials that were tested. The second section will discuss the analysis and results of the biaxial experiments. Next, the third section will discuss the pressure deflection analysis, as well as show the results of the materials tested. Finally section five will be an overview of all the results and discuss which material(s) is/are suited as a skin for a morphing wing. Also, shown in the fifth section will present a comparison matrix chart showing the final conclusions of the characteristics for each material.

The uniaxial and biaxial sections will present the force and strain results of the material. Also, discussed in the uniaxial and biaxial sections is the amount of force needed to hold the material stationary at a given strain. The prediction is less force will be needed over time to hold the material at a strained location due to the plastic deformation characteristics of the material. The final result that is presented is the ability or inability of the material to recover after it has been deformed. It is important for the material to recover to its original size because the excess material could increase the drag of the aircraft.

The fourth section of this chapter discusses the ability of the material to hold a pressure load. The results presented in this section show the results from the pressure deflection test stand. These results determine if the material can sustain the aerodynamic loads of the aircraft while in flight. If the material cannot carry the aerodynamic loads, it is not a suitable material for a morphing wing.

The final section of this chapter will present a comparison matrix of all the materials with their corresponding results. This matrix will help characterize the performance of each material and compare the results against one another.

## 4.2 Uniaxial Experimental Results

### 4.2.1 Results Overview

This section will give an in-dept discussion of how the results were obtained. By going in-dept of how the analysis was completed for one material will allow a more straightforward discussion of just the results for the other materials tested. The uniaxial experiments allowed the investigation of how the material performed.

For the uniaxial experiments the strain was calculated by using equation 4.2-1. Figure 4.2-1 shows a visual representation of how equation 4.2-1 was utilized.

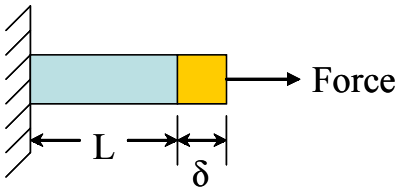


**Figure 4.2-1.** Picture of a member that is strain.

$$strain = \varepsilon = \frac{\delta}{L} \qquad 4.2\text{-}1$$

where δ is the total elongation of the member and

$L$ is the original length of the member.

The following graph, Figure 4.2-2, shows a visual representation of the analysis that was completed for each experiment. The blue "+," shows the data that was collected during the experiment. The green line represents the curve fit of the data. Finally, the error bounds were determined by normalizing the data and centering it at the zero mean. The error bounds, upper and lower bound, was determined using a ± 2 standard deviation that corresponded to a 95 percent confidence interval. The upper and lower bound lines are shown as black dashed lines and red dashed lines, respectively.

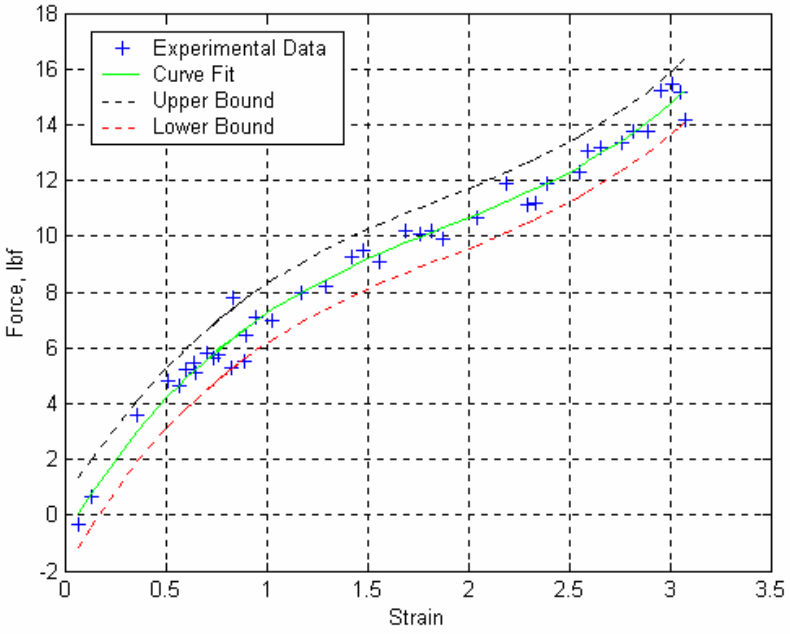


**Figure 4.2-2.** Experimental results of Tecoflex® 80A.

The importance of the analysis was to make sure the curve fit is consistent with the experimental data. The curve fit used was a 3rd degree polynomial using MATLAB.

The same material was also deformed two more additional times to determine if the material exhibits different force characteristics. Figure 4.2-3 shows the curve fitted results depicting the differences in the required forces necessary to strain the material. After the material is strained the first time, the material required less force at a given strain. The reason for this characteristic is the material exhibits plastic material properties. For the Tecoflex® 80A experiments the material was not strained beyond the yield strength point.

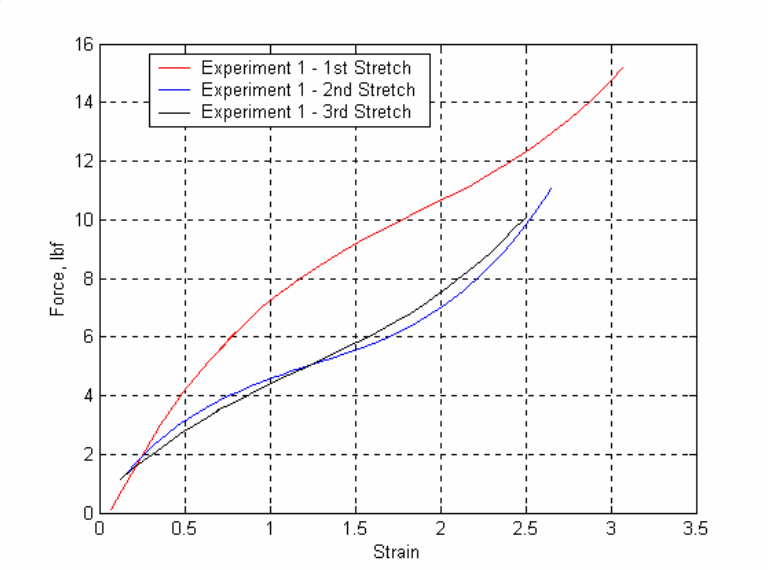


**Figure 4.2-3.** Difference in the force requirements for a given strain (Tecoflex® 80A).

The same experiment was completed again for the same material and analyzed, as shown in Figure 4.2-4. The reason for running the same experiment was to make sure the results are reproduced.

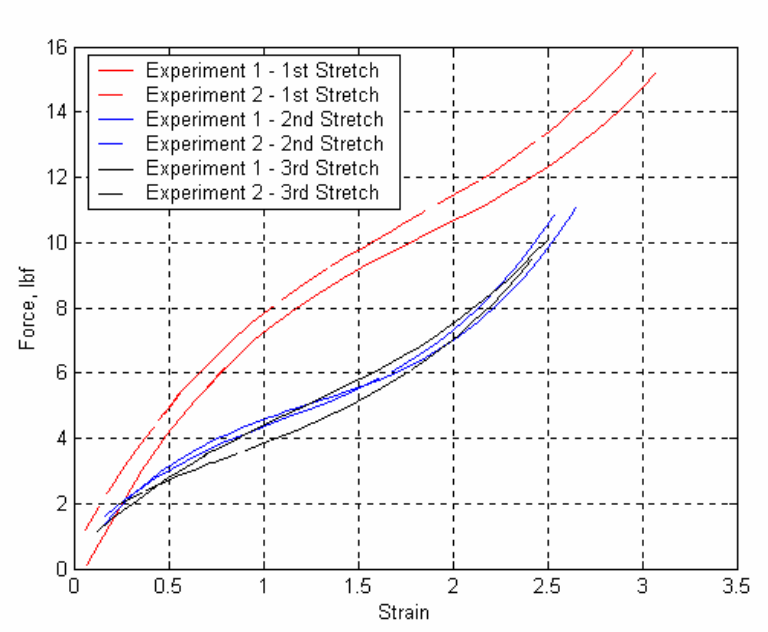


**Figure 4.2-4.** Duplicated results for Tecoflex® 80A.

**Necking.** The uniaxial experiments allowed two sides of the material to have a free boundary condition, as shown in Figure 4.2-5. Therefore, the non-constrained parts of the material exhibited necking effects.

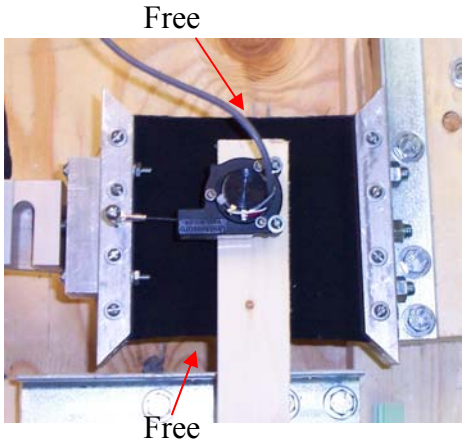


**Figure 4.2-5.** Boundary constrains for uniaxial deformation.

The data gathered due to the necking attributes was quantified by measuring the width of the material at center, relative to the axis of the material that is being deformed, as shown in Figure 4.2-6.

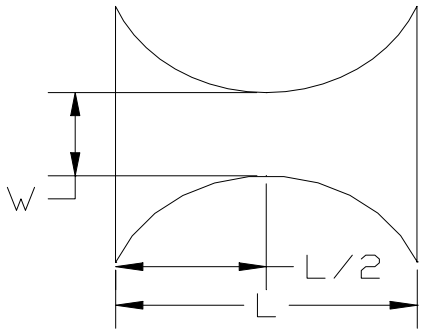


**Figure 4.2-6.** Analysis used to determine necking characteristics of the material.

Throughout this section the necking attributes are quantified in the following way. The axis the material is being strained by pulling the material is called the "Axial Strain," while the axis the material is necking is called the "Lateral Strain." A picture representing this is shown in Figure 4.2-7.

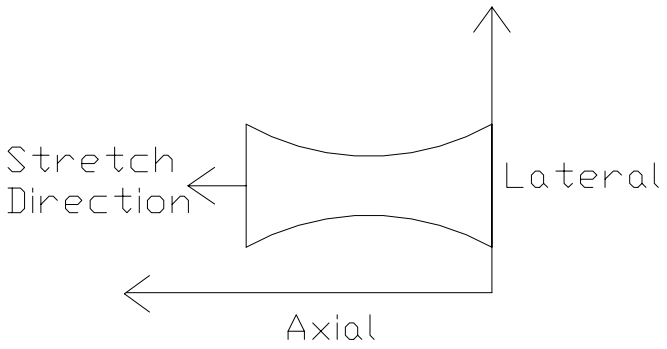


**Figure 4.2-7.** Schematic presenting the different terms used for the measured strains.

For Tecoflex® 80A, the necking properties were consistent with each experiment, as shown in Figure 4.2-8.

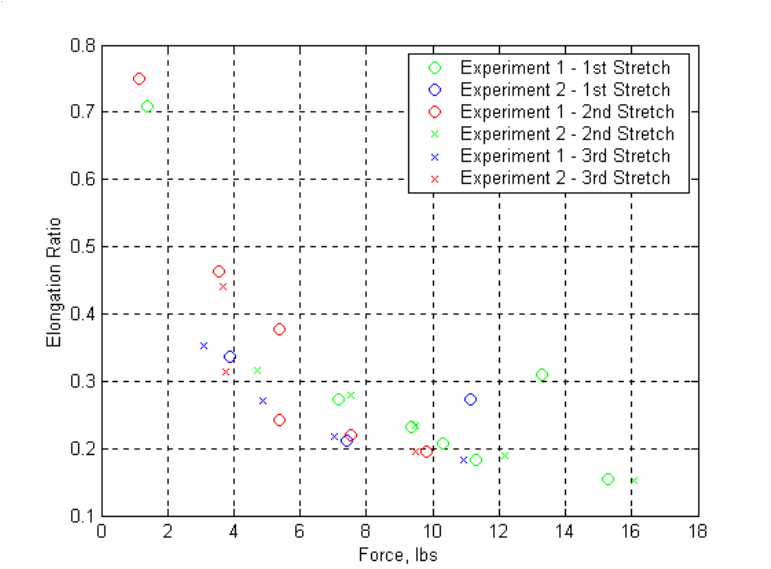


**Figure 4.2-8.** Necking response of Tecoflex® 80A as it is strained.

After determining the lateral and axial strains of the material, the elongation ratio was calculated.

$$\nu = -\frac{\text{lateral strain}}{\text{axial strain}} = \frac{\varepsilon_w}{\varepsilon_l} = \frac{\delta_w / w}{\delta_l / l} \tag{4.2-2}$$

where $\delta_w$ is the elongation of the material in the lateral direction,

$w$ is the original material length in the lateral direction,

$\delta_l$ is the elongation in the axial direction, and

$l$ is the original material length in the axial direction.

After calculating the elongation, a graph was produced, as shown in Figure 4.2-9. Notice the elongation ratio is not constant.

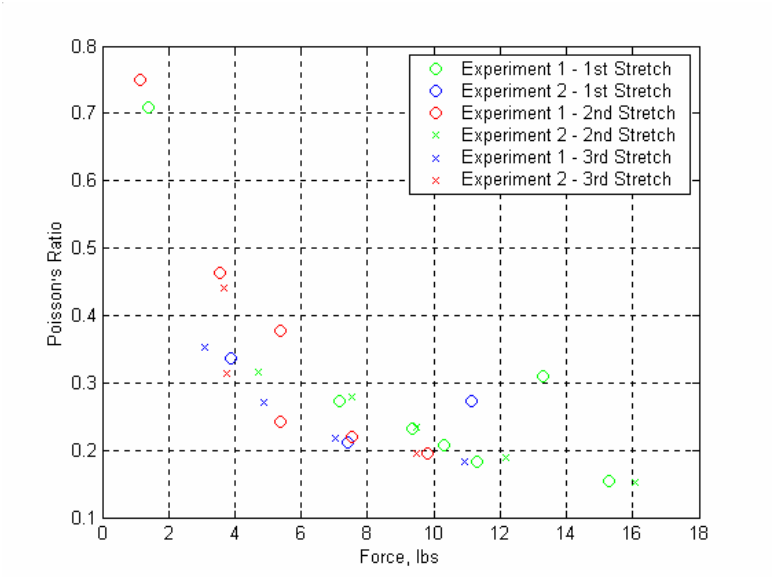


**Figure 4.2-9.** Elongation ratio difference for Tecoflex® 80A.

**Young's Modulus.** To determine the stiffness of Tecoflex® 80A, the Young's modulus was calculated at different strain locations. The following equation was used to calculate the Young's Modulus.

$$E = \frac{\sigma}{\varepsilon} = \frac{F}{A} \times \frac{L}{\delta} \tag{4.2-3}$$

where $F$ is the applied force,

$A$ is the cross-sectional area,

$L$ is the orginal length of the member, and

$\delta$ is the total elongation of the member.

The thickness of Tecoflex® 80A was 4.5 mil thick while the width was 5.25 inches thick. Therefore, the Young's Modulus could be calculated where the results are shown in Table 4.2-1. The necking affects were not taken into account, therefore the original cross-sectional area was held constant.

**Table 4.2-1.** Young's Modulus at different strains for Tecoflex® 80A.

| Strain | 0.213 | 0.592 | 1.046 | 2.118 | 2.513 |
|---|---|---|---|---|---|
| Young's Modulus kpsi (MPa) | 0.156 (1.07) | 0.287 (1.98) | 0.266 (2.01) | 0.202 (1.84) | 0.208 (1.43) |

**Strain and Hold.** Figure 4.2-10 shows how much force is needed to hold the material at a given strain amount. The forces are decreasing since the material is undergoing plastic deformation. During these experiments the material was strained to approximately 200 percent strain.

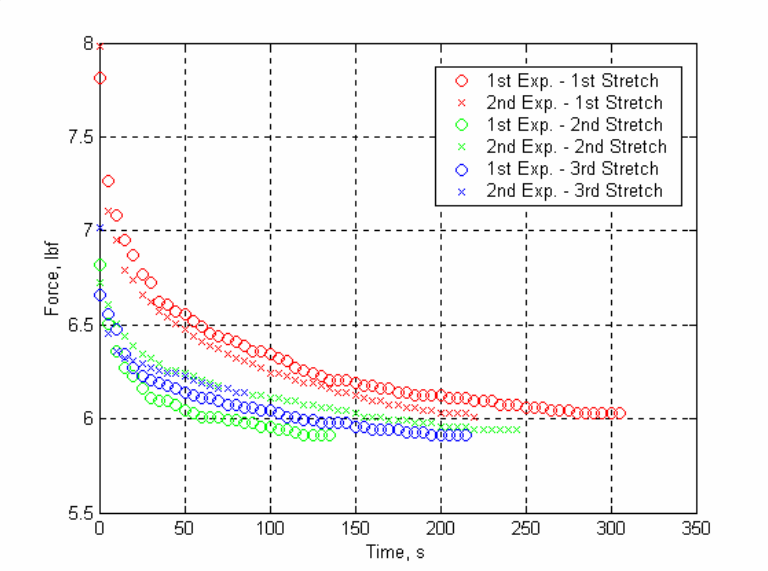


**Figure 4.2-10.** Reduction of force needed to hold Tecoflex® 80A at a given strain.

**Recovery.** The recovery results were conducted by doing the following analysis. The material was first measured before being strained. Once the material was strained, the material was measured again. Finally the material was allowed to recover and then was measured. The tables below have two columns. One column, "Max Strain," is the strained amount the material was deformed. The second column, "Recovery Strain," is the excess strain that is a result of being deformed. This recovery strain is the result of the material undergoing plastic deformation.

The first table presented, Table 4.2-2, shows the recovery results of Tecoflex® 80 A during the force and strain experiment. The gathered data during the force and strain experiment was done by stretching the material to the limits of the string potentiometer.

**Table 4.2-2.** Strain recovery of Tecoflex® 80A during the force and strain experiments.

| Test | Maximum Strain | Recovery Strain |
|---|---|---|
| Experiment 1 – Stretch 1 | 3.076 | 0.101 |
| Experiment 1 – Stretch 2 | 2.651 | 0.157 |
| Experiment 1 – Stretch 3 | 2.510 | 0.182 |
| Experiment 2 – Stretch 1 | 2.957 | 0.125 |
| Experiment 2 – Stretch 2 | 2.548 | 0.150 |
| Experiment 2 – Stretch 3 | 2.423 | 0.175 |

The second table presents the results of the ability for the material to recover when the strain and hold experiment was conducted, as shown in Table 4.2-3. Although the material was not strained to the limits of the string potentiometer or the breaking point of the material, it was important to understand how the material recovered under a different strain situation.

**Table 4.2-3.** Strain recovery of Tecoflex® 80A during the strain and hold experiments.

| Test | Maximum Strain | Recovery Strain |
|---|---|---|
| Experiment 1 – Stretch 1 | 1.994 | 0.050 |
| Experiment 1 – Stretch 2 | 1.988 | 0.050 |
| Experiment 1 – Stretch 3 | 2.000 | 0.050 |
| Experiment 2 – Stretch 1 | 1.994 | 0.044 |
| Experiment 2 – Stretch 2 | 2.000 | 0.068 |
| Experiment 2 – Stretch 3 | 1.988 | 0.068 |

### 4.2.2 Tecoflex® 100A

The data analyses of the uniaxial experiments for Tecoflex® 100A are shown in Appendix E. Figure 4.2-11 shows the force and strain comparison of Tecoflex® 100A. The material broke during both experiments after the last strain was recorded. The results presented in Figure 4.2-11 seemed to be inconclusive since the strain ability is not the same for each experiment. During the first experiment the material was able to strain to 1.44, while during the second experiment the material only strained to 1.20. Since the availability of the material was limited, more testing could not be conducted. Since the material broke during both experiments, the material was strained beyond the yield strength.

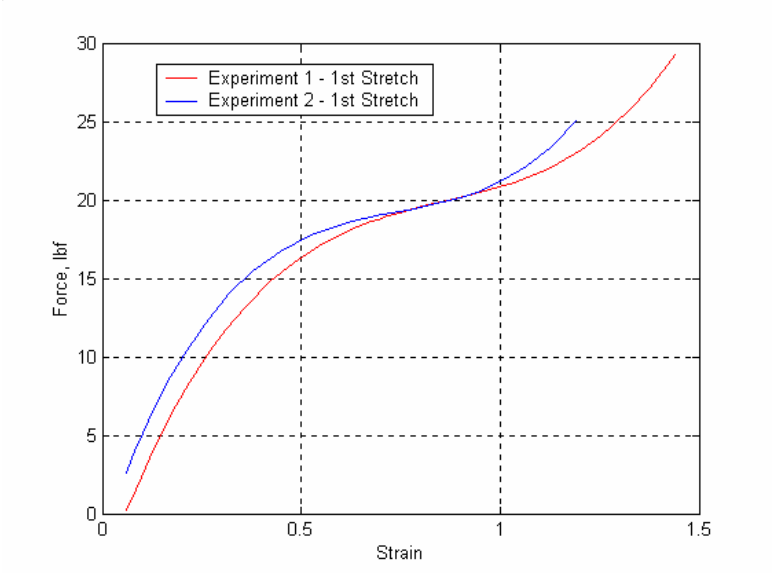


**Figure 4.2-11.** Force versus strain results for Tecoflex® 100A.

Although the results of the force and strain for Tecoflex® 100A are different, the necking characteristics were similar for the uniaxial experiments. The necking of the material seems to have a linear response as it was strained, as shown in Figure 4.2-12.

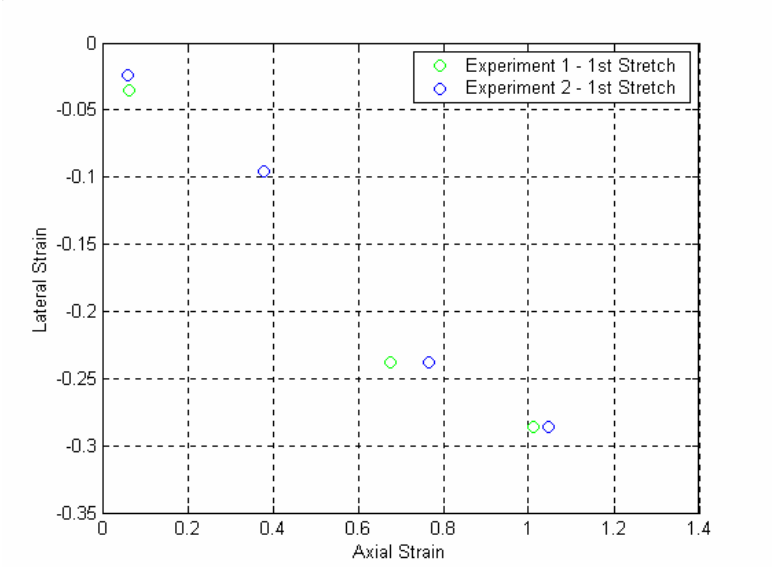


**Figure 4.2-12.** Necking response of Tecoflex® 100A as it is strained.

Once the axial and lateral strains were determined, the elongation ratio was calculated using equation 4.2-2. Figure 4.2-13 shows that the elongation ratio is not constant.

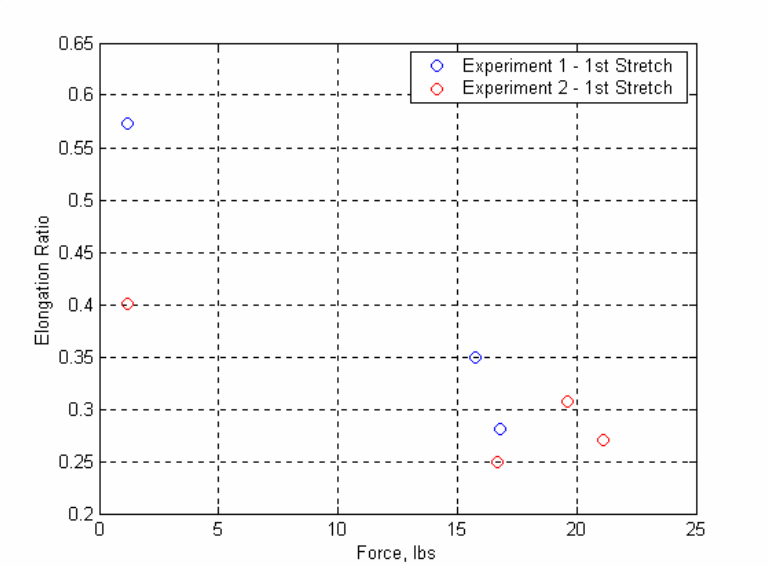


**Figure 4.2-13.** Elongation ratio difference for Tecoflex® 100A.

To determine the stiffness of Tecoflex® 100A, the Young's Modulus was calculated using equation 4.2-3. The thickness of Tecoflex® 100A was 1.5 mil thick while the width was 5.25 inches thick. Therefore, the Young's Modulus was calculated where the results are shown in Table 4.2-4. The necking affects were not taken into account, therefore the original cross-sectional area was held constant. By observing the values of the Young's Modulus, Tecoflex® 100A is a stiffer material when compared to Tecoflex® 80A.

**Table 4.2-4.** Young's Modulus at different strains for Tecoflex® 100A.

| Strain | 0.208 | 0.505 | 1.020 | 1.530 | 2.053 |
|---|---|---|---|---|---|
| Young's Modulus kpsi (MPa) | 2.42 (16.6) | 2.94 (20.2) | 2.25 (15.5) | 1.69 (11.7) | 1.49 (10.3) |

The next analysis conducted was the response of the material once it was strained and held at a stationary location, hence the strain and hold experiment. As the material was held at the strained location, the force decreased over time, as shown in Figure 4.2-14. After the material is stretched the first time, the amount of force needed to hold the material at the strained location decreases. The reason for this phenomenon is because the material had undergone plastic deformation.

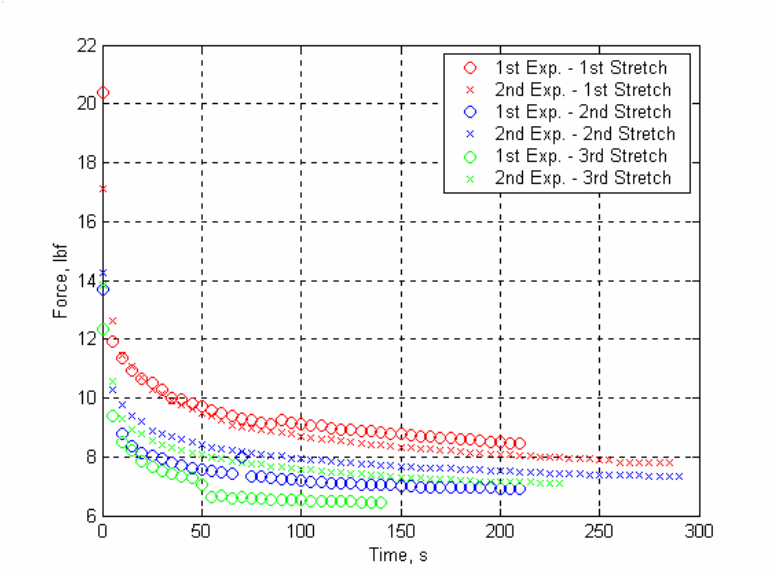


**Figure 4.2-14.** Reduction of force needed to hold Tecoflex® 100A at a given strain.

The final results for Tecoflex® 100A presented for the different uniaxial experiments are the recovery results. As stated before, the material broke during the force and strain experiments. Therefore, extracting the ability for the material to recover was difficult for the force and strain experiments. The way the recovery analysis was done was determining the strain before the material broke and measuring the broken material. The results for the recovery of the material during the force and strain experiments are shown in Table 4.2-5. Since there is an excess of material, plastic deformation occurred.

**Table 4.2-5.** Strain recovery of Tecoflex® 100A during the force and strain experiments.

| Test | Maximum Strain | Recovery Strain |
|---|---|---|
| Experiment 1 – Stretch 1 | 1.443 | 0.122 |
| Experiment 2 – Stretch 1 | 1.195 | 0.106 |

Since Tecoflex® 100A ripped during one of the force and strain experiments when the material was strained to 1.2, it was determined when conducting the strain and hold experiments the material should be strained less. Therefore, it was concluded the material should not be strained more than 0.6 when conducting the strain and hold experiments. Table 4.2-6 shows the recovery results of the material during the strain and hold experiments. The recovery results are different when comparing Tables 4.2-5 and 4.2-6. If the material is strained more, the recovery strain should be greater. This is not the case with this material. But, it could be the fact that the material did break and the recovery was extrapolated by measuring the broken material.

**Table 4.2-6.** Strain recovery of Tecoflex® 100A during the strain and hold experiments.

| Test | Maximum Strain | Recovery Strain |
|---|---|---|
| Experiment 1 – Stretch 1 | 0.548 | 0.155 |
| Experiment 1 – Stretch 2 | 0.480 | 0.167 |
| Experiment 1 – Stretch 3 | 0.480 | 0.167 |
| Experiment 2 – Stretch 1 | 0.571 | 0.132 |
| Experiment 2 – Stretch 2 | 0.576 | 0.118 |
| Experiment 2 – Stretch 3 | 0.581 | 0.118 |

### 4.2.3 Tecoflex® 93A

The results presented here are for the force and strain experiments that were conducted for Tecoflex® 93A. The data analyses of the uniaxial experiments for Tecoflex® 93A are shown in Appendix E. Tecoflex® 93A needed a higher rated force transducer to record the required force for a given strain, as shown in Figure 4.2-15. The required forces needed to strain the material are similar for both experiments. It was determined that the material would be strained no more than 2 since the required force was nearing the limits of the force transducer. Also the material was only stretched one time during each experiment for two reasons. The first reason is the material's width was considerably smaller as it was strain when compared to Tecoflex® 80A and 100A and because of the poor recovery results, these differences will be discussed in later in this report. Although the material recovered poorly, the material was not strained beyond the yield strength point.

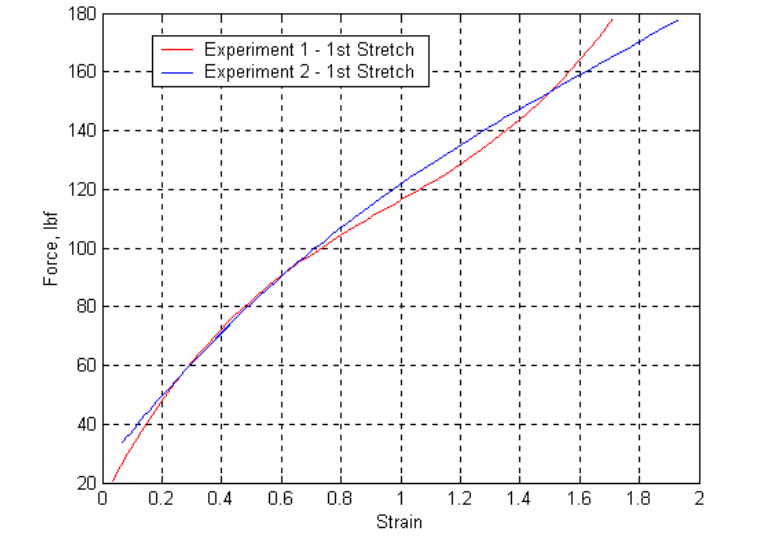


**Figure 4.2-15.** Force versus strain results for Tecoflex® 93A.

When the force and strain experiments were conducted, the width of the material was recorded. Both experiments resulted in similar necking characteristics. As the strain increased, the necking of the material decreased, as shown in Figure 4.2-16. When Tecoflex® 93A necking characteristics were compared to Tecoflex® 80A and 100A, the materials deforms more.

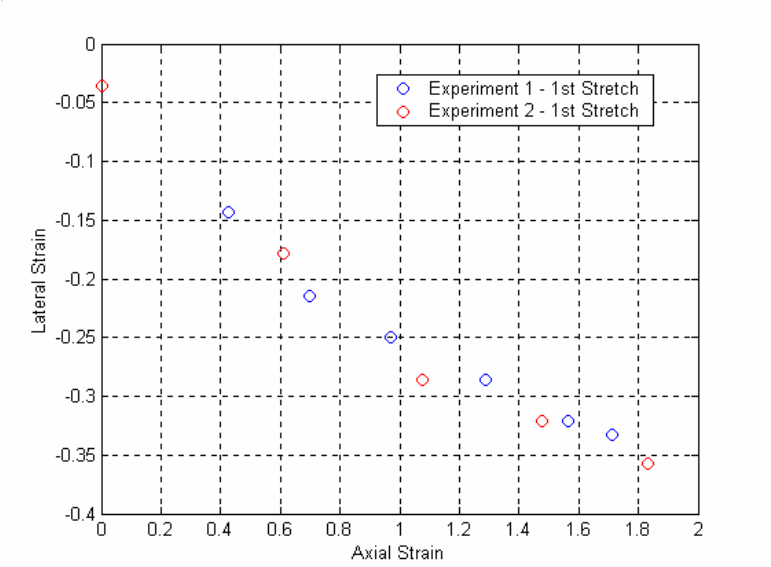


**Figure 4.2-16.** Necking response of Tecoflex® 93A as it is strained.

Once the axial and lateral strains were determined, the elongation ratio was calculated using equation 4.2-2. Figure 4.2-17 shows that the elongation ratio is not constant.

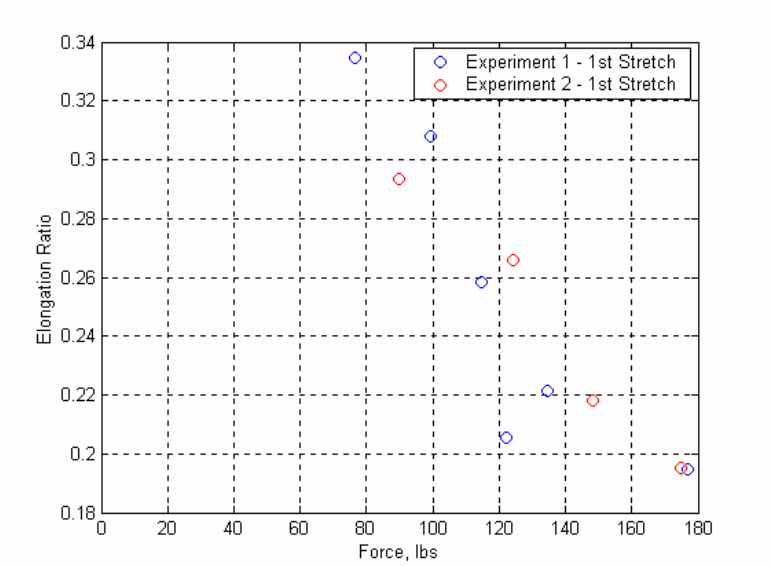


**Figure 4.2-17.** Elongation ratio difference for Tecoflex® 93A.

To determine the stiffness of Tecoflex® 93A, the Young's Modulus was calculated using equation 4.2-3. The thickness of Tecoflex® 93A was 22 mil thick while the width was 5.25 inches thick. Therefore, the Young's Modulus was calculated where the results are shown in Table 4.2-7. The necking affects were not taken into account, therefore the original cross-sectional area was held constant. Initially Tecoflex® 93A seemed to be a stiffer material because of the force requirements needed to strain the material. Since, the material was thicker than Tecoflex® 80A and Tecoflex® 100A the Young's Modulus clearly shows the Tecoflex® 93A is not stiffer than Tecoflex® 100A.

**Table 4.2-7.** Young's Modulus at different strains for Tecoflex® 93A.

| Strain | 0.229 | 0.504 | 1.018 | 1.541 |
|---|---|---|---|---|
| Young's Modulus kpsi (MPa) | 1.96 (13.5) | 1.42 (9.78) | 1.00 (6.88) | 0.88 (6.10) |

The next result presented for Tecoflex® 93A is the force needed to hold the material at a given strain. Since the Tecoflex® 93A materials were limited, this test was conducted with one material. The material was strained to approximately 200 percent strain and the forces required to hold the material were recorded, as shown in Figure 4.2-18. The required forces to hold the material were almost identical when the same material was stretched both times.

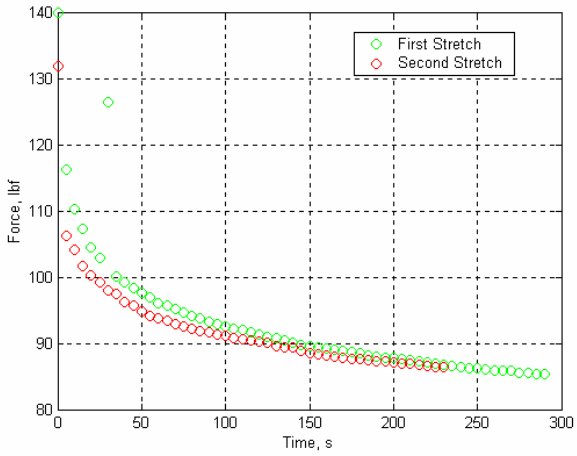


**Figure 4.2-18.** Reduction of force needed to hold Tecoflex® 93A at a given strain.

The final results presented for Tecoflex® 93A are the recovery results. Even though the maximum strain is similar to the maximum strains for Tecoflex® 80A and 100A, the recover strain is greater, as shown in Table 4.2-8. This excess material would not work well as a skin for

a morphing wing since it could cause additional drag. Since there is excess material, plastic deformation occurred.

**Table 4.2-8.** Strain recovery of Tecoflex 93A during the force and strain experiments.

| Test | Maximum Strain | Recovery Strain |
|---|---|---|
| Experiment 1 – Stretch 1 | 1.710 | 0.185 |
| Experiment 2 – Stretch 1 | 1.935 | 0.235 |

When conducting the strain and hold experiments the material was strain to approximately 1. One good characteristic of this material was the recovery strains were the same during both tests, as shown in Table 4.2-9.

**Table 4.2-9.** Strain recovery of Tecoflex 93A during the strain and hold experiments.

| Test | Maximum Strain | Recovery Strain |
|---|---|---|
| Experiment 1 – Stretch 1 | 0.927 | 0.073 |
| Experiment 2 – Stretch 1 | 1.012 | 0.073 |

### 4.2.4 Riteflex® 640

The results presented here are for the force and strain experiments that were conducted for Riteflex® 640, which is a product of Ticona. The data analysis of the uniaxial experiment for this material is shown in Appendix E. Figure 4.2-19 shows the both the force and strain results as well as the necking results of the material. This particular material ripped after it was strain to 2.20. The necking characteristics are similar to the Tecoflex® materials that were tested. Although additional test were needed, the availability of this material was very limited. Since the material failed after being strained to 2.20, the material was strained beyond the yield strength point.

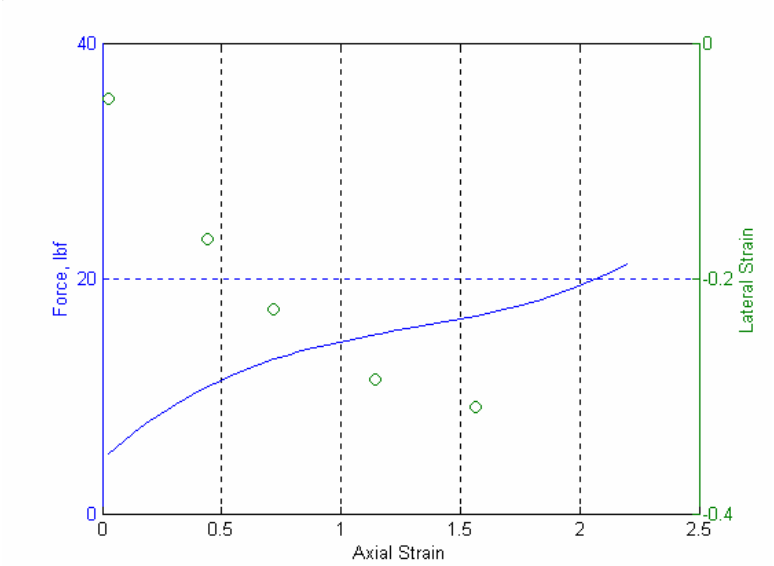


**Figure 4.2-19.** Force versus strain results for Riteflex® 640 are shown in blue. The green circles are the necking characteristics of Riteflex® 640.

Once the axial and lateral strains were determined, the elongation ratio could be calculated using equation 4.2-2. Figure 4.20 shows that the elongation ratio is not constant.

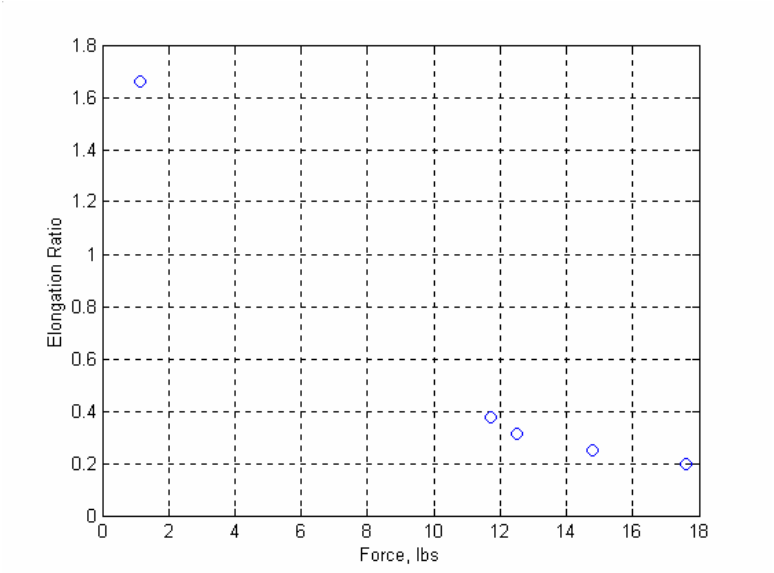


**Figure 4.2-20.** Elongation ratio difference for Riteflex® 640.

To determine the stiffness of Riteflex® 640, the Young's Modulus was calculated using equation 4.2-3. The thickness of Riteflex® 640 was 1.4 mil thick while the width was 5.25 inches

thick. Therefore, the Young's Modulus was calculated where the results are shown in Table 4.2-10. The necking affects were not taken into account, therefore the original cross-sectional area was held constant. The Young's Modulus results of Riteflex® 640 presented show that it is a stiffer material when compared to the Tecoflex® materials.

**Table 4.2-10.** Young's Modulus at different strains for Riteflex® 640A.

| Strain | 0.222 | 0.519 | 1.002 | 1.537 | 2.066 |
|---|---|---|---|---|---|
| Young's Modulus kpsi (MPa) | 5.04 (35.8) | 3.05 (21.0) | 2.00 (13.7) | 1.49 (10.3) | 1.33 (9.20) |

The next experiment strained the material and recorded the amount of force that was required to hold the material. Since the material underwent plastic deformation, the amount of force needed to hold the material at a given strain decreased. Figure 4.2-21 shows the force decreasing as the four separate tests were completed with the same material. For each stretch experiment, the material was strained to approximately 100 percent strain.

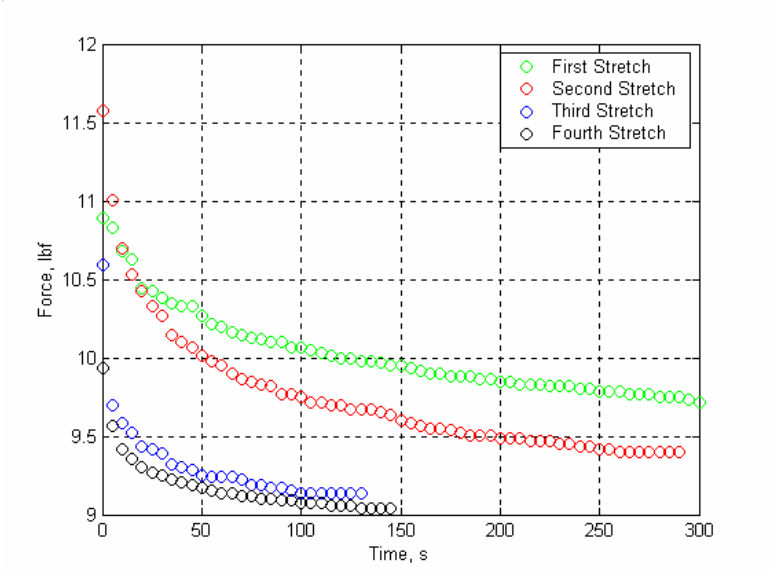


**Figure 4.2-21.** Reduction of force needed to hold Riteflex® 640 at a given strain.

As stated before, the experiment where the force and strain comparison were conducted the material broke**.** Therefore, extracting the ability for the material to recover was difficult for the force and strain experiment. The way the recovery analysis was done was determining the strain before the material broke and measuring the broken material. The results for the recovery of the material during the force and strain experiments are shown in Table 4.2-11. Since the recovery strain was poor, plastic deformation has occurred.

**Table 4.2-11.** Strain recovery of Riteflex® 640 during the force and strain experiments.

| Test | Maximum Strain | Recovery Strain |
|---|---|---|
| Experiment 1 – Stretch 1 | 2.202 | 0.788 |

When conducting the strain and hold experiments the material was strain to approximately 1. One good characteristic of this material was the recovery strains relatively the same, as shown in Table 4.2-12.

**Table 4.2-12.** Strain recovery of Riteflex® 640 during the strain and hold experiments.

| Test | Maximum Strain | Recovery Strain |
|---|---|---|
| Experiment 1 – Stretch 1 | 0.975 | 0.350 |
| Experiment 1 – Stretch 2 | 1.000 | 0.363 |
| Experiment 1 – Stretch 3 | 1.000 | 0.388 |
| Experiment 1 – Stretch 4 | 1.000 | 0.410 |

### 4.2.5 Riteflex® 663

The results presented here is for the force and strain experiment that were conducted for Riteflex® 663, which is another product of Ticona. The data analysis of the uniaxial experiment for Riteflex® 663 is shown in Appendix E. Since the quantity of this material was limited only one test was performed for each experiment. Te required forces necessary to strain Riteflex® 663 were similar to Tecoflex® 80A and 100A. But, the amount the material could strain before failing was only 1.28, as shown in Figure 4.2-22. Since the material failed while being strained beyond 1.28, the material was strained beyond the yield strength point.

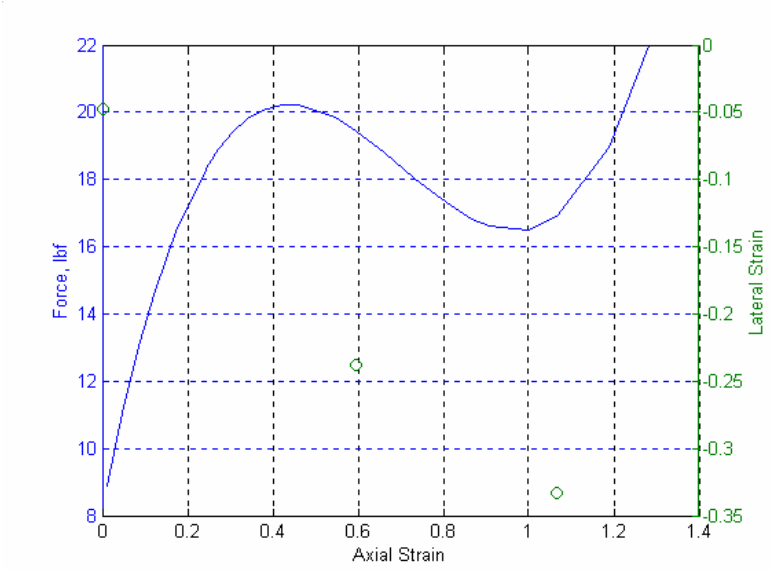


**Figure 4.2-22.** Results of the force and strain experiment for Riteflex® 663 are shown in blue. The green circles are the necking characteristics of Riteflex® 663.

Using the results from Figure 4.2-22, specifically the axial and lateral strain results, the elongation ratio was calculated using equation 4.2-2. As shown in Figure 4.2-23, the elongation ratio was not constant.

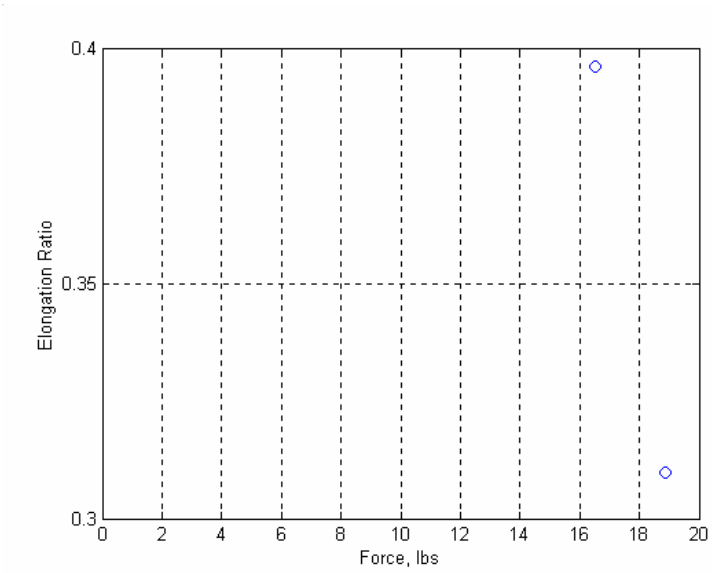


**Figure 4.2-23.** Elongation ratio difference for Riteflex® 663.

To determine the stiffness of Riteflex® 663, the Young's Modulus was calculated using equation 4.2-3. The thickness of Riteflex® 663 was 1.4 mil thick while the width was 5.25 inches

thick. Therefore, the Young's Modulus was calculated where the results are shown in Table 4.2-13. The necking affects were not taken into account, therefore the original cross-sectional area was held constant. Riteflex® 663 is a stiffer material when compared to Riteflex® 640 and the Riteflex® material that were tested.

**Table 4.2-13.** Young's Modulus at different strains for Riteflex® 663A.

| Strain | 0.238 | 0.536 | 1.048 |
|---|---|---|---|
| Young's Modulus kpsi (MPa) | 11.2 (77.1) | 4.14 (28.5) | 2.36 (16.3) |

The next result presented for Riteflex® 663 is for the strain and hold experiment. The material was strained to approximately half of the breaking strain. Since the material ripped when it was strained to 1.28, for this experiment the material was strained to 60 percent strain. Figure 4.2-24 shows that as time went on, the material needed less force to hold the material at the given strain. Although additional test were needed, there was a limited quantity of this particular material. Also, since Riteflex® 663 recovered poorly due to the straining of the material, additional strain and hold test were not conducted for the material, which will be discussed below.

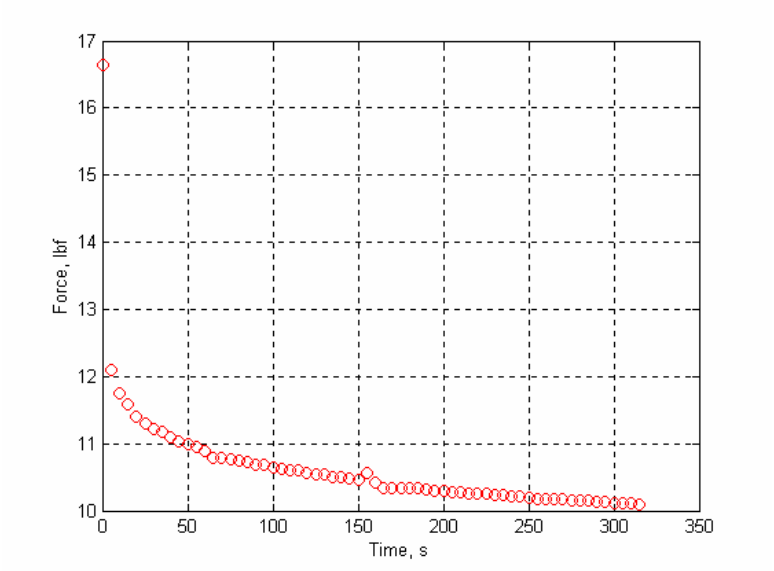


**Figure 4.2-24.** Reduction of force needed to hold Riteflex® 663 at a given strain.

As stated before, the experiment where the force and strain comparison were conducted the material broke. Therefore, extracting the ability for the material to recover was difficult. The way the recovery analysis was conducted was determining the strain before the material broke

and measuring the broken material. The result for the recovery of the material during the force and strain experiment is shown in Table 4.2-14.

**Table 4.2-14.** Strain recovery of Riteflex® 663 during the force and strain experiment.

| Test | Maximum Strain | Recovery Strain |
|---|---|---|
| Experiment 1 – Stretch 1 | 1.283 | 0.950 |

When conducting the strain and hold experiment the material was strain to approximately 0.6. The recoverability of this material was poor, therefore the experiment was only conducted once. The recovery result for the strain and hold test is presented in Table 4.1-15.

**Table 4.2-15.** Strain recovery of Riteflex® 640 during the strain and hold experiment.

| Test | Maximum Strain | Recovery Strain |
|---|---|---|
| Experiment 1 – Stretch 1 | 0.613 | 0.213 |

### 4.2.6 Arnitel®

The results presented here is for the force and strain experiment that were conducted for Arnitel®. The data analyses of the uniaxial experiment for Arnitel are shown in Appendix E. The material was only stretched once, since the material broke both times during each test. The results are inconclusive because the material did not break at the same strain. Figure 4.2-25 shows the results of the required forces needed to strain the material. The initial strain results are similar when the material is strained to 0.8, but the material responded differently beyond being strained 0.8. Since the material failed while being strained, it was strained beyond the yield strength point.

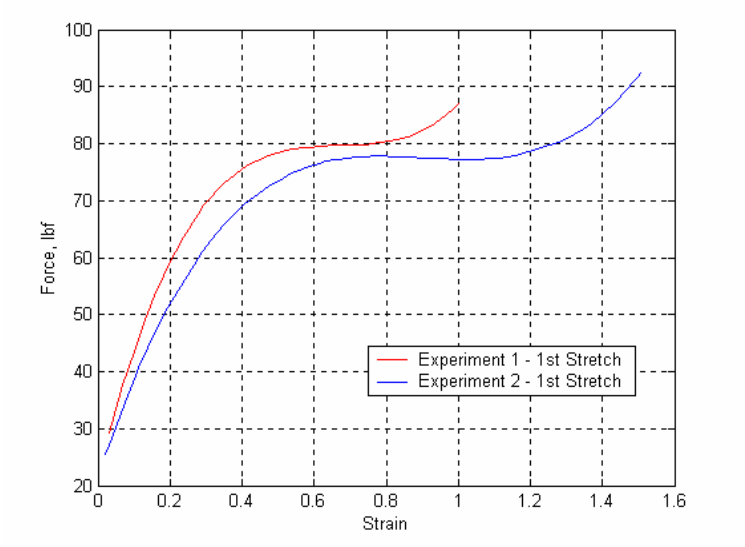


**Figure 4.2-25.** Force versus strain results for Arnitel®.

Although the force and strain comparison did not correlate well, the necking characteristics did for Arnitel®. The measured strains used to determine the elongation ratio for both experiments seemed to follow the same pattern, as shown in Figure 4.2-26.

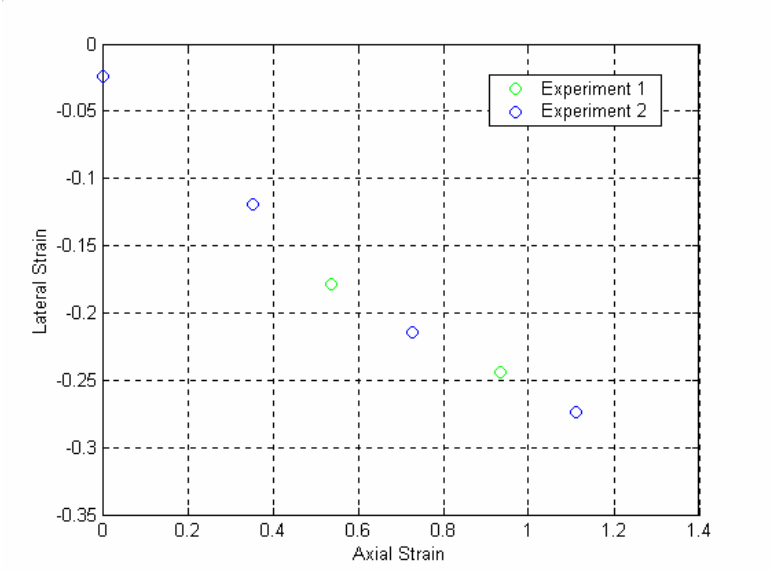


**Figure 4.2-26.** Necking response of Arnitel® as it is strained.

Once the axial and lateral strains were determined, the elongation ratio was calculated using equation 4.2-1. Figure 4.2-27 shows that the elongation ratio was not constant for each of the experiments.

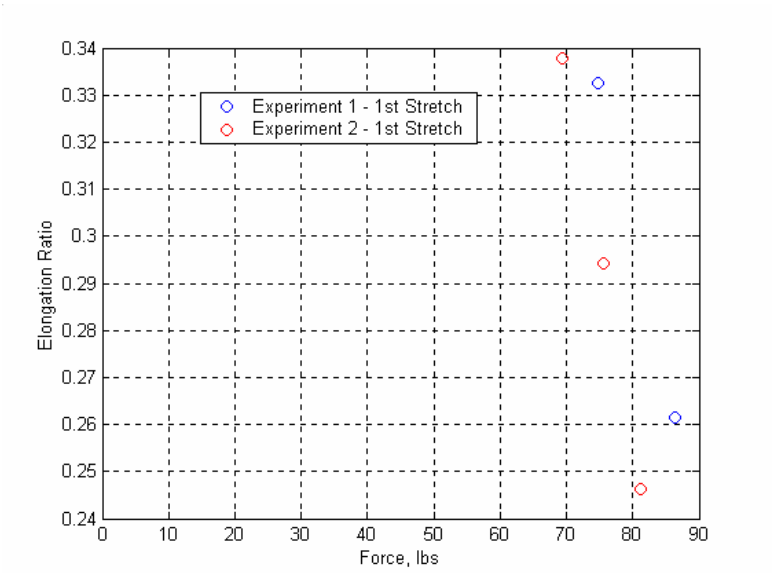


**Figure 4.2-27.** Elongation ratio difference for Arnitel®.

To determine the stiffness of Arnitel®, the Young's Modulus was calculated using equation 4.2-3. The thickness of Arnitel® was 15 mil thick while the width was 5.25 inches thick. Therefore, the Young's Modulus was calculated where the results are shown in Table 4.2-16. The necking affects were not taken into account, therefore the original cross-sectional area was held constant. The calculated Young's Modulus of Arnitel® produced similar results when compared to Tecoflex ® 93A.

**Table 4.2-16.** Young's Modulus at different strains for Arnitel®.

| Strain | 0.237 | 0.523 | 1.00 |
|---|---|---|---|
| Young's Modulus kpsi (MPa) | 3.41 (23.5) | 1.91 (13.2) | 1.10 (7.61) |

The final uniaxial test conducted was the strain and hold experiment. Since the material ripped the force and strain experiment was conducted, it was determined to strain the material to approximately 100 percent strain. Once the material was strained, the required forces to hold the material at that particular strained location were measured, as shown in Figure 4.2-28. If the same material was strained again, it took less force to hold the material.

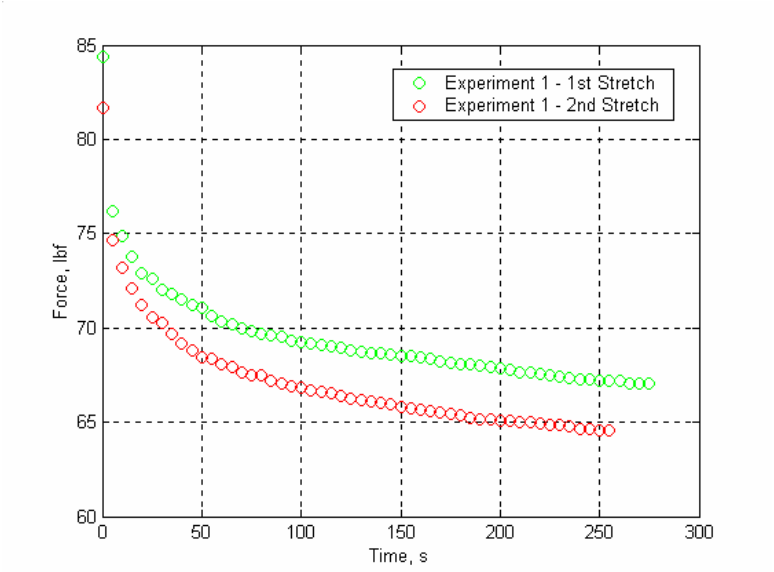


**Figure 4.2-28.** Reduction of force needed to hold Arnitel® at a given strain.

Next, the recovery results were analyzed for both the strain and force experiments and the strain and hold comparison. Table 4.2-17 shows the recovery results for the force and strain experiments. As a reminder, the material ripped while conducting the experiments. Therefore, extracting the ability for the material to recover was difficult. The way the recovery results were conducted was determining the strain before the material broke and measuring the broken material. Since the material could not recover, the material underwent plastic deformation.

**Table 4.2-17.** Strain recovery of Arnitel® during the force and strain experiment.

| Test | Maximum Strain | Recovery Strain |
|---|---|---|
| Experiment 1 – Stretch 1 | 1.005 | 0.342 |
| Experiment 2 – Stretch 1 | 1.511 | 0.439 |

The final recovery results are for the strain and hold experiments. The same material was strained again and by observing Table 4.2-18, even though the material was strained slightly less than the first stretch, the material did not recover as much. The reason is the material underwent plastic deformation.

**Table 4.2-18.** Strain recovery of Arnitel® during the strain and hold experiments.

| Test | Maximum Strain | Recovery Strain |
|---|---|---|
| Experiment 1 – Stretch 1 | 1.243 | 0.356 |
| Experiment 1 – Stretch 2 | 1.193 | 0.429 |

### 4.2.7 Shape Memory Polymer

Figure 4.2-29 shows the results of the amount of force needed to strain the shape memory polymer. The maximum strain the material was able to attain before breaking was 2, which needed a force of 11.09 pounds. Since the material failed while being strained, the experiment strained the material beyond the yield strength point. This material was exposed to a constant temperature of 105 degrees Celsius during this experiment. According to the product engineer at Cornerstone Research Group, the material would not be able to be strained beyond 2, therefore these results match. It is important to not that the temperature was measured at one location of the shape memory polymer. Although the temperature was kept constant during the experiment, there might be a temperature gradient along the material.

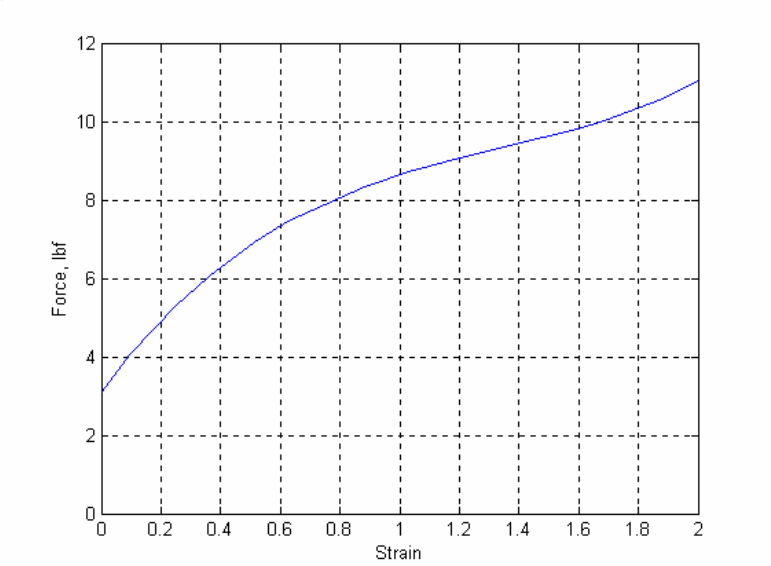


**Figure 4.2-29.** Force versus strain results for the shape memory polymer at 105 degrees Celsius.

Another important result of the material characteristic of the shape memory polymer was the necking. Figure 4.2-30 shows the necking response as the material was strained.

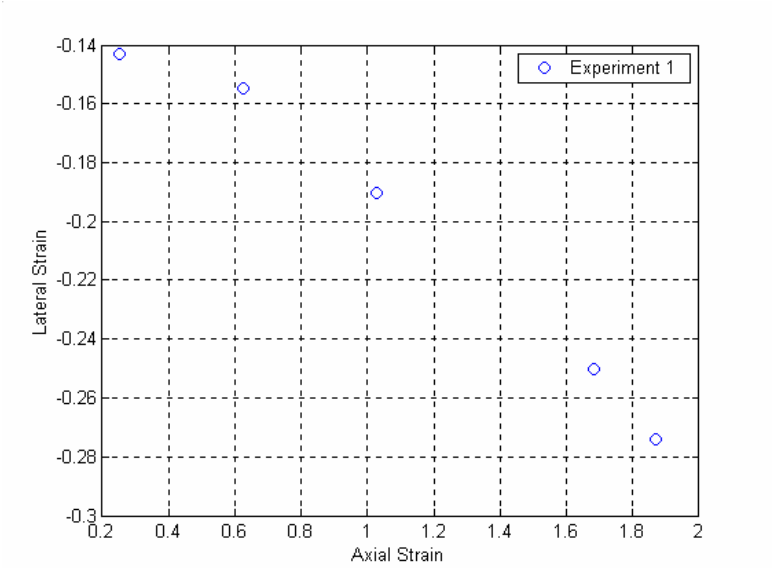


**Figure 4.2-30.** Necking response of the shape memory polymer as it is strained.

Using the experimental results from the necking results, the elongation ratio was calculated using equation 4.2-2. The results show that the elongation ratio is not constant, as shown in Figure 4.2-31.

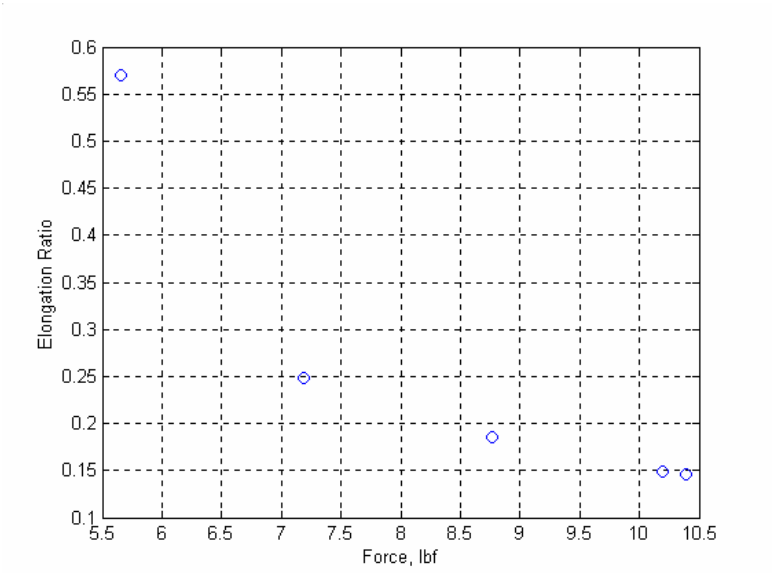


**Figure 4.2-31.** Elongation ratio difference for the shape memory polymer.

To determine the stiffness of the shape memory polymer, the Young's Modulus was calculated using equation 4.2-3. The thickness of the shape memory polymer was 100 mil thick while the width was 5.25 inches thick. Therefore, the Young's Modulus was calculated where the

results are shown in Table 4.2-19. The necking affects were not taken into account, therefore the original cross-sectional area was held constant. The shape memory polymer was the least stiff material while it was heated. The calculation of the Young's Modulus when the shape memory was below the glass transition temperature was not conducted, since the shape memory polymer needed to be heated above the glass transition temperature to be strained.

**Table 4.2-19.** Young's Modulus at different strains for the shape memory polymer (105 degrees Celsius).

| Strain | 0.250 | 0.512 | 1.029 | 1.595 | 2.001 |
|---|---|---|---|---|---|
| Young's Modulus psi (MPa) | 43.1 (0.30) | 24.6 (0.17) | 16.5 (0.11) | 11.8 (0.08) | 10.6 (0.07) |

The final test conducted using the uniaxial test stand for the SMP was the strain hold experiment. Figure 4.2-32 shows the results of the strain and hold test. The material was heated to a constant temperature of 106 degrees Celsius so the material would become viable to strain. The shape memory polymer was strained to 1.04 and the forces were recorded. Once the forces decreased to a plateau while still in the heated environment, the material was exposed to ambient air temperature of 60 degrees Celsius, allowing the material to become rigid again. As a reminder, the glass transition temperature is 85 degrees Celsius. Although the temperature was held constant, the temperature of the material was only measured at one location. Therefore the temperature of the material might be different at other locations. Again, the required forces to hold the material at the given strain decreased. At around 140 seconds, the necessary forces start increasing again. The reason for this phenomenon is the material is trying to recover to its original shape. The shape memory polymer then hardens, becoming a rigid body. The "Line Tension" line is force that was measured from the sensor even though the material was deformed and not moving. The winch was relaxed, where the measured force from the force transducer was 0. Yet, the material was still in the strained position, since the shape memory polymer was a rigid body.

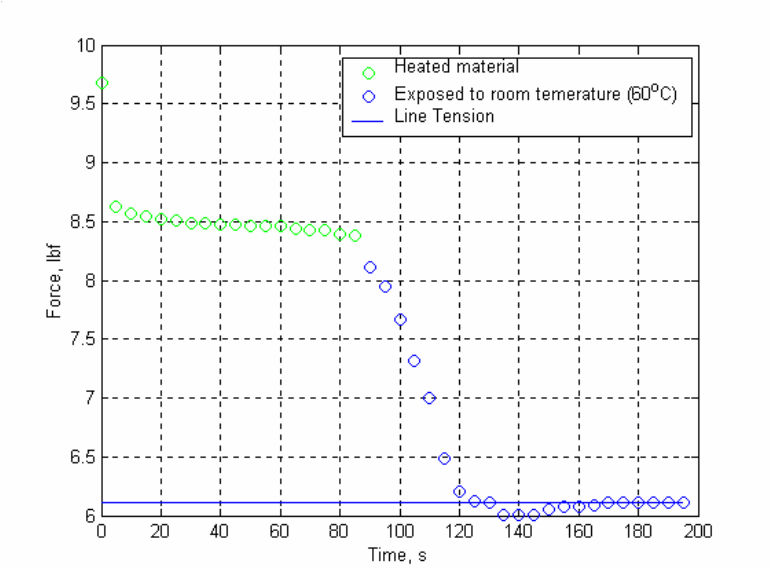


**Figure 4.2-32.** Reduction of force needed to hold the shape memory polymer at a given strain (106 degrees Celsius).

The following two tables present the results of the recovery ability of the shape memory polymer. During the force and strain experiment, the material broke, yet, the material did recover. Even thought the material broke, the material clearly recovered. Table 4.2-20 shows the recovery result of the force and strain experiment.

**Table 4.2-20.** Strain recovery of the shape memory polymer during the force and strain experiment.

| Test | Maximum Strain | Recovery Strain |
|---|---|---|
| Experiment 1 – Stretch 1 | 2.00 | 0.167 |

Since the material broke beyond a strain of 2 for the force and strain experiment, during the strain and hold experiment the material was strained to approximately 100 percent strain. When the material was allowed to recover, the shape memory polymer almost recovered to its original length. This result is shown in Table 4.2-21.

**Table 4.2-21.** Strain recovery of the shape memory polymer during the strain and hold experiments.

| Test | Maximum Strain | Recovery Strain |
|---|---|---|
| Experiment 1 – Stretch 1 | 1.040 | 0.043 |

### 4.2.8. Spandura®

One advantage of using a woven material is it did not break. On the other hand, when the material was deformed one could clearly see air could pass through the weaves of the yarns. Also the ability for material to recover was not as good as Tecoflex® 80A, Tecoflex® 100A, and the shape memory polymer. The data analyses of the uniaxial experiment for Spandura® are shown in Appendix E.

During the force and strain comparison, a piece of Spandura® material was tested twice. Figure 4.2-33 shows the results of the force that is needed to strain the material. The reason the strain is different for the second stretch case is during the first stretch case the yarns deformed. Yet the material was not strained beyond the yield strength point. The reason the experiments were at the rated limits of the force transducer. Notice, the force needed to strain the material is greater when compared to Tecoflex® 80A and 100A, Riteflex® 640 and 663, as well as the shape memory polymer.

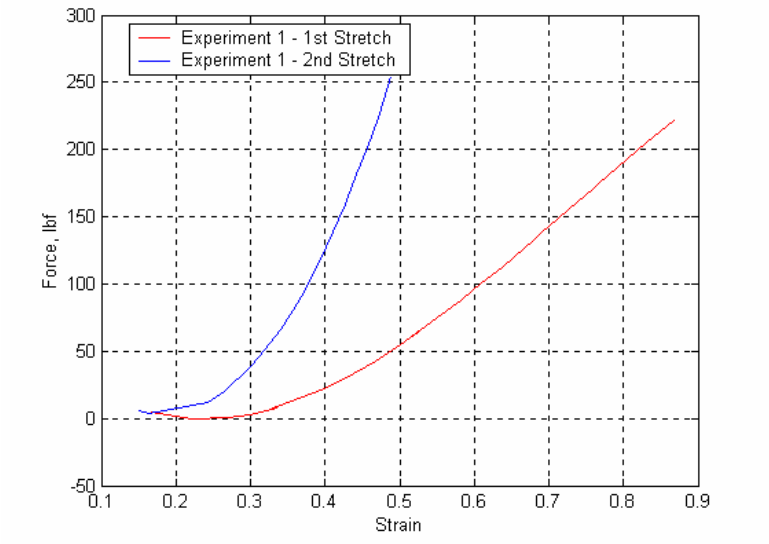


**Figure 4.2-33.** Force versus strain results for Spandura®.

One advantage of Spandura® is the necking effects relatively does not change, as shown in Figure 4.2-34. The reason for this phenomenon is the way the yarns are woven.

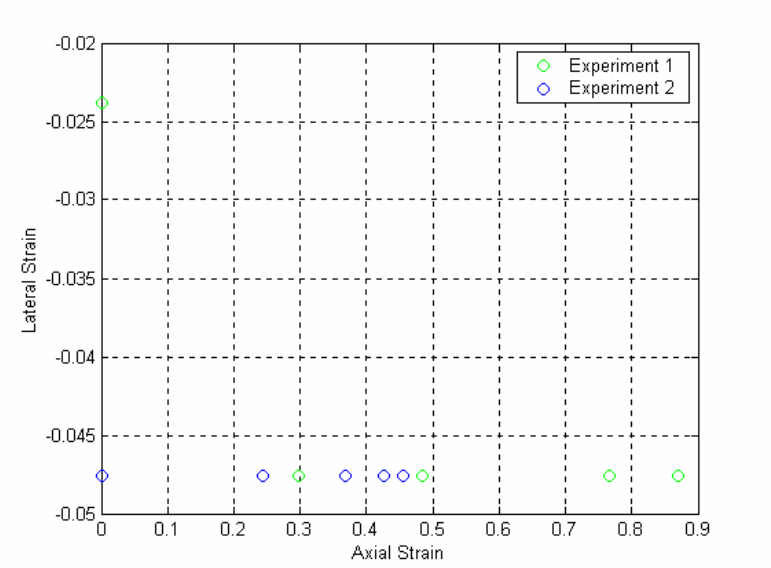


**Figure 4.2-34.** Necking response of Spandura® as it is strained.

Once the axial and lateral strains were determined, the elongation ratio could be calculated from the experimental strain results. Figure 4.2-35 shows that the elongation ratio is not constant.

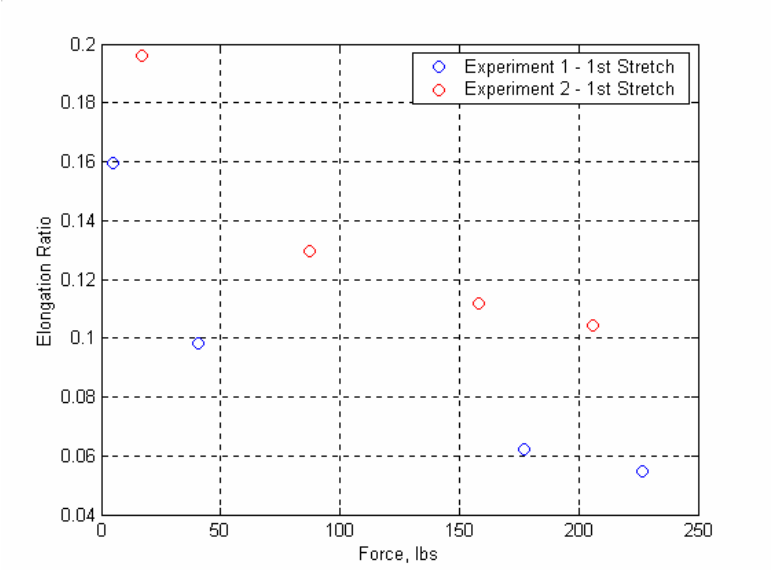


**Figure 4.2-35.** Elongation ratio difference for Spandura®.

To determine the stiffness of Spandura®, the Young's Modulus was calculated using equation 4.2-3. The thickness of Spandura® was 14 mil thick while the width was 5.25 inches thick. Therefore, the Young's Modulus was calculated where the results are shown in Table 4.2-

22. The necking affects were not taken into account, therefore the original cross-sectional area was held constant. As Spandura® was strained more the stiffness of the material increased. The stiffness of Spandura® exhibited similar Young's Modulus values as the straining of the material increased.

**Table 4.2-22.** Young's Modulus at different strains for Spandura®.

| Strain | 0.220 | 0.525 | 0.870 |
|---|---|---|---|
| Young's Modulus kpsi (MPa) | 0.03 (0.23) | 1.66 (11.5) | 3.48 (24.0) |

Next, the strain and hold results are presented in Figure 4.2-36. When the material was strained to approximately 80 percent strain, it took a considerable amount of force to strain the material. But, when the material was strained again to the same location, it needed less force. The reason this occurred is the yards are made out of polyurethane, which deformed when the material was initially strained.

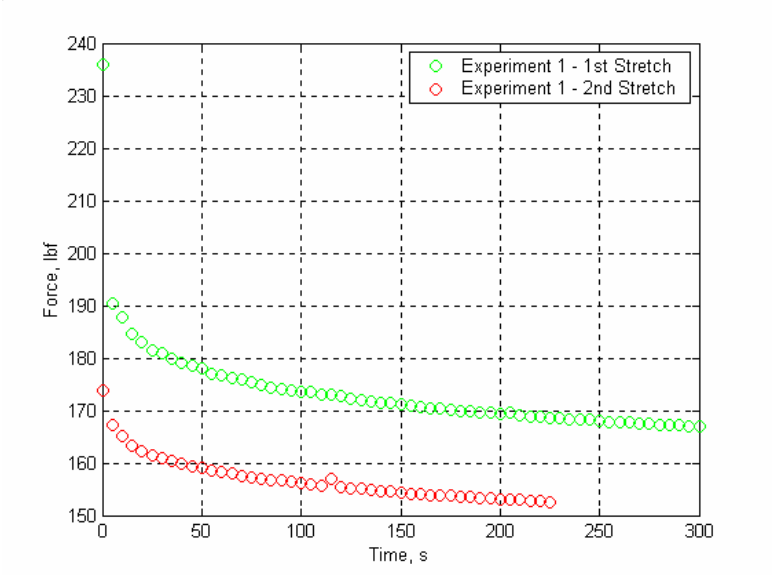


**Figure 4.2-36.** Reduction of force needed to hold Spandura® at a given strain.

The final results presented for the uniaxial testing of Spandura® is the ability for it to recover. During the second force and strain stretch test, the maximum strain was measured from where the material recovered, therefore the maximum strain for the second stretch is less than the first stretch. Since the material did not recover, it underwent plastic deformation. The results for the recovery of Spandura® for the force and strain comparison are shown in Table 4.2-23.

**Table 4.2-23.** Strain recovery of Spandura® during the force and strain experiments.

| Test | Maximum Strain | Recovery Strain |
|---|---|---|
| Experiment 1 – Stretch 1 | 0.870 | 0.342 |
| Experiment 1 – Stretch 2 | 0.489 | 0.341 |

The recovery results for the strain and hold experiments are shown in Table 4.2-24. Although the material was strained the same amount, the recovery strain was greater during the second stretch test. The reason for the increase in the recovery strain is the yards deformed.

**Table 4.2-24.** Strain recovery of Spandura® during the strain and hold experiments.

| Test | Maximum Strain | Recovery Strain |
|---|---|---|
| Experiment 1 – Stretch 1 | 0.781 | 0.244 |
| Experiment 1 – Stretch 2 | 0.781 | 0.293 |

### 4.2.9 Tru-Stretch®

The final woven material that was tested was Tru-Stretch®. As a reminder, the yarns in Tru-Stretch were not woven uniformly. Therefore, the material performed differently depending on how the material was deformed. The easiest way to differentiate how the material is woven is either "stiffly woven" or "lightly woven."

The first step that was completed was analyzing the data of the uniaxial experiments for Tru-Stretch®, which is shown in Appendix E. Figure 4.2-37 shows the strain and force response of the stiffly woven Tru-Stretch®. During the experiments for Tru-Stretch® the material was not strained beyond the yield strength point. The reason is the amount of force needed to strain the material was at the limits of the force transducer, which was rated for 250 lb.

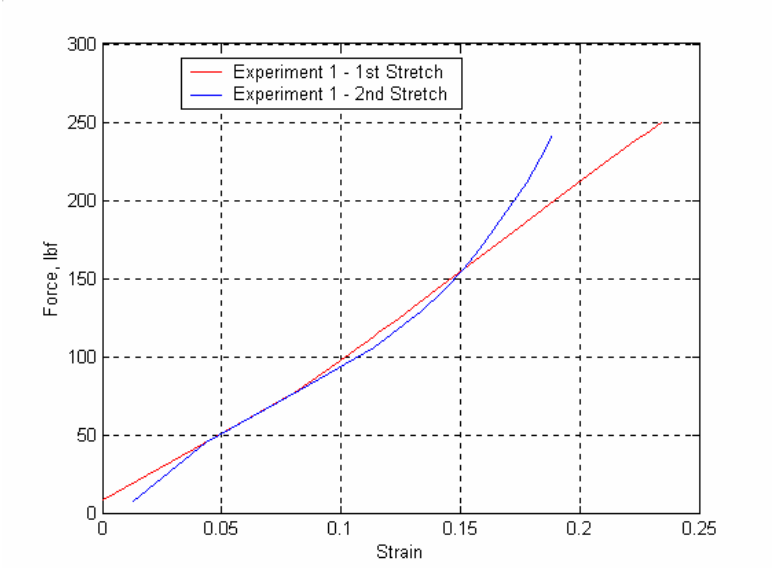


**Figure 4.2-37.** Force versus strain results for True-Stretch® (stiffly woven).

On the other hand when the lightly woven Tru-Stretch® material was deformed, it was allowed to stretch more. The force and strain results are shown in Figure 4.2-38. The reason the strain is different for the second stretch case is during the first stretch case the yarns deformed, since the yarns are made out of polyurethane. The responses of the force and strain results for the lightly woven Tru-Stretch® material are similar to Spandura®.

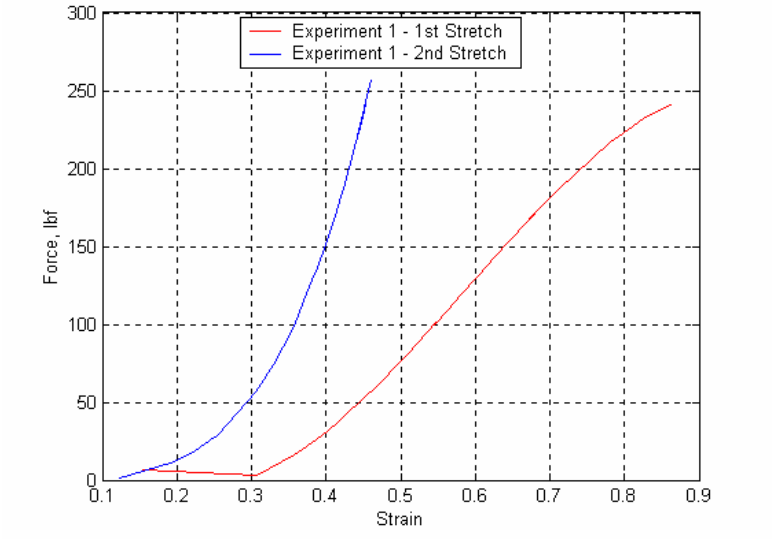


**Figure 4.2-38.** Force versus strain results for True-Stretch® (lightly woven).

The necking characteristics were the same for both the stiffly and the lightly woven Tru-Stretch® material, as shown in Figure 4.2-39and 4.2-40. Tru-Stretch is woven in such a manner that the lateral strain was 0, hence the material did not undergo necking effects. This characteristic is also similar to Spandura®.

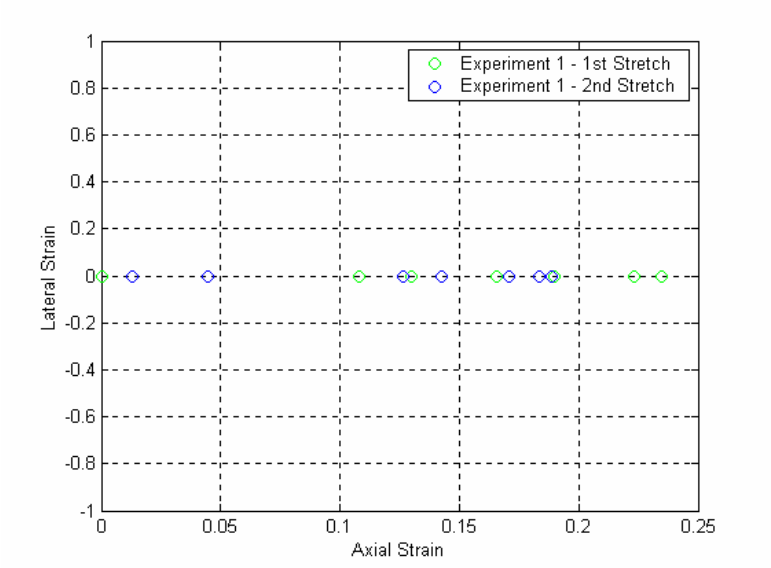


**Figure 4.2-39.** Necking response of Tru-Stretch® (Stiffly woven) as it is strained.

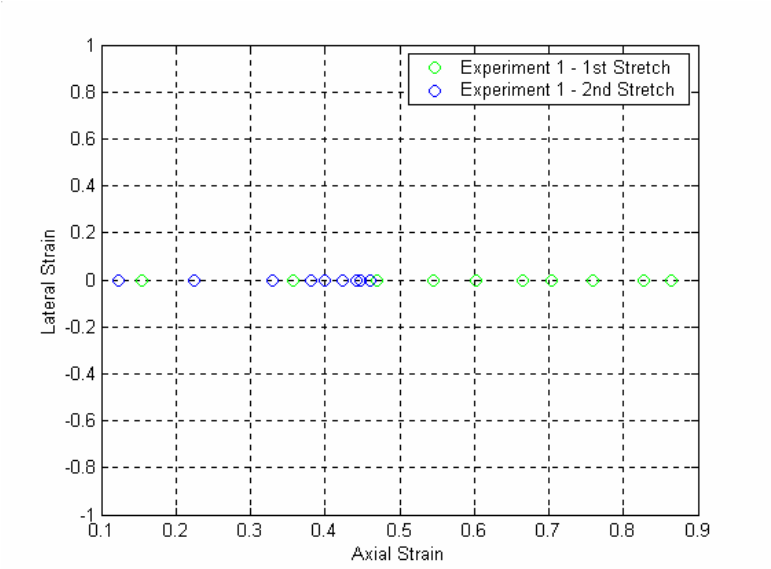


**Figure 4.2-40.** Necking response of Tru-Stretch® (lightly woven) as it is strained.

Once the axial and lateral strains were determined, the elongation ratio could be calculated using equation 4.2-4. Figures 4.2-41 and 4.2-42 show the elongation ratio for the

stiffly and lightly woven Tru-Stretch®, respectively. Since the lateral strains did not change, the elongation ratio should be 0 because the lateral strains were 0.

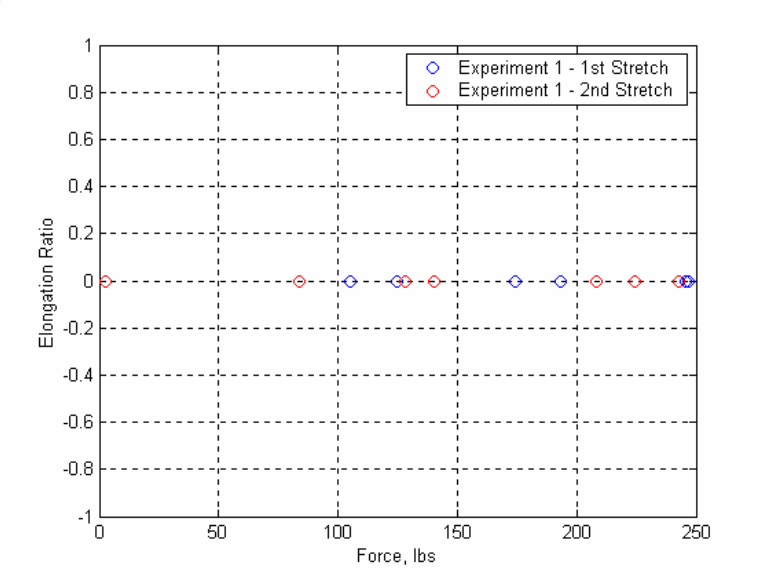


**Figure 4.2-41.** Elongation ratio comparison for Tru-Stretch® (Stiffly woven).

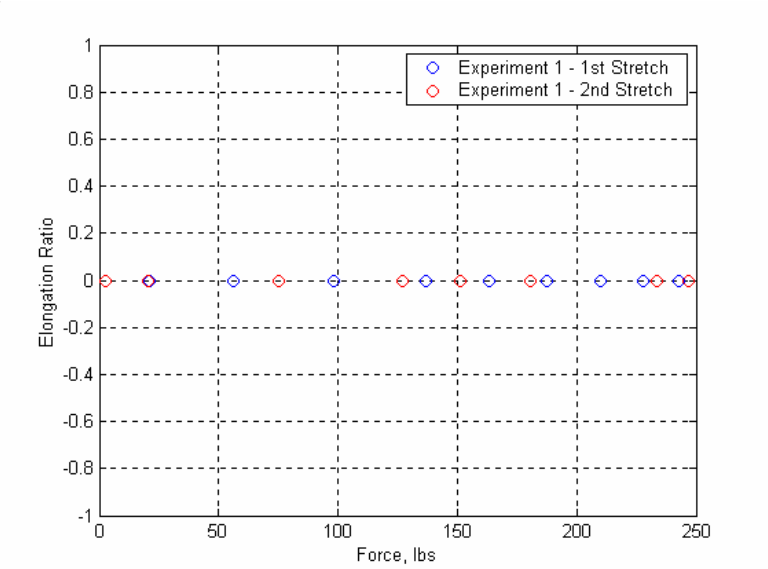


**Figure 4.2-42.** Elongation ratio comparison for Tru-Stretch® (Lightly woven).

To determine the stiffness of Tru-Stretch®, the Young's Modulus was calculated using equation 4.2-3. The thickness of Tru-Stretch® was 15 mil thick while the width was 5.25 inches thick. Since Tru-Stretch® exhibits different characteristics because of how the material is woven, Table 4.2-25 presents the results where the material is stiffly woven and Table 4.2-26 presents the results when the material is lightly woven. The necking affects were not taken into account,

therefore the original cross-sectional area was held constant. Tru-Stretch® (stiffly woven) was the stiffest material when comparing the Young's Modulus to the other materials tested. But, the ability for the material to strain was the least. On the other hand Tru-Stretch® (lightly woven) produced similar results when compared to Spandura®.

**Table 4.2-25.** Young's Modulus at different strains for Tru-Stretch® (stiffly woven).

| Strain | 0.108 | 0.208 | 0.229 |
|---|---|---|---|
| Young's Modulus kpsi (MPa) | 12.5 (86.2) | 13.5 (93.2) | 13.5 (93.3) |

**Table 4.2-26.** Young's Modulus at different strains for Tru-Stretch® (lightly woven).

| Strain | 0.155 | 0.510 | 0.704 | 0.865 |
|---|---|---|---|---|
| Young's Modulus kpsi (MPa) | 0.51 (3.49) | 2.03 (14.0) | 3.30 (22.8) | 3.55 (24.5) |

The stretch and hold experiments also exhibited different results, depending on if the material was either stiffly or lightly woven. For the stiffly woven material, the material was strained to 20 percent strain and the forces required to hold the material were recorded, as shown in Figure 4.2-43. Since the yarns are made out of polyurethane the amount of force necessary to hold the material at the same displaced amount as the first stretched was less. The polyurethane yarns deformed enough that plastic deformation occurred.

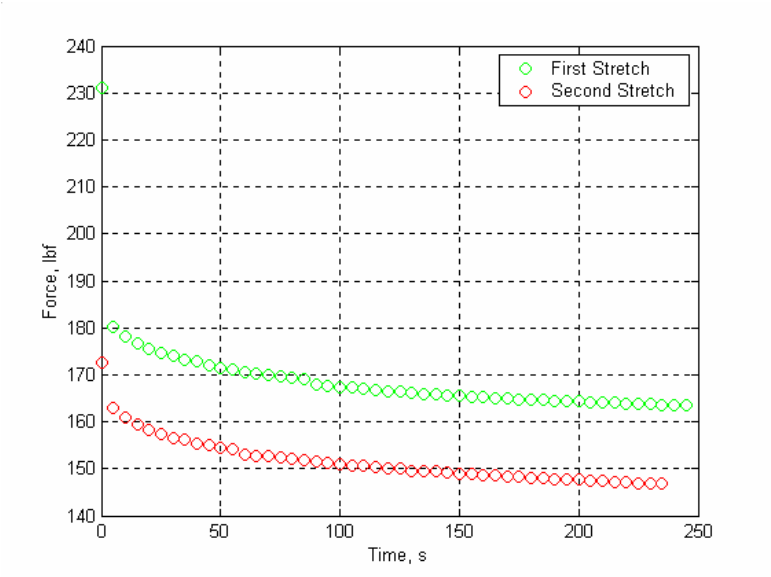


**Figure 4.2-43.** Reduction of force needed to hold Tru-Stretch® at a given strain (stiffly woven).

Although the lightly woven Tru-Stretch® material was allowed to deform more, the responses are similar when the material was strained and held. The responses are shown in Figure 4.2-44. Since the yarns are made out of polyurethane the amount of force necessary to hold the material at the same displaced amount as the first stretched test was less. The yarns underwent plastic deformation during the first stretched, which is the reason the required force to hold the material at the given displaced amount was less.

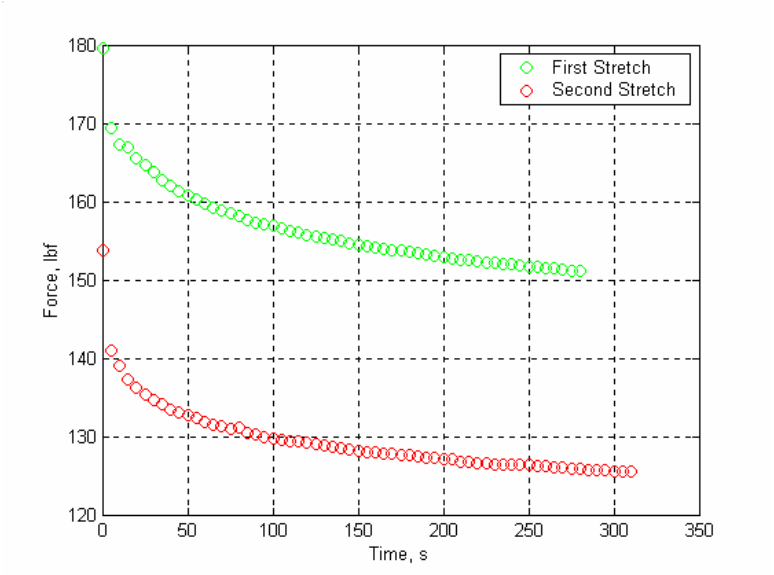


**Figure 4.2-44.** Reduction of force needed to hold Tru-Stretch® at a given strain (lightly woven).

The final results presented in this section for this material are the recovery abilities of Tru-Stretch for both the stiffly woven and the lightly woven Tru-Stretch® materials.

For the stiffly woven materials, the material was not allowed to strain beyond approximately 25 percent strain because the required forces would be beyond the range of the force transducer. But, when the material was strained the recoverability performed better for the stiffly woven when compared to the lightly woven, as shown in Table 4.2-27. Even though the material recovered, it still underwent plastic deformation.

**Table 4.2-27.** Strain recovery of Tru-Stretch during the force and strain experiments.

| Test | Maximum Strain | Recovery Strain |
|---|---|---|
| Stiffly woven Experiment 1 – Stretch 1 | 0.235 | 0.073 |
| Stiffly woven Experiment 1 – Stretch 2 | 0.189 | 0.061 |
| Lightly woven Experiment 1 – Stretch 1 | 0.865 | 0.281 |
| Lightly woven Experiment 1 – Stretch 2 | 0.461 | 0.317 |

When the material was strained to the same displaced amount and held, the recovery results were relatively the same for both the stiffly woven and lightly woven Tru-Stretch® experiments. The recovery results for the strain and held experiments are shown in Table 4.2-28.

**Table 4.2-28.** Strain recovery of Tru-Stretch during the strain and hold experiments.

| Test | Maximum Strain | Recovery Strain |
|---|---|---|
| Stiffly woven Experiment 1 – Stretch 1 | 0.202 | 0.056 |
| Stiffly woven Experiment 1 – Stretch 2 | 0.135 | 0.056 |
| Lightly woven Experiment 1 – Stretch 1 | 0.700 | 0.213 |
| Lightly woven Experiment 1 – Stretch 2 | 0.402 | 0.225 |

# 4.3 Biaxial Experimental Results

## 4.3.1 Results Overview

The previous section discussed the uniaxial responses of the candidate skin materials for a morphing wing. This section will concentrate on reporting the biaxial response of the same materials that were experimented with in the uniaxial experimental results section. Although recovery results were sought when performing the biaxial experiments, most of the material ripped. Also for most materials, the ability for the material to strain was significantly less when compared to the uniaxial experiments. Explanations of how the materials performed will be discussed in each of the separate material's sub-section in further detail throughout this section of the report.

Throughout this section, the figure will be referring to how much force is required to strain the material. Since this section deals with biaxial loading conditions, the figures will have a legend depicting which way the material was strained. The coordinate system that was used for the experiments is shown in Figure 4.3-1.

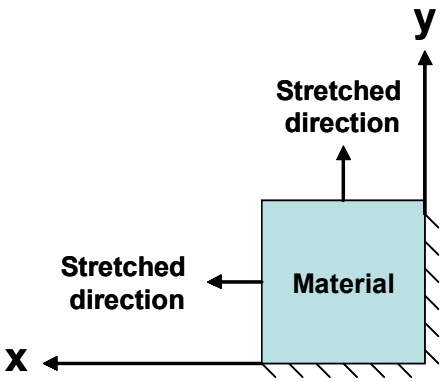


**Figure 4.3-1.** Coordinate system used for the biaxial experiments.

The materials presented here will follow the same order as the uniaxial results were presented. Therefore, the first material that will be discussed in this section will be Tecoflex® 80A.

### 4.3.2 Tecoflex® 80A

For both experiments that were conducted for the force and strain comparison of Tecoflex® 80A, the material broke. Although for both experiments the trends are the same, the breaking point of the material was different, as shown in Figure 4.3-2. During the first experiment the material was able to be strained in both directions to approximately 0.45, while for the second experiment the material was strained to approximately 0.3 before ripping. Although more testing was needed, the limited supply only permitted two experiments.

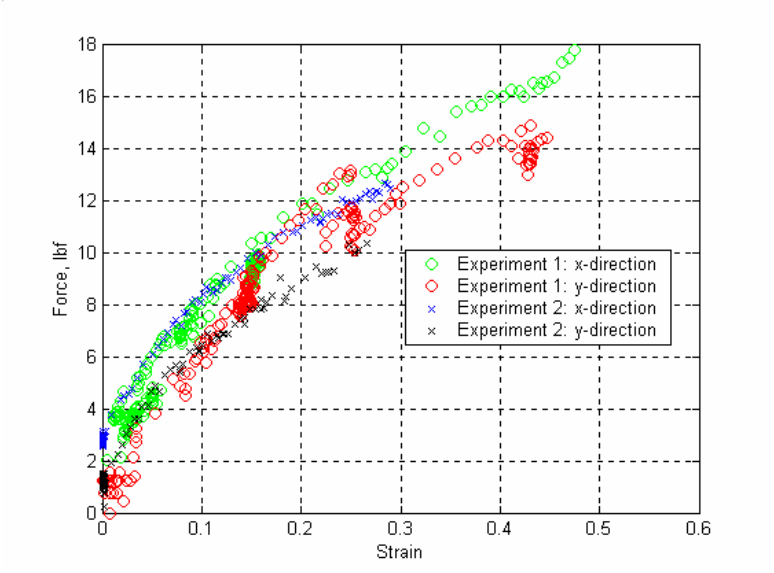


**Figure 4.3-2.** Force and strain comparison for Tecoflex 80A.

The next test performed was to determine if the holding force decayed after the material was strained. The material was strained to 0.30 in the x-direction, while the material was strained to 0.20 in the y-direction. Over time, the force needed to the hold the material decayed over time, as shown in Figure 4.3-3. The reason is the material under went plastic deformation, which allowed the material to relax.

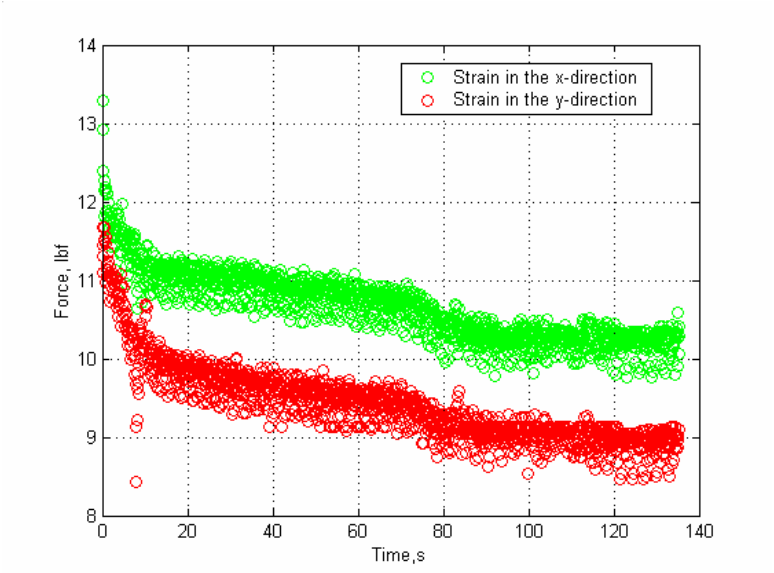


**Figure 4.3-3.** Reduction of force needed to hold Tecoflex 80A® at a given strain.

### 4.3.3 Tecoflex® 100A

Tecoflex® 100A material characteristics were similar to Tecoflex® 80A for the biaxial experiments. When determining the force and strain relationship Tecoflex® 100A ripped. Since the material ripped, the recovery results of this material could not be conducted.

During the first experiment, the material was strained to approximately 0.225 and 0.175, in the x-direction and y-direction respectively. During the second experiment, the material was strained to approximately 0.225 for both the x and y-direction. Figure 4.3-4 shows that although the same trends are seen for both experiments, the required forces are slightly different when the material is being strained.

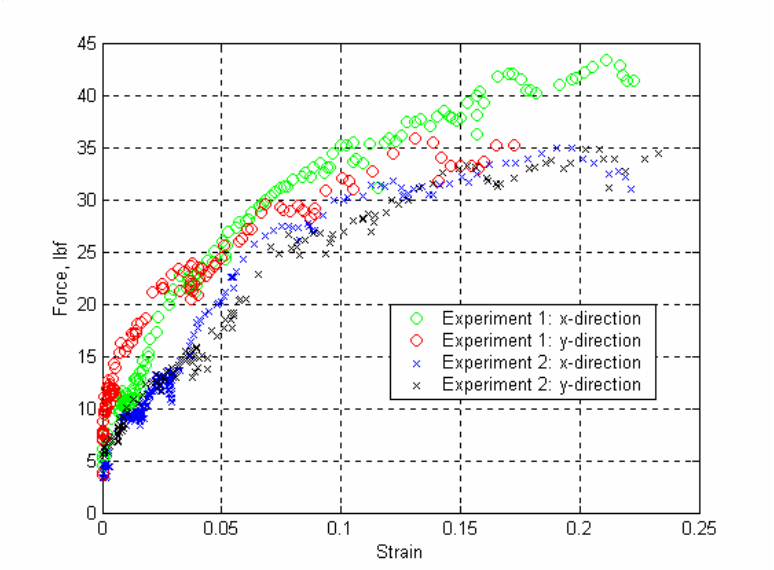


**Figure 4.3-4.** Force and strain comparison for Tecoflex® 100A.

The next experiment conducted using Tecoflex® 100A was determining the required forces to hold the material once it had been strained. The material was strained to 0.05 and 0.04, in the x and y-direction respectively. As time went on, the material exhibited a decaying behavior in the amount of force that was needed to hold the material at the given strain locations, as shown in Figure 4.3-5.

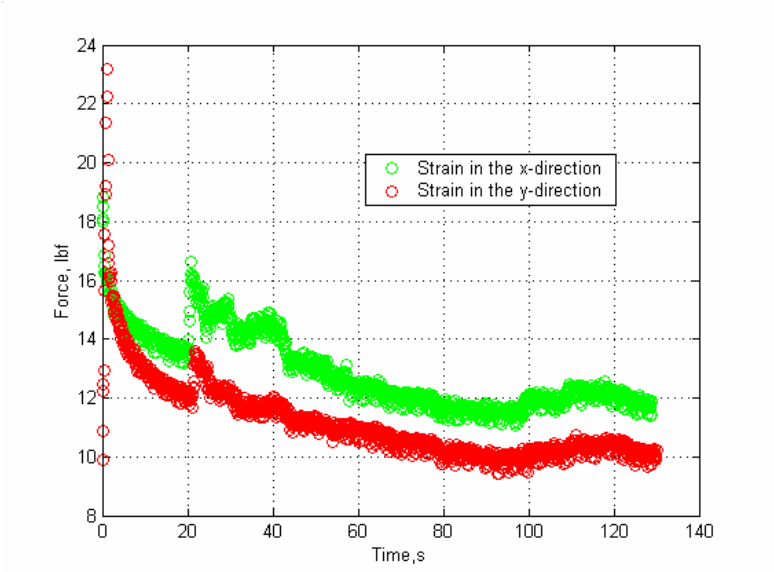


**Figure 4.3-5.** Reduction of force needed to hold Tecoflex 100A® at a given strain.

### 4.3.4 Tecoflex® 93A

Like the other Tecoflex® materials, there was a limited quantity of Tecoflex® 93A. Figure 4.3-6 shows the force and strain comparison for this material. The material was strained to approximately 0.325 in the y-direction and approximately 0.25 in the x-direction before the material broke. Since the material broke, a recovery analysis could not be completed.

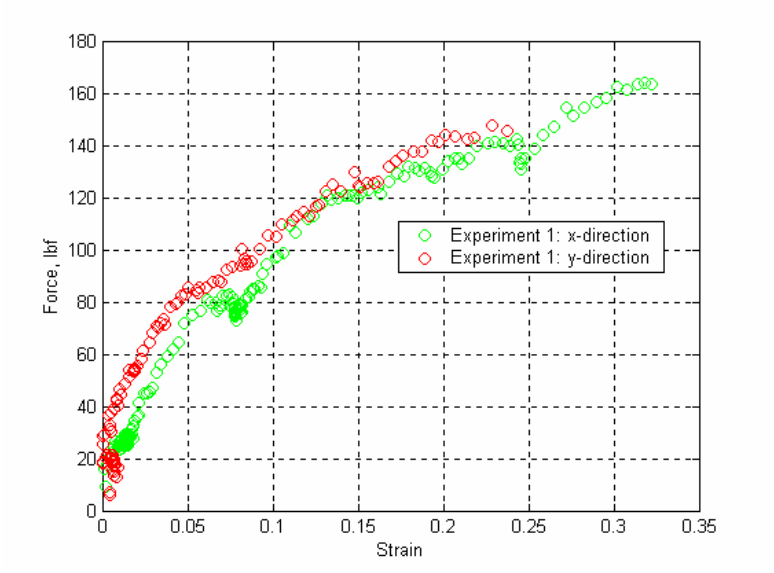


**Figure 4.3-6.** Force and strain comparison of Tecoflex® 93A.

Unlike the other Tecoflex materials that were tested this is the only result that was determined. The reason was there was another sample of Tecoflex® 93A, but the thickness of the material was different from all the other Tecoflex® 93A tested.

### 4.3.5 Riteflex® 640

Since the quantity of the material was limited, only one experiment was conducted for each test. The first test conducted was the force and strain comparison. Figure 4.3-7 shows the force and strain comparison for Riteflex® 640. The material was strained to approximately 0.055 in the x-direction and 0.03 in the y-direction before the material ripped. Since the material ripped, a recovery analysis could not be completed.

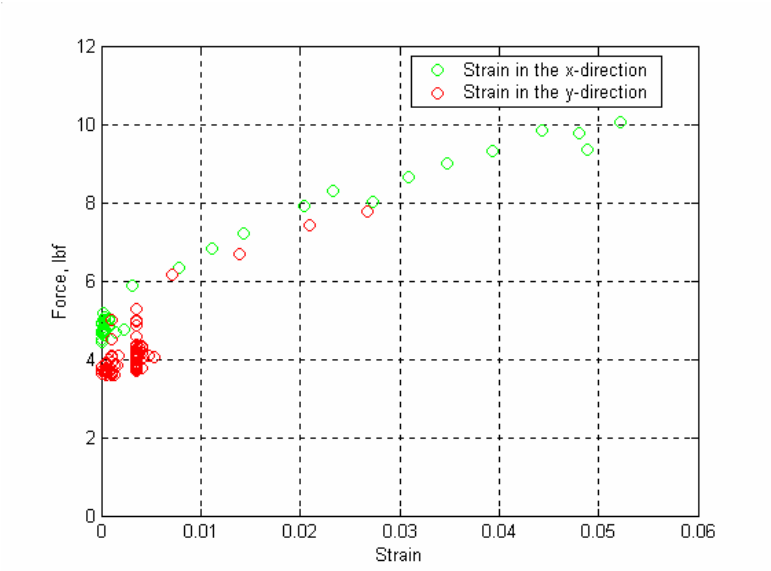


**Figure 4.3-7.** Force and strain comparison of Riteflex® 640.

The next results presented are the necessary force to sustain a given strain, as shown in Figure 4.3-8. The material was strained to 0.89 and 0.06, in the x- and y-direction, respectively. The required forces to hold the material at the given strain decreased over time. After approximately 30 seconds the material finally relaxed and the material needed a constant force to hold the material at the given strains.

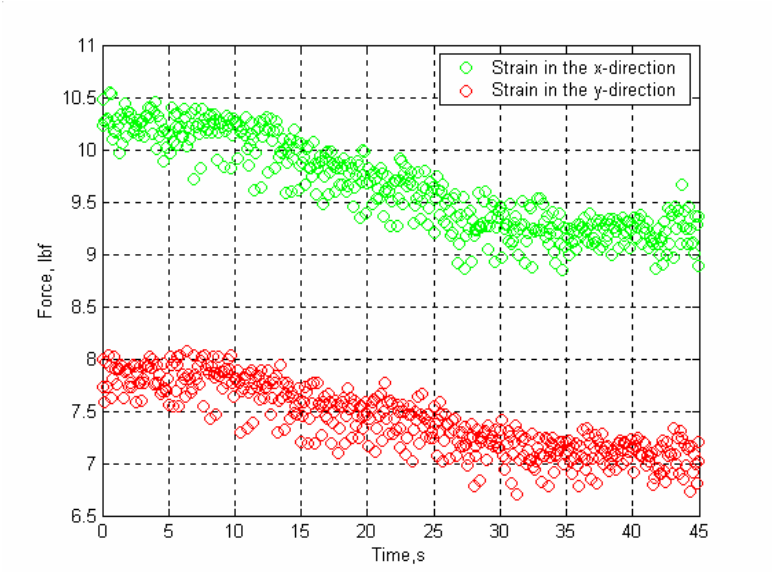


**Figure 4.3-8.** Reduction of force needed to hold Riteflex 640® at a given strain.

### 4.3.6 Riteflex® 663

The final material tested from Ticona was Riteflex® 663. Since there was a limited quantity of this material, only one test was conducted for each experiment. The first experiment conducted determined the required forces needed to strain the material. The material was strained to approximately 0.075 in the x- and y-direction before tearing, as shown in Figure 4.3-9. Although additional experiments were not completed, a material comparison can be completed. The straining ability of Riteflex® 663 was better than Riteflex® 640. Riteflex ® 663 needed more force at a given strain when compared to Riteflex® 640. Since the material ripped, a recovery result can not be completed.

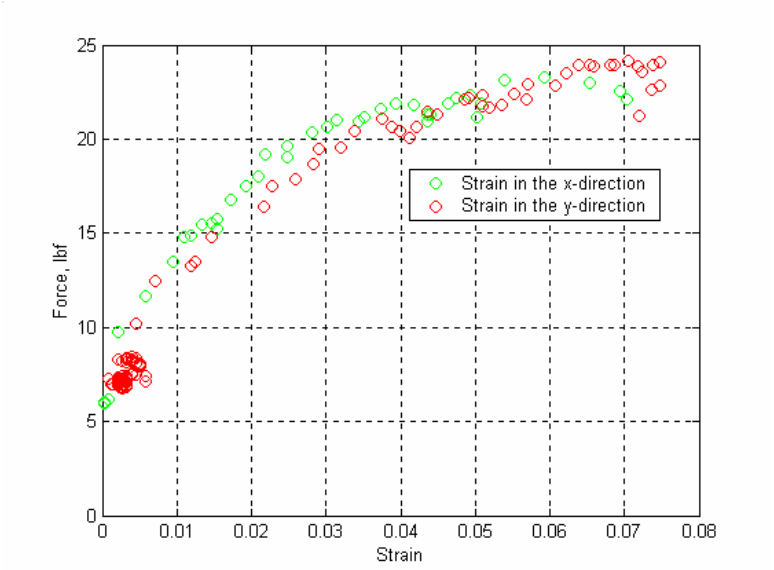


**Figure 4.3-9.** Force and strain comparison of Riteflex® 663.

The next figure, Figure 4.3-10, shows the required forces to hold the material after being strained to 0.07 and 0.08 in the x- and y-direction, respectively. Once the material is strained, the amount of force needed to hold the material at the given strain decreases. The reason less forces are needed is the material relaxes after undergoing plastic deformation.

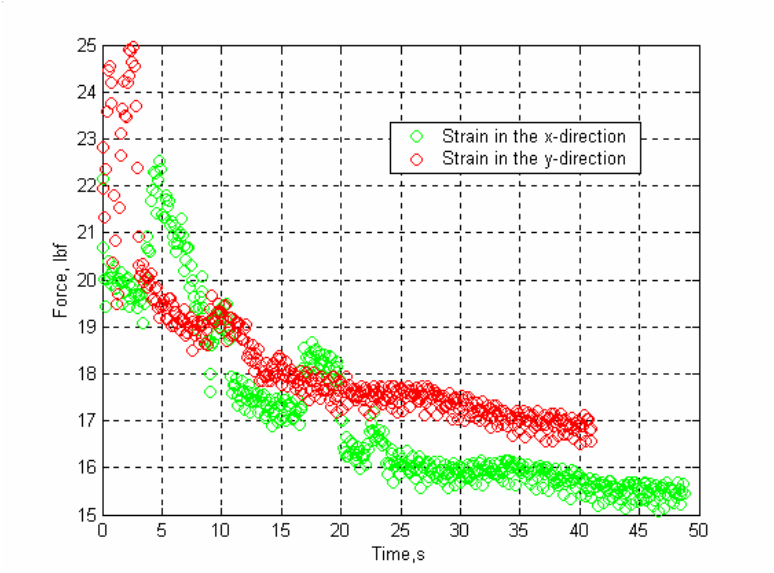


**Figure 4.3-10.** Reduction of force needed to hold Riteflex® 663 at a given strain.

### 4.3.7 Arnitel®

The following results presented here are for Arnitel®. Two experiments were conducted for the force and strain comparison test. For the first experiment, the material was strained to approximately 0.225 in the x-direction and 0.35 in the y-direction. After the material was strained to a greater amount, the material broke. During the second experiment the material was strained to 0.275 and 0.325 in the x- and y-direction, respectively before tearing. These results are shown in Figure 4.3-11. Although the material followed the same trend, the material failed at different strained amounts. Additional testing was needed, but the quantity of the material was limited. Since the material ripped, a recovery analysis could not be performed.

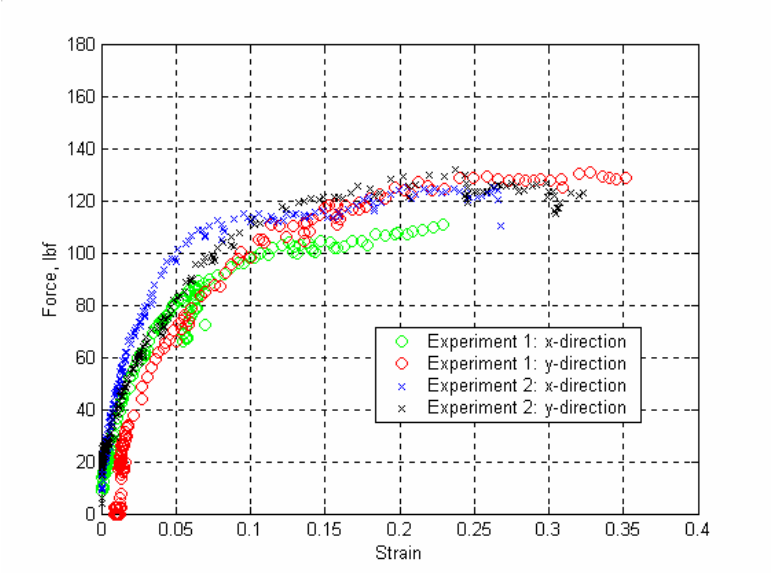


**Figure 4.3-11.** Force and strain comparison of Arnitel®.

The next experiment that was going to be conducted was the strain and hold test. While placing the material in the test stand, the material accidentally got ripped. Therefore, the experiment could not be performed. Since the experiment was not performed, there are no results to present showing the required forces needed to hold the material for the biaxial experiment. Yet, Arnitel® acted in a similar manner as other polyurethane based materials. Therefore, it is a good hypothesis that the amount of force to hold the material after being strained would have decreased over time.

### 4.3.8 Shape Memory Polymer

Although biaxial testing was originally planned for the shape memory polymer, the tests were not completed. The shape memory polymer was very brittle, which made it hard to handle. Even though the shape memory polymer was heated to the viable temperature to work with, the polymer was still hard to handle. For one test specimen of the shape memory polymer, while placing it in the grippers, it shattered. Also, since there was a limited quantity of this material, there was no more material left to test.

### 4.3.9 Spandura®

The first woven material tested was Spandura®. Figure 4.3-14 shows the results for the force and strain comparison. Two experiments were conducted, and the trends are similar. For the first experiment, the material was strained to approximately 0.5 in the x-direction and approximately 0.3 in the y-direction. During the second experiment the material was strained to approximately 0.5 and 0.25, in the x- and y-direction respectively.

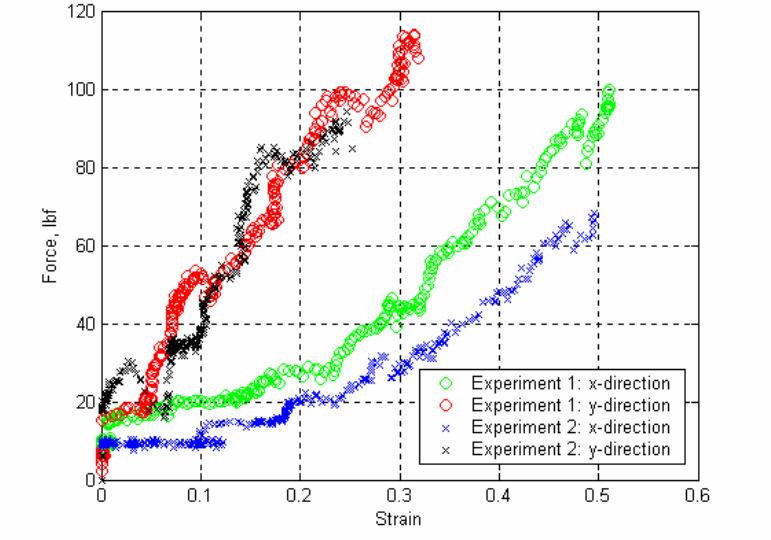


**Figure 4.3-12.** Force and strain comparison of Spandura®.

Although the material did not rip, the material was not strained more. The reason was the material deformed in a manner that air would pass through, as shown in Figure 4.3-15. This would not be suitable as a skin for a morphing wing, since the material would not be able to sustain the loads of the aircraft.

**Figure 4.3-13.** Picture showing the deformation of Spandura®.

The next experiment that was completed for Spandura was the strain and hold test. The material was strained to 0.5114 and 0.3186, in the x- and y-direction, respectively. Figure 4.3-16 shows that as the material relaxed, less force was needed to hold the material at the given strain. Although this experiment was completed for the purpose of showing the results, as previously stated the material deformed in such a way that air could easily pass through. Since air could pass through the material, it is not a suitable candidate material for a morphing wing skin.

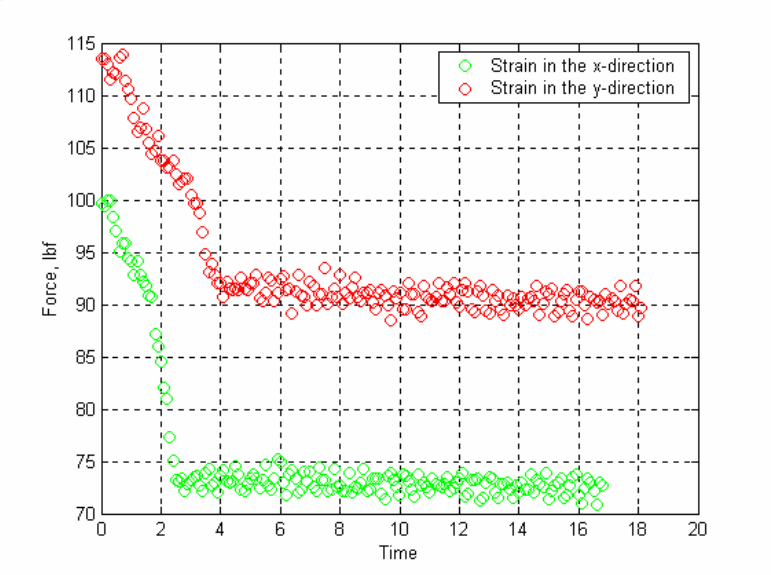


**Figure 4.3-14.** Reduction of force needed to hold Spandura® at a given strain.

### 4.3.10 Tru-Stretch®

The final woven material tested was Tru-Stretch®. The force and strain comparisons are shown in Figure 4.3-17. The trends for both experiments are very similar. Notice, when the material was strained in the y-direction, the forces increased to the limit of the force transducer with minimal strain compared to the x-direction. The reason, as stated in the material's chapter, due to the weaving of the yarns the material was only elastic in one direction. While when the material was strained in the y-direction, the material was able to strain more before reaching the limits of the force transducer, when compared with the ability for the material being strained in the x-direction.

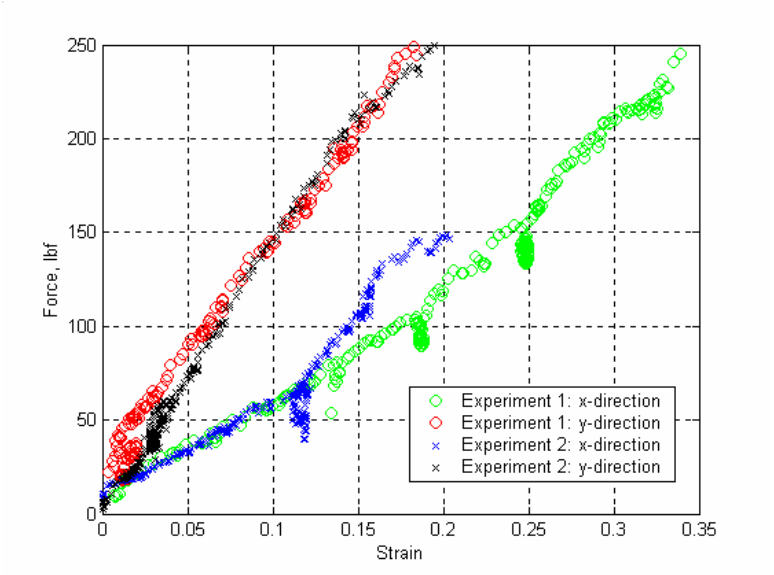


**Figure 4.3-15.** Force and strain comparison of Tru-Stretch®.

Even though the material did not rip, the material was not strained more since the required forces were greater than the rated limits of the force transducers. Also as the material was strained, the yarns separated, which would allow air to pass through the material. When the material was strained in this manner, the material looked similar to Spandura®, which is shown in Figure 4.3-13. This would not be a suitable material for a morphing wing, since the skin of a wing has to be able to handle the aerodynamic loads of the aircraft.

For the strain and hold results, the material was strained to 0.23 in the x-direction and 0.07 in the y-direction. The required forces to hold the material at the given strained amount decreased, as shown in Figure 4.3-18. Even though the material is woven with yarns, the yarns are made with polyurethane chains. Therefore, the required forces needed to hold the material decreased as the material relaxed.

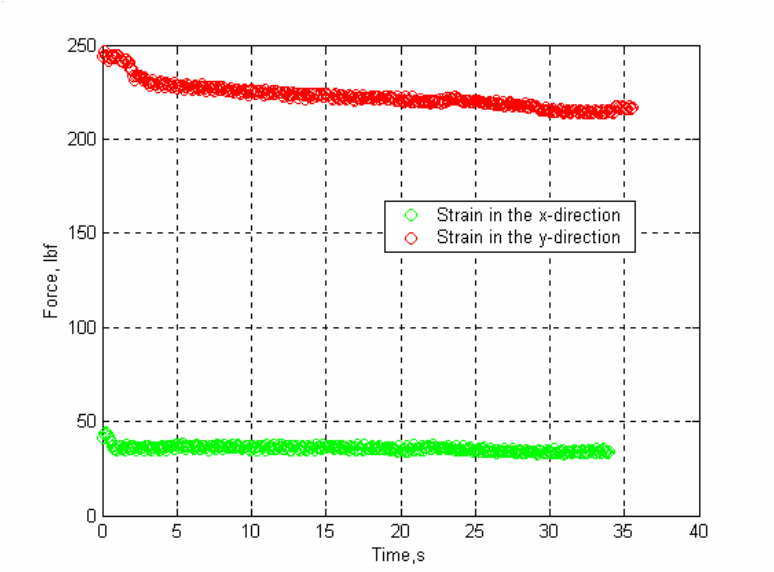


**Figure 4.3-16.** Reduction of force needed to hold Tru-Stretch® at a given strain.

### 4.3.11 Biaxial Deflection Discussion

As stated throughout this section some materials ripped while conducting the force and strain comparison. The only materials that did not rip were the woven materials, Spandura® and Tru-Stretch®. The only explanation why theses materials did not rip is the way the yarns were woven. For the materials that did rip, they started to rip in one of three locations. The locations are shown in Figure 4.3-19 by the red circles.

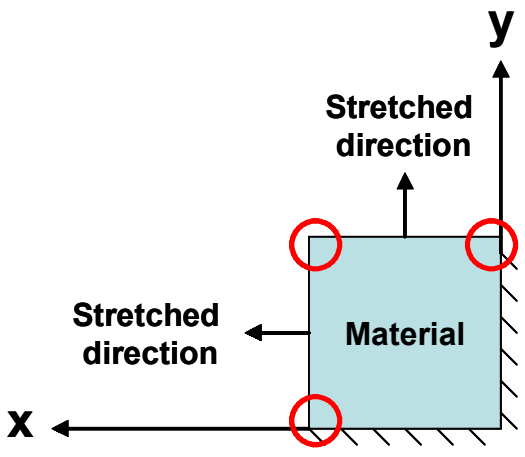


**Figure 4.3.17.** The red circles represent the locations where the material ripped while conducting the biaxial experiments.

The reason the bottom right-hand side of the material did not rip is the material is grounded. The other three corners were free to deform, therefore allowing the material to undergo deformation. As stated in the biaxial test stand section, the gripping devices were cut at 45 degree angles, allowing a perfect square. Figure 4.3-20 shows a picture of a slightly deformed material. Notice at the unbounded corners the gripping device is instantaneously stretching a very small area of the material. Therefore, the material is ripping while being strained a small amount.

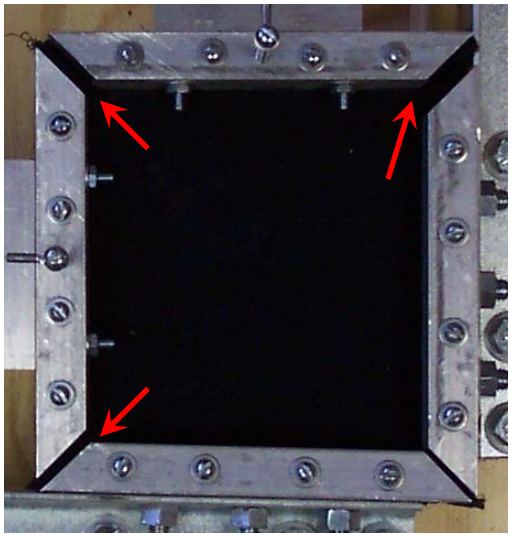

**Figure 4.3-18.** Picture showing where the material is ripping during the biaxial experiments.

# 4.4 Pressure Deflection Results

## 4.4.1 Pressure Deflection Overview

The final results shown in this report identifies the ability for the material to handle the aerodynamic loads of an aircraft while in flight. As the pressure increased, the material expanded. Therefore, the data that was recorded was the applied constant pressure load and the deflection of the material. The deflection of the material was measured from the center of the material, shown in the blue circle in Figure 4.4-1. Also, the pressure load was applied over a constant area of the material, as shown in Figure 4.4-1. The test stand was design for a boundary constraint of four square inches.

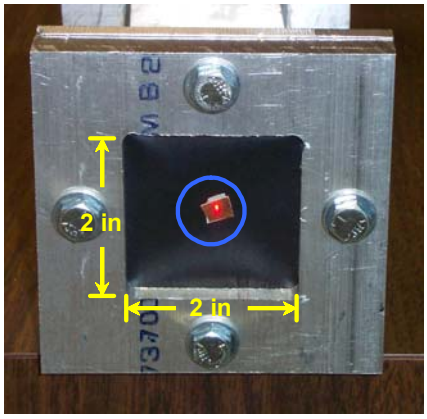


**Figure 4.4-1.** Picture showing measuring location for the pressure-deflection experiments.

Figure 4.4-2 shows a material that has been deformed under a constant pressure load. The measured displacement recorded is shown between the yellow arrows.

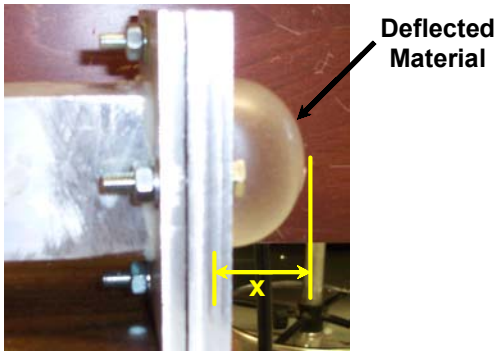


**Figure 4.4-2.** A test material representing the measured deflection under a constant pressure load.

The following sections will present the results of the pressure deflection experiments in the same order that the uniaxial and biaxial results were presented.

### 4.4.2 Tecoflex® 80A

The results presented here are for Tecoflex® 80A. The material was tested at 4, 7, and 10 psi. When the constant pressure load of 4 psi was applied to the material it deflected a maximum of 0.62 inches. However when a pressure load of 7 psi was applied to the material, it deflected by

1.25 inches. These results are shown in Figure 4.4-3. The material failed when a pressure load of 10 psi was applied.

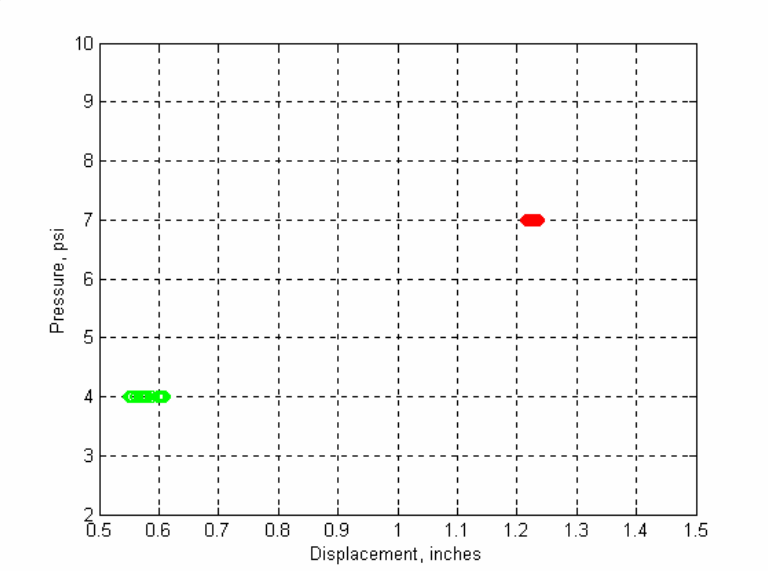


**Figure 4.4-3.** Pressure deflection results of Tecoflex® 80A.

### 4.4.3 Tecoflex® 100A

Tecoflex® 100A was test with a pressure load of both 5 and 10 psi. Figure 4.4-4 shows the pressure deflection results of Tecoflex® 100A. While undergoing a pressure load of 5 psi, the material deflected a maximum of 1.2 inches. When the material was applied a pressure load of 10 psi, the material failed.

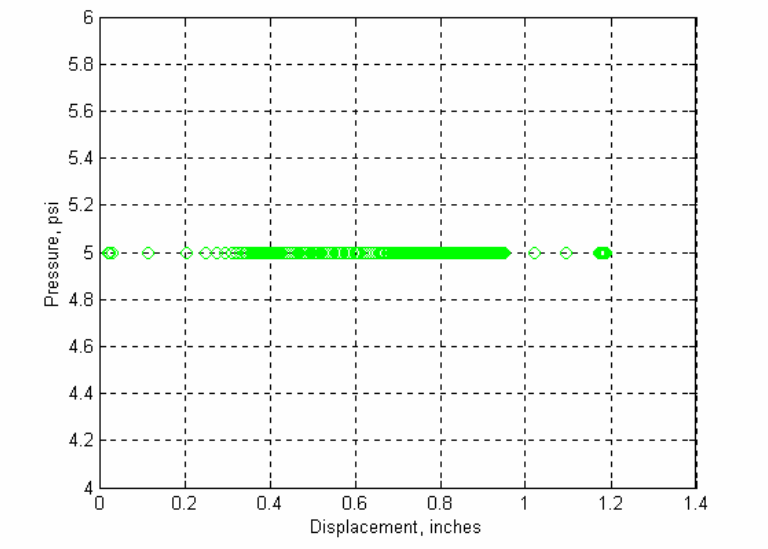


**Figure 4.4-4.** Pressure deflection results of Tecoflex® 100A.

### 4.4.4 Tecoflex® 93A

Tecoflex® 93A was able to handle the maximum pressure the air compressor could produce, which was 56 psi. Also the material did not deflect as much as the other Tecoflex® materials that were tested. Even though a pressure load of 56 psi was applied to the material, the material only deflected 1.05 inches. Furthermore, the material did not break. The results of the different pressures and the amount the material deflected are shown in Figure 4.4-5.

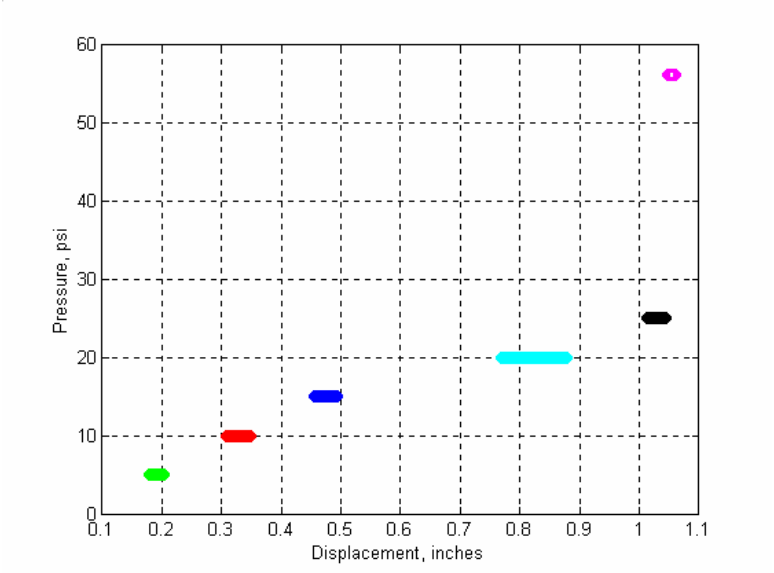


**Figure 4.4-5.** Pressure deflection results of Tecoflex® 93A.

### 4.4.5 Riteflex® 640

Riteflex® 640 performed similarly to Tecoflex® 100A. Pressure loads of 5 and 10 psi were applied to both materials. While both materials were able to handle the pressure loads of 5 psi, they failed when a pressure load of 10 psi was applied to the material. A pressure load of 5 psi was applied to Riteflex® 640 and it deflected approximately 0.4 inches, as shown in Figure 4.4-6. When this material underwent a pressure load of 10 psi the material failed.

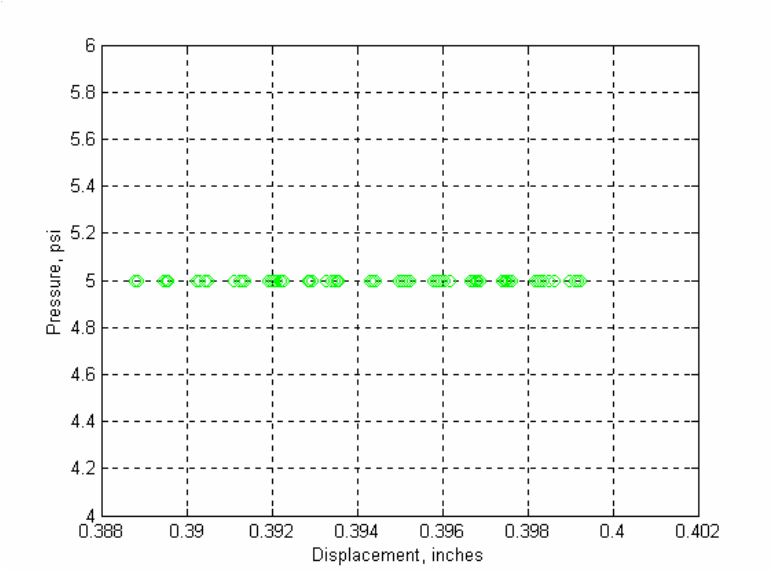


**Figure 4.4-6.** Pressure deflection results of Riteflex® 640.

### 4.4.6 Riteflex® 663

Riteflex® 663 deflected less than Riteflex® 640. When a pressure load o f5 psi was applied to Riteflex® 663 the material deflected by 0.28 inches, as shown in Figure 4.4-7. On the other hand, when a pressure load of 10 psi was applied, the material failed. As a comparison, both Riteflex® 640 and 663 failed when a pressure load of 10 psi was applied to the materials.

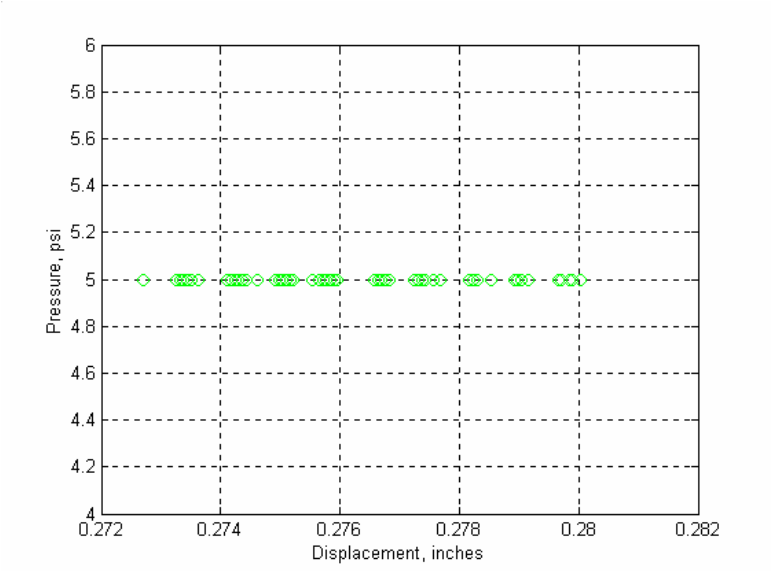


**Figure 4.4-7.** Pressure deflection results of Riteflex® 663.

### 4.4.7 Arnitel®

Arnitel® underwent pressure loads of 5, 10, 15, and 20 psi. The material performed well when subject to the 5, 10, and 15 psi pressure loads, as shown in Figure 4.4-8. When a pressure load of 5 psi was applied, the material deflected by 0.36 inches. While a pressure load of 10 psi was applied, the material deflected by 0.48 inches. The maximum amount the Arnitel® deflected was 0.63 inches, when a 15 psi pressure load was applied. The material failed when it was subjected to a 20 psi pressure load.

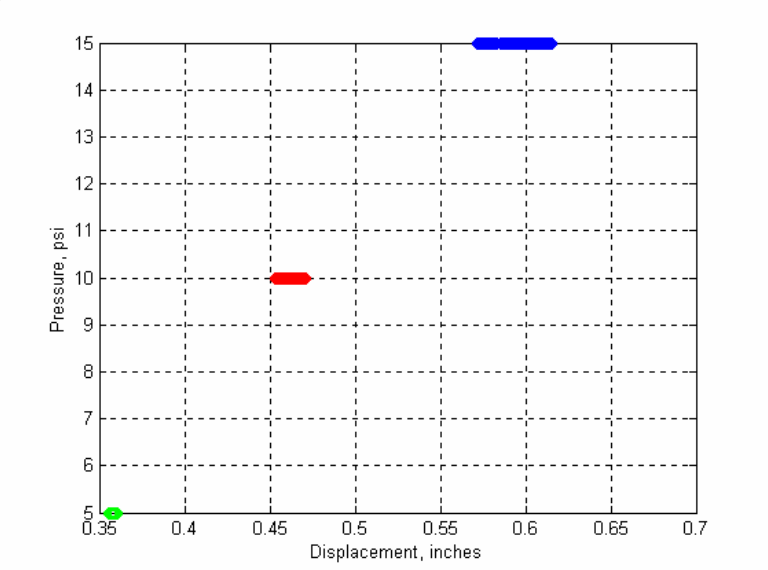


**Figure 4.4-8.** Pressure deflection results of Arnitel®.

### 4.4.8 Shape Memory Polymer

The shape memory polymer material was applied a pressure load of 10, 20, 30, 40, and 50 psi. The amount the material deflected is shown in Figure 4.4-9. While undergoing the 50 psi pressure load the material broke, therefore this result is shown. The shape memory polymer was able to sustain the pressure loads of all the other test pressures. Since the shape memory polymer had to be viable to cut the material to fit in the pressure deflection test stand, it was heated to 100 degrees Celsius. Once the material was cut, it was allowed to cool to ambient air temperature and placed in the test stand.

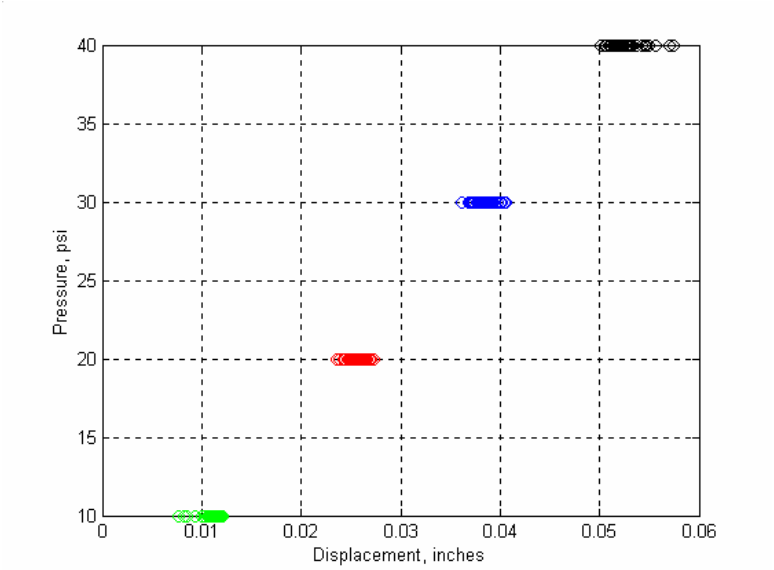


**Figure 4.4-9.** Pressure deflection results of the SMP (solid state).

The previous results were concluded when the shape memory polymer was in the solid state. The following results are for when the material was in its rubbery state (105 degrees Celsius). When the material was heated, a pressure load of 5 psi was applied and the shape memory polymer deflected by 1.32 inches, as shown in Figure 4.4-10. When the pressure was increased to 8 psi, the shape memory polymer failed.

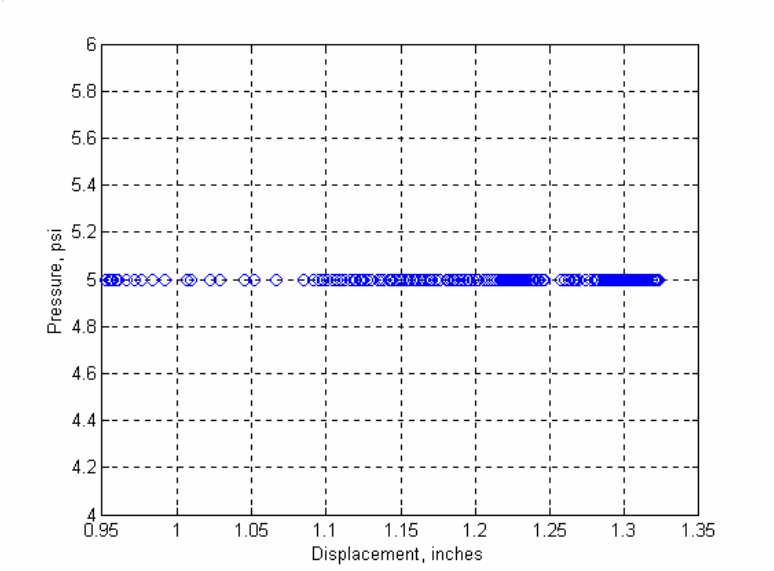


**Figure 4.4-10.** Pressure deflection results of the SMP (rubbery state, 105$^{o}$C).

### 4.4.9 Spandura®

Since Spandura® was woven, it allowed air to pass through. Therefore the woven materials could not sustain a suitable pressure load. The only pressure load that was sustained was approximately 1 psi. While a pressure load of 1 psi was sustained the material deflected by 0.32 inches, as shown in Figure 4.4-11. But, this deflected was caused by the velocity of the air compressor. If one placed their hand next to the material one could feel the air passing through the material. Essentially this material could not hold any loads, therefore is not a good candidate material for a morphing wing.

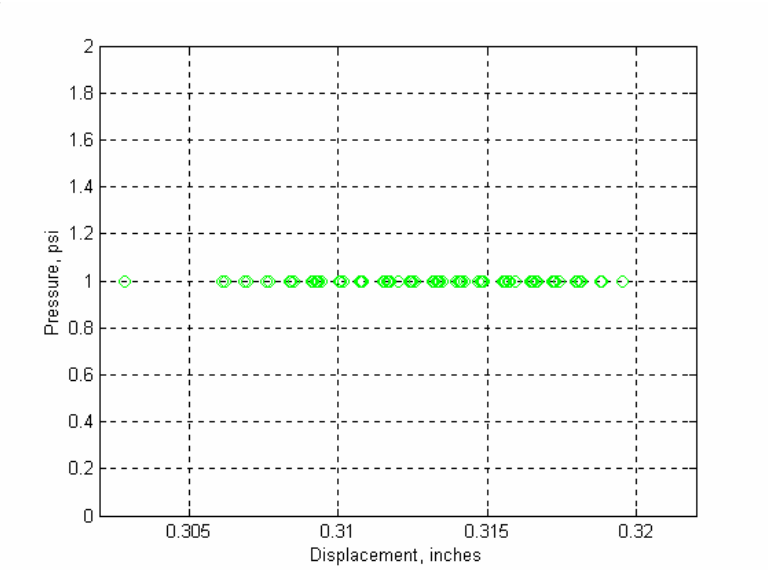


**Figure 4.4-11.** Pressure deflection results of Spandura®.

### 4.4.10 Tru-Stretch®

Although Tru-Strech and Spandura are woven materials, they produced different results. As a reminder, in the material section of the report the difference in the ability for Tru-Stretch® and Spandura® to stretch was discussed. The maximum pressure load Tru-Strech® could sustain was 1 psi and in conjunction the material deflected by 0.3 inches. This result is shown in Figure 4.4-12. Just like Spandura®, the deflection of Tru-Stretch® was caused by the output velocity of the air compressor. By placing a hand next to the material, one could feel the air passing through the material. Since air was passing through Tru-Stretch®, this material could not handle the aerodynamic loads of an aircraft while in flight.

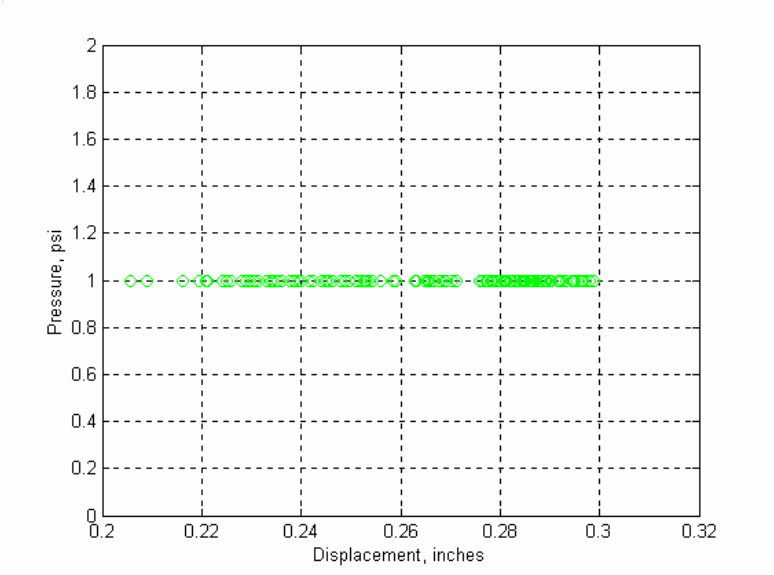


**Figure 4.4-12.** Pressure deflection results of Tru-Stetch®.

## 4.5 Comparison of the Results

This section compares the results from all the experiments and all of the different materials. This includes the uniaxial, the biaxial, and the pressure deflection experiments. The easiest way to compare the materials is by presenting a matrix chart of how the materials performed during each experiment.

Table 4.5-1 shows the results of all the material for the uniaxial experiments. One part of the table is for the force and strain comparison experiments. The results presented the maximum experimental strain, and the worst recovery strain. The reason for reporting the worst recovery strain is when determining if the candidate material is suitable for a morphing wing, there cannot be any excess material because it could increase the drag. Also shown in Table 4.5-1 is a column depicting if the elongation ratio is constant. As a reminder, the elongation ratio was calculated from the experimental axial and lateral strain data that was recorded. The final main column presented in Table 4.5-1 is the comparison of the Young's Modulus. The Young's Modulus column presents both the minimum and maximum values.

**Table 4.5-1.** Material comparison matrix of the uniaxial experiments.

| | Force and Strain Comparison | | | Elongation Ratio | Young's Modulus | |
|---|---|---|---|---|---|---|
| | **Strain** | **Max. Force** | **Recovery Strain** | **Constant** | **min** | **max** |
| **Material** | (Max) | (lbs) | (Worst) | (Y/N) | kpsi (Mpa) | |
| Tecoflex® 80A | 3.07 | 15.91 | 0.182 | N | 0.156 (1.07) | 0.266 (2.01) |
| Tecoflex® 100A | 1.44 | 28.86 | 0.122 | N | 1.49 (10.3) | 2.92 (20.2) |
| Tecoflex® 93A | 1.93 | 178.23 | 0.235 | N | 0.88 (6.10) | 1.42 (9.78) |
| Riteflex® 640A | 2.20 | 21.28 | 0.788 | N | 1.33 (9.20) | 5.04 (35.8) |
| Riteflex® 663A | 1.28 | 21.97 | 0.950 | N | 2.36 (16.3) | 11.2 (77.1) |
| Arnitel® | 1.51 | 87.36 | 0.439 | N | 1.10 (7.61) | 3.41 (23.5) |
| Shape Memory Polymer | 2.00 | 11.09 | 0.167 | N | 0.010 (0.07) | 0.043 (0.3) |
| Spandura® | 0.87 | 222.87 | 0.342 | N | 0.03 (0.23) | 3.48 (24.0) |
| Tru-Stretch® (stiffly woven) | 0.23 | 250.00 | 0.073 | Y* | 12.5 (86.2) | 13.5 (93.2) |
| Tru-Stretch® (lightly woven) | 0.86 | 241.91 | 0.317 | Y* | 0.51 (3.49) | 3.55 (24.5) |

Table 4.5-2 presents the results of the strain and hold experiments. The results presented for this part of the table are strain, max force, dissipated force, and the recovery strain. The "strain" is the strain amount the material was displaced to hold the material constant. The "max force" is the maximum amount of force it took to strain the material to the displaced location. While, the "dissipated force" is the constant force the material needed once the material relaxed after undergoing plastic deformation. The "force difference" column shows the percentage difference in the required forces necessary to hold the material once being strained. The final result presented in the strain and hold part of Table 4.5-2 is the worst excess strain that is the consequence of straining the material, "recovery strain."

**Table 4.5-2.** Material comparison matrix of the strain and hold test from uniaxial experiments.

| | Strain and Hold | | | | |
|---|---|---|---|---|---|
| **Material** | **Strain** (Max) | **Max. Force** (lbs) | **Max Dissipated Force** (lbs) | **Force Difference** (%) | **Recovery Strain** (Worst) |
| Tecoflex® 80A | 2 | 7.98 | 6.10 | 23.56 | 0.068 |
| Tecoflex® 100A | 0.581 | 20.62 | 7.87 | 61.83 | 0.167 |
| Tecoflex® 93A | 1.12 | 139.88 | 85.84 | 38.63 | 0.073 |
| Riteflex® 640A | 1.00 | 11.57 | 9.40 | 18.76 | 0.41 |
| Riteflex® 663A | 0.613 | 16.63 | 10.10 | 39.27 | 0.213 |
| Arnitel® | 1.24 | 81.64 | 64.59 | 20.88 | 0.429 |
| Shape Memory Polymer | 1.04 | 9.68 | 0 | 100.00 | 0.043 |
| Spandura® | 0.78 | 235.96 | 167.00 | 29.23 | 0.293 |
| Tru-Stretch® (stiffly woven) | 0.2 | 231.22 | 163.51 | 29.28 | 0.059 |
| Tru-Stretch® (lightly woven) | 0.70 | 179.47 | 151.11 | 15.80 | 0.225 |

As stated before, a material that could be used as a skin for a morphing wing has to be elastic, while having the ability to recovery. This was the main purpose of the uniaxial experiments. From Table 4.5-1, notice the material that was allow to strain the most without break is Tecoflex® 80A. Another material that was to strain without breaking was the shape memory polymer. For both Tecoflex® 80A and the shape memory polymer the required force to strain the material were the least out of all the materials tested. The final result to take note of was the ability of Tecoflex® 80A and the shape memory polymer to recover. Although the materials were strained the most, they have the best overall recovery results. By observing the first and third column under the "Force and Strain Comparison" one can notice Tecoflex® 80A and the shape memory polymer recovered the best. For the strain and hold section of the table, the column to take notice of is the "Force Difference" column. This column is the reduction on

the force necessary to hold the material at a given strain amount. Once the shape memory polymer was allowed to cool to ambient air temperature, which is well below the glass transition temperature, the required force to keep the material strained was 0. Also for Tecoflex® 80A, the percentage isn't as high as the other materials but overall it still needs less force to strain the material, while still having the ability to recover the best.

Tecoflex® 80A is a type of thermoplastic polyurethane, while Riteflex and Arnitel are copolyester materials, and Spandura and Tru-Stretch are woven materials. Shape memory polymers are in a class by themselves since they have the ability to change their material properties, but they need to me thermally induced to change their material properties. It seems the thermoplastic polyurethanes and the shape memory polymer type of materials provided the best strain and force results, while conducting the uniaxial experiments. Although, the stiffer materials that were presented in Table 4.5-1 need more force at a given strain they are better suited to handle to aerodynamic loads of the aircraft.

The next two tables are a material comparison matrix from the results of the biaxial experiments. Table 4.5-3 presents the results of the materials for the force and strain comparison biaxial experiments. The main purpose of the biaxial test stand was to get a better understand how the material would perform as a skin material if it was on a wing that had all the morphing capabilities that were discussed in Chapter 1, section 1.3. Basically, the biaxial test stand was design to try and mimic extreme condition that the material would be subjected to as a skin on a morphing wing.

The results presented in Table 4.5-3 show the maximum experimental strain that was recorded before the material ripped. Since this table is presenting the biaxial results the maximum strains shown are for the x- and y-direction. Also the forces relating to the maximum strains are shown. Although recovery results were sought while conducting the experiments, most of the materials ripped while only being strained a short amount when compared to the uniaxial straining amounts. The shape memory polymer was the only material that was not tested while conducting the biaxial experiments. The reason was the material was very difficult to handle, since the material had to be headed to 100 degrees Celsius to be viable to handle. A test was attempted, but the material broke while placing the shape memory polymer in the gripping devices. Since there were limited quantities of this material, no more shape memory polymer materials were left to test.

**Table 4.5-3.** Material comparison matrix of the force and strain experiments due to biaxial loading.

| | Force and Strain Comparison | | | | |
|---|---|---|---|---|---|
| **Material** | **Strain (x-dir)** (Max) | **Strain (y-dir)** (Max) | **Max. Force (x-dir)** (lbs) | **Max. Force (y-dir)** (lbs) | **Recovery Strain** (Worst) |
| Tecoflex® 80A | 0.454 | 0.426 | 17.79 | 14.40 | broke |
| Tecoflex® 100A | 0.222 | 0.233 | 41.37 | 34.44 | broke |
| Tecoflex® 93A | 0.322 | 0.238 | 163.99 | 147.42 | broke |
| Riteflex® 640A | 0.060 | 0.026 | 10.05 | 7.77 | broke |
| Riteflex® 663A | 0.077 | 0.072 | 23.25 | 24.14 | broke |
| Arnitel® | 0.268 | 0.323 | 125.21 | 131.94 | broke |
| Shape Memory Polymer | N/A | N/A | N/A | N/A | NA |
| Spandura® | 0.511 | 0.319 | 100.00 | 113.85 | inconclusive |
| Tru-Stretch® | 0.340 | 0.185 | 245.43 | 249.18 | inconclusive |

The first noticeable difference is the material's ability to strain while under a biaxial loading condition when it is compared to the uniaxial loading. The reported strains in Table 4.5-3 are strains that were recorded before the material ripped. Since the material ripped a recovery result could not be completed. But, there is still vital information that was used to make a conclusion. Again, Tecoflex® 80A performed the best under while undergoing biaxial deformation. The ability for it to strain the most, while requiring the least amount of force makes it a good material candidate for a morphing wing. Although a recovery analysis could not be done, the hypothesis is the material would be able to recover well. The reason is the results from the uniaxial experiment of the same material, Tecoflex® 80A, it was able to recover the best.

The material comparison for the strain and hold tests are shown in Table 4.5-4. The results presented for this part are strain in the x- and y-direction, max force, dissipated force, and the recovery strain. The "strain" is the strain amount the material was displaced to hold the material stationary. The "max force" is the maximum amount of force it took to strain the material to the displaced location. While, the "dissipated force" is the constant force the material needed once the material relaxed after undergoing plastic deformation. The "force difference" column shows the percentage difference of the reduction of force that was needed to hold the material at the strained location. Although a recovery strain was warranted, the materials were strained a limited amount, which would not allow a conclusive determination of how much the material recovered.

**Table 4.5-4.** Material comparison matrix of the strain and hold experiments due to biaxial loading.

| | Strain and Hold | | | | | | | | |
|---|---|---|---|---|---|---|---|---|---|
| **Material** | **Strain (x-dir) (Max)** | **Strain (y-dir) (Max)** | **Max. Force (x-dir) (lbs)** | **Max. Force (y-dir) (lbs)** | **Dissipated Force (x-dir) (lbs)** | **Dissipated Force (y-dir) (lbs)** | **Force Difference (x-dir) (%)** | **Force Difference (y-dir) (%)** | **Recovery Strain (Worst)** |
| Tecoflex® 80A | 0.300 | 0.200 | 13.28 | 11.68 | 9.76 | 8.43 | 26.50 | 27.84 | Inconclusive |
| Tecoflex® 100A | 0.050 | 0.040 | 18.85 | 23.16 | 11.05 | 9.43 | 41.36 | 59.29 | Inconclusive |
| Tecoflex® 93A | N/A | N/A | N/A | N/A | N/A | N/A | N/A | N/A | N/A |
| Riteflex® 640A | 0.080 | 0.060 | 10.55 | 8.07 | 8.85 | 6.70 | 16.14 | 17.04 | Inconclusive |
| Riteflex® 663A | 0.074 | 0.083 | 22.54 | 24.96 | 15.06 | 16.50 | 33.17 | 33.88 | Inconclusive |
| Arnitel® | N/A | N/A | N/A | N/A | N/A | N/A | N/A | N/A | N/A |
| Shape Memory Polymer | N/A | N/A | N/A | N/A | N/A | N/A | N/A | N/A | N/A |
| Spandura® | 0.511 | 0.319 | 100.00 | 113.85 | 72.73 | 90.47 | 27.27 | 20.53 | Inconclusive |
| Tru-Stretch® | 0.224 | 0.071 | 44.45 | 246.40 | 32.85 | 213.53 | 26.10 | 13.34 | Inconclusive |

While the strain and hold test were completed with data being gathered for the stain and force, the recovery of the material was not gathered. The reason is the material was not strained enough without breaking to notice any recovery. Therefore, the results for the recovery are inconclusive. On the other hand, notice that even though the material is being strained biaxially, the amount of forced required to hold the material at a given displacement does reduce.

Tecoflex® 93A, Arnitel®, and the shape memory polymer were not tested for the strain and hold experiments. The reason why is simply there were no more materials left to test of those particular materials. But, some important conclusions can be determined form the other results presented in Table 4.5-4. Again Tecoflex® 80A performed the best. The ability for this material to strain while needing the least force seems to make it the prime candidate to be used as a skin material for a morphing wing.

The final material comparison is from the results of the pressure deflection experiments. Table 4.5-5 shows the maximum pressure the material could sustain before breaking with the associated amount the material deflected. As a reminder, the applied pressure load was applied on a surface area of 4 square inches.

**Table 4.5-5.** Material comparison matrix of the pressure deflection experiments.

| Material | Max Sustained Pressure (psi) | Deflection (in) |
|---|---|---|
| Tecoflex® 80A | 7 | 1.25 |
| Tecoflex® 100A | 5 | 1.20 |
| Tecoflex® 93A | 56* | 1.05 |
| Riteflex® 640A | 5 | 0.40 |
| Riteflex® 663A | 5 | 0.28 |
| Arnitel® | 15 | 0.63 |
| Shape Memory Polymer (hard) | 45 | 0.06 |
| Shape Memory Polymer (soft) | 5 | 1.32 |
| Spandura® | 1 | 0.32 |
| Tru-Stretch® | 1 | 0.30 |

* Maximum pressure allowed by air compressor

Although Tecoflex® 80A results were the best for the uniaxial and biaxial experiments, the material could not sustain a high pressure load. On the other hand, materials that had a higher Young's Modulus such as Tecoflex® 80A, like Tecoflex® 93A and Arnitel® were able to sustain a

higher pressure load. When the shape memory polymer was in its solid state it was able to sustain a pressure load of 45 psi. But, when the shape memory polymer was in its rubbery state, it was only able to sustain a pressure load of 4 psi. Since a morphing wing changes shape, the material will have to have to ability to change shape. For an shape memory polymer to change shape it has to be heated up to it's rubbery state, during this state the shape memory polymer can not handle a high pressure load. Even though Spandura® and Tru-Stretch® seemed to be stiff materials, based off the uniaxial and biaxial experiments, they performed the worst for the pressure deflection tests. The reason is the material is woven, which allows air to pass through the material. Therefore, it is not a prime candidate for a skin material.

Based off the results that were presented, there is a contradiction in the material requirements. On one hand there is a need for the material to be elastic and have a high recovery, yet the material needs to be strong enough to hold the aerodynamic loads of an aircraft. If a material was able to strain and recovery well, it was not able to sustain a high pressure load. While if the material was not woven, a material that did not strain and recover well could handle a higher sustained pressure load. Currently, none of the material tested for this research effort meet the requirements to be a suitable material for a morphing wing.

## 4.6 Chapter Summary

The first section of this chapter gave a brief summary of what this chapter presented and identified the separate sections of the chapter. The second section of this chapter first went into an in-depth discussion of how the data was analyzed for the uniaxial experiments.

The third section of this chapter presented the biaxial experimental results. At the beginning of this section there was a brief overview concerning how the results would be presented. Within this section, each material had its own subsection where the results were presented. This would allow each material's results to be presented separately.

The fourth section presents the performance of each material when subjected to a pressure load. At the beginning of the section, the there was on overview how the experiments were conducted. Then, the results of each material were presented in their separate subsections.

The most important section of this chapter was the fifth section. This section directly compared each material to one another by using a comparison matrix. Although the comparison matrixes were separate for each experiment (uniaxial deformation, biaxial deformation, and pressure deflection) it allowed an easy visual of how the material performed. Also this section showed that the material's performance contradicted the criteria. Hence, a material that was able to strain and recover well was not able to carry a high sustain load, and vise-a-versa.

# Chapter 5

# Conclusion

## 5.1 Brief Thesis Summary

At the beginning of the thesis, a background of the different morphing wing configurations was discussed. These different wing configurations helped prove that a rigid body material could not be used as a skin material for the wing. Understand the different wing shapes, criteria were determined to assist in determining different materials that are readily available in the commercial market to test. In the material's section of the thesis, each material that was tested was presented, specifically discussing how the material met the criteria that were determined for a candidate skin material for a morphing wing. Next, Chapter 3 gave an overview of the test stands used to conduct the different experiments. Specifically for each test stand, the different components and sensors were presented. Chapter 4 went over the results of the each material for the uniaxial, biaxial, and pressure deflection experiments. At the end of Chapter 4, comparison charts compared the performance of each material against one another.

Although none of the materials tested were suitable to be a material for a skin of a morphing wing, the results help show the direction engineers should take in the future when investigating other candidate materials. Two specific materials that seemed to work the best are Tecoflex 80A and the shape memory polymer. Materials similar to those should be investigated in the future. Section 5.3 will discuss other candidate materials that could be used for a morphing wing.

## 5.2 Improvements for the Test Stands

An enhancement that could be considered for the uniaxial deformation test stand is designing a system that would keep the material from necking. The performance of the material will probably change if the material was not allowed to neck. Specifically, the material might not be able to strain as much before it breaks, also the necessary forces to strain the material might increase. It would be interesting to see the comparison of the strain and force when the material is allowed to neck and when the material is not allowed to neck.

Another improvement is for the pressure deflection test stand. The applied pressures were recorded from a gage regulator. The reason for using a gage regulator is the sustained pressures the material could handle was sought. A better way to gather the pressure would be to use a pressure transducer that could be screwed into the regulator and using dSPACE to record the data. This would also allow engineers to compare the dynamic changes in the pressure as well as the displacement, since the laser vibrometer already use dSPACE to record the data.

When conducting the experiments for the shape memory polymer an improvement would be to use thermocouples throughout the housing unit, instead of using one thermometer. This would make sure the shape memory polymer material being tested is exposed to a constant temperature at all the locations of the material.

## 5.3 Other Candidate Materials

The materials tested gave a good representation of the type of materials that are currently available in the commercial market. It was determined that none of the materials tested are good candidate materials for a morphing wing. Therefore, there needs to be forum where the morphing wing community and the materials community can get together and discuss specifically what material characteristics are needed for a candidate material for a morphing wing skin. In the material's section of this report, it was determined a candidate material needs to be able to be elastic, flexible, high recovery, resistant different weather conditions, resistant to abrasions and chemicals, and having a hardness number high enough to handle the aerodynamic loads of an aircraft while in flight.

Even though the shape memory polymers did not perform as well as anticipated, these types of materials meet the fundamental criteria for a morphing wing skin. If the shape memory polymer could be engineered to be easier to handle, while still having the similar material characteristics as Tecoflex® 80A while above the glass transition temperature, and having a lower glass transition temperature that is slightly higher than room temperature it could be the future material for a morphing wing skin. The only downside to these types of materials is the need for a heat source to allow the material to deform.

Tecoflex® 80A overall performed the best out of all the other candidate materials. The only downside is the inability for the material to handle high sustained pressure loads. If this material could be slightly modified so the material could handle higher pressure loads, while still having the same strain abilities it would make a material that could meet all the specifications that are required for a morphing wing skin.

Another possibility is combining yarn materials like Spandura® and Tecoflex® 80A together. The yarns that are made out of Spandura® were formulated with more hard chains than soft polyurethane chains. If yarns could be designed with more soft polyurethane chains that is layered with a material like Tecoflex® 80A it might work better. The increase in the soft polyurethane chains would allow the yarns to deform more with less force. Yet, the yarns would act like rebar giving the material the strength it by carrying the pressure loads. The Tecoflex® 80A material would keep the air from passing through the woven yarns.

## 5.4 Analytical Solution

Although analytical solutions were not performed in this report, there is a need for predictive analytical models and solutions. In the material's section of this report, a literature review was completed discussing possible avenues that could be taken for an analytical solution. An analytical solution would give engineers an advantage, since a MATLAB program can be coded to output general performance results. These initial results could be used to determine if a material meets the criteria for a morphing wing skin. If the initial solutions meet the criteria, testing can then be completed. This would decrease the time an engineer has to spend in the lab performing experiments for an initial understanding how the material would perform.

## 5.5 Future Work

The test stands that were designed allow engineers an initial understanding how a candidate morphing wing skin material will perform. Specifically, determining the required forces needed to strain the material. Also, the test stands can be used to determine if less force is needed to hold the material once it's been strained. The pressure deflection test stand determines the maximum pressure load the material can handle before being damaged. The pressure deflection test stand allows engineers to compare how much the material will deflect while undergoing a pressure load. These test stands can be used in the future to test other candidate materials, as well as help the engineering community set standards for testing candidate morphing wing materials. One intuitive result that was not determine is the comparison of how much force is required and how much the material can strain at different strain rates. This result will also be a determining factor for a successful skin material for a morphing wing.

Engineers need standards to follow. These standards allow engineers to compare the results of different materials that are conducted by performing the exact same experiments. The test stands that were designed to gather the results that were presented in this report could help set the standards. Also, for the morphing wing program to be successful in the future, it is vital that a suitable skin material is designed. As stated before, the material engineers and the morphing wing engineers get together to discuss what type of material is needed.

## 5.6 Contributions

This research effort is a starting point to further investigate plausible skin materials for a morphing wing. Although none of the materials tested are suitable, the results determined that woven materials cannot sustain a pressure load, since air is allowed to pass through the material. The experiments also showed that the stiffer materials could sustain a higher pressure load, yet needed more force to strain the material and vise-versa. Although shape memory polymers can be strained easily, they need to be thermally induced. Finally, the results provided in this research effort can be use to set standards. In the future, engineers will be able to compare their material(s) to the materials tested in this report. By comparing the same results engineers will be able to easily discuss other candidate materials for morphing wings.

# Bibliography


| | |
|---|---|
| Bunker Corporation's website: | http://www.bunkercorp.com/pages/hypr_fx.htm,14 October 2003 |
| Cordura's website: | http://www.cordura.com/FAQ.html, 11 October 2003 |
| DMS's website: | http://www.dsm.com/en_US/html/dep/arnitel.htm, 12 October 2003 |
| Lycra's website: | http://www.invista.com/lycra.html, 11 October 2003 |
| Omega's website: | http://www.omega.com, 20 May 2003 |
| Seattle Fabric's website: | http://www.seattlefabrics.com/stretch.html, 11 October 2003 |
| Thermedics Polymer Products: | http://www.thermedicsinc.com/english/en/products/medical, 12 October 2003 |
| Ticona's website : | http://www.ticona.com, 11 October 2003 |
| Unimeasure's website: | http://www.unimeasure.com, 20 May 2003 |

Arrison, Laura, et al. "2002-2003 AE/ME Morphing Wing Design," Senior Design Final Report, Virginia Tech, 1 May 2003.

Barr, Larine. News@afrl: November 2002, Volume III, Issue 11. 13 October 2003. Available: http://www.afrl.af.mil/news/nov02/

Barry, L. Patrick. "Buck Rogers, Watch Out!" Science@NASA. Internet. 13 October 2003. Available: http://science.nasa.gov/headlines/y2001/ast01mar_1.htm.

Bhattacharyya, A., "Isothermal Mechanical Response of Shape Memory Polymers (SMP)-Based Hybrid Models and SMP-Composites." In Press.

Boresi, Arthur P., Richard J. Schmidt, and Omar M. Sidebottom. *Advanced Mechanics of Materials 5th edition.* United States of America: John Wiley & Sons, 1993.

Chen, Wei, Chengye Zhu, and Xuerong Gu, 2002. "Thermosetting Polyurethanes with Water-Swollen and Shape Memory Properties," *Journal of Applied Polymer Science*, Vol. 94, pp. 1504-1512.

Cone Jr., Clarence D. "The theory of induced lift and minimum induced drag of nonplanar lifting systems." NASA TR R-139, 21 February 1962.

Flick, Pete. News@afrl: November 2002, Volume III, Issue 11. 13 October 2003. Available: http://www.afrl.af.mil/news/nov02/.

Fourné, R., GmbH, Fourné Polmertechik, 2001. "Melt Spinning of Elastane Yarns," *Chemical Fibers International*, Vol. 51, pp 46-48.

Freakley, P.K. and A.D. Payne. *Theory and Practice of Engineering with Rubber*. Essex: Applied Sciences Publishers LTD, 1978.

Gaymans, R.J., J. Krijgsman, and M. C. E. Niesten , 2000. "Melt Spinnable Elastane (Spandex) Fibers from Segmented Copolyetheresteraramids," *Chemical Fibers International*, Vol. 50, pp. 257-260.

Hayashi, Shunichi and Kondo Satoru, 1995. "Room-Temperature-Functional Shape-Memory Polymers." *Plastic Engineering*, February 1995: pp. 29-31.

Hayashi, S., P.H. Lin, and H. Tobushi, 1994. "Deformation properties of polyurethane shape memory polymers." Proceedings of the First International Conference on Shape Memory and Superelastic Technologies, 1994, Pacific Grove California, pp. 109-114.

Hayashi, Shunichi, Shinichi Kojima, and Hisaaki Tobushi, 1992. "Mechanical Properties of Shape Memory Polymer of Polymer of Polyurethane Series (Basic Characteristic of Stress-Strain Temperature Relationship)," *JSME International Journal*, Series I, Vol. 35, No.3, pp. 296-302.

Indian Head Institute. *Rubber Engineering*. New Delhi, India, McGraw-Hill, 2000.

Mainer-Schneider, Maibach, and Obermeir, 1995. "A New Analytical Solution for the Load-Deflection of Square Membranes," *Journal of Microelectromechanical systems*, Vol. 4, No. 4, pp. 238-241.

Kroo, Ilan., 2001, "Drag due to lift: Concepts for prediction and reduction," *Annual Reviews: Fluid Mech.,* Vol. 33, pp. 587-617.

Lee, Yup, Kim, Kyu Byung, and Mao Xu, 1996. "Polyurethanes Having Shape Memory Effects," *Polymer*, Vol. 37, No.26, pp. 5781-5793.

Liang, C., E. Malafeew, and C.A. Rogers, 1997. "Investigation of Shape Memory Polymers and Their Hybrid Composites," *Journal of Intelligent Material Systems and Structures*, Vol.8, No. 1, pp. 380-386.

Lui, Changdeng, et al, 2002. "Tailored Shape Memory Polymers: Not all SMPs are Created Equial." Proceedings of The First World Congress on Biomimetics, December 9-11, Albuquerque, New Mexico, pp. 1-7.

McBowan, Anna-Maria R., et al. "Research Activities within NASA's Morphing Program." Proceedings of the NATO-RTO Workshop on Structural Aspects of Flexible Aircraft Control, October 18-21, 1999, Ottawa, Canada.

Monkman, G.J, 2000. "Advances in shape memory polymer actuation," *Mechatronics*, Vol. 10, No. 4/5, pp 489-498.

Pettit, Greg. Pictures captured from a movie showing different morphing wing configurations. Center for Intelligent Materials Systems and Structures, Virginia Tech. Blacksburg, Virginia, 2001.

F/A-18 with AAWNASA Dryden photo. Picture. NASA. 1 October 2003. Available: http://www.dfrc.nasa.gov/Gallery/Photo/AAW.

Ugural, A.C. and Fenster, S.K. *Advanced Strength and Applied Elasticity*. New York: Elsevier Science Publishing Co., Inc, 1981.

van Dam, C.P. Letter. Nature January 29, 1987. "Efficiency characteristics of crescent-shaped wings and caudal fins."

## **Appendix A:** Material Properties of Tecoflex

| | ASTM | EG-80A | EG-85A | EG-93A | EG-100A | EG-60D | EG-65D | EG-68D | EG-72D |
|---|---|---|---|---|---|---|---|---|---|
| **Durometer (Shore Hardness)** | D2240 | 72A | 77A | 87A | 94A | 51D | 60D | 63D | 67D |
| **Spec Gravity** | D792 | 1.04 | 1.05 | 1.08 | 1.09 | 1.09 | 1.10 | 1.10 | 1.11 |
| **Flex Modulus (psi)** | D790 | 1,000 | 2,300 | 3,200 | 10,000 | 13,000 | 37,000 | 46,000 | 92,000 |
| **Ultimate Tensile (psi)** | D412 | 5,800 | 6,200 | 7,700 | 8,200 | 8,300 | 8,300 | 8,300 | 8,100 |
| **Ultimate Elongation (%)** | D412 | 660 | 550 | 390 | 370 | 360 | 360 | 350 | 310 |
| **Tensile (psi) @ 100%** | D412 | 300 | 600 | 1,000 | 1,600 | 1,800 | 2,200 | 2,600 | 3,400 |
| **Tensile (psi) @ 200%** | D412 | 500 | 900 | 1,900 | 3,000 | 2,900 | 3,000 | 3,700 | 4,800 |
| **Tensile (psi) @ 300%** | D412 | 800 | 1,400 | 4,300 | 5,600 | 5,600 | 6,000 | 6,300 | 7,100 |
| **Melt Index g/10 min at 2160 g load** | D1238 | 3.5 (175C) | 4.0 (165C) | 5.3 (170C) | 4.8 (175C) | 3.4 (175C) | 3.8 (175C) | 3.5 (175C) | 4.0 (175C) |
| **Mold Shrinkage** | D955 | .008 to .012 | .008 to .012 | .006 to .010 | .006 to .010 | .004 to .008 | .004 to .008 | .004 to .008 | .004 to .006 |

Taken from: http://www.thermedicsinc.com/english/en/products/medical/med1

## **Appendix B:** Material Properties of Arnitel PM381

| MECHANICAL PROPERTIES* | Unit | Test Method | PM381 |
|---|---|---|---|
| Tensile Strength, (500 mm/minute) | MPa ( psi ) | ISO 527 | 14 ( 2,030 ) |
| Tensile Modulus (1 mm/minute) | MPa ( psi ) | ISO 527 | 60 ( 8,700 ) |
| Tensile Elongation, break | % | ISO 527 | 450 |
| Tensile stress ( 5% / 10% / 50% strain ) | MPa | ISO 527 | 2.6 / 4.2 / 7.1 |
| Initial Tear Resistance | kN/m | ASTM 1004 | 40 |
| Izod Impact, notched, 23°C | $kJ/m^2$ ( ft-lbs/in ) | ISO 1801A | No Break (ductile failure) |
| Izod Impact, notched, -30°C | $kJ/m^2$ ( ft-lbs/in ) | ISO 1801A | No Break (ductile failure) |
| **PHYSICAL PROPERTIES*** | | | |
| Density | $gm/cm^3$ | ISO 1183 | 1.16 |
| Hardness | Shore D | ASTM D2240 | 38 |
| Mold Shrinkage, 2 mm thickness | % | ISO 2577 | 1.5 - 1.8 |
| Equilibrium Water Absorption 50% R.H. / 23°C | % | ISO 62 | 0.4 |
| Tabor Abrasion, H-18 Wheel | mg/1000 cycles | ASTM D1044 | 274 |
| UL Flame Class | - | UL94 | UL94-HB |
| **THERMAL PROPERTIES*** | | | |
| Vicat Softening Temperature (10 N Load) | °C ( °F ) | ISO 306 | 140 ( 284 ) |
| Melting Point | °C ( °F ) | ISO 3146 | 212 ( 414 ) |
| Melt Flow Index ( 240°C / 2.16 kg ) | gms / 10 minutes | ASTM D1238 | 6 |
| Coef. of Linear Thermal Expansion | E-5 / °C | ASTM E831 | 15 |
| **ELECTRICAL PROPERTIES*** | | | |
| Dielectric Strength | kV/mm | IEC 243 | 20 |
| Dielectric Constant, 1 kHz | - | IEC 247 | 5.6 |
| Dissipation Factor, 1 kHz | E-4 | IEC 247 | 370 |
| Comparitive Tracking Index | V | IEC 112 | 600 |
| Volume Resistivity | ohm-cm | IEC 93 | 1E +12 |
| Surface Resistivity | ohm/sq | IEC 93 | 1E +14 |

Taken from: http://www.dsmep.com/america/products/data_sheets/arnitel/al_pm381.pdf

# Appendix C: Specifications for the Transducers

### LC-101-50:

**SPECIFICATIONS**
**Excitation:** 10 Vdc, 15 Vdc max
**Output:** 3 mV/V ±.0075 mV/V
**Linearity:** ±0.03% FSO (0.1% 40 K)
**Hysteresis:** ±0.02% FSO(0.1% 40 K)
**Repeatability:** ±0.01% FSO (0.05% 40 K)
**Zero Balance:** ±1% FSO
**Agency Approval:** FM Intrinsically Safe IS/I.II.III/1/CDEFG - Standard
**Operating Temp Range:** -40 to +93°C (-40 to 200°F)
**Compensated Temp Range:** 17 to 71°C (60 to 160°F)
**Thermal Effects:**Zero: 0.001% FSO/°F Span: 0.001%FSO/°F
**Safe Overload:** 150% of Capacity
**Ultimate Overload:** 300% of Capacity
**Input Resistance:** 350 ±10 Ohms
**Output Resistance:** 350 ±10 Ohms
**Full Scale Deflection:** 0.010 to 0.020"
**Construction:** 17-4 PH Stainless Steel
**Electrical:** LC101: up to 200 lb = 30 ft 24 AWG; 250-2000 lb = 30 ft 20 AWG; 3000 lb and up= 15 ft 20 AWG 4-conductor shielded cable, LC111:up to 200 lbs 4 pin connector mating connector: PT06F8-4S (not included) >200 lbs, 6 pin connector, mating connector: PT06F10-6S (not included)

Specifications provided by Omega's website: http://www.omega.com/ppt/pptsc.asp?ref=LC101

**LC-105-250:**

**SPECIFICATIONS:**
Excitation: 10 Vdc, 15 Vdc max
Output: 3 mV/V ±.0075 mV/V
Linearity: ±0.03% FSO
Hysteresis: ±0.02% FSO
Repeatability: ±0.01% FSO
Zero Balance: ±1% FSO
Agency Approval: FM Intrinsically Safe IS/I.II.III/1/CDEFG Standard.
Operating Temp Range: -40 to 93°C (-40 to +200°F)
Compensated Temp Range: 17 to 71°C (60 to 160°F)
Thermal Effects: Zero: 0.001% FSO/°F Span: 0.001% Rdg/°F
Safe Overload: 150% of Capacity
Ultimate Overload: 300% of Capacity
Bridge Resistance: 350 ± 5 ohms
Full Scale Deflection: .010 to .020"
Construction: Aluminum
Electrical: <200 lb: 30 ft (9.1 m) 24 AWG >250 lb: 30 ft (9.1 m) 20 AWG
4-conductor shielded PVC cable

Specifications provided by Omega's website: http://www.omega.com/ppt/pptsc.asp?ref=LC105

# Appendix D: Specifications for the String Potentiometers

## *LX-PA* SERIES
### *RATIOMETRIC VOLTAGE OUTPUT*

The **UniMeasure LX-PA Series** linear position transducer with analog output is a low cost, compact alternative for use in light to moderate duty applications in dry environments. The plastic bodied device is ideal for high volume OEM situations where cost is a major consideration and in applications where small size or low weight are of paramount importance.

Model LX-PA is available in eleven different measurement ranges with a maximum range of 50" (1250 mm). The output is voltage from a potentiometric voltage divider circuit. In standard form, the electrical connections are made directly to the contacts on the potentiometer of the unit. Optional electrical cable attached to the potentiometer is available in various lengths. Standard potentiometer value is 1K ohm with optional values of 2K, 5K and 10K ohm available.

SPECIFICATIONS

General

| | |
|---|---|
| Measurement Ranges | See Table 1 |
| Sensing Device | Precision Potentiometer |
| Resolution | Essentially Infinite |
| Linearity | |
| 2", 2.8", 3.8" 4.7" ranges | ±1.0% Full Scale |
| 10" to 25" ranges | ±0.5% Full Scale |
| 30" to 50" ranges | ±0.25% Full Scale |
| Repeatability | ±0.03% Full Scale |
| Construction | Thermoplastic Body |
| Cable | Ø.018 (0.46 mm) Jacketed Stainless Steel |
| Wire Rope Tension | See Table 1 |
| Weight | 3 oz. (85 gm) |
| Connections | Solder terminals |
| Dimensional Information | See Next Page |
| Life | |
| Ranges to 4.7" | 1,000,000 full stroke cycles |
| Ranges 10" to 25" | 250,000 full stroke cycles |
| Ranges 30" to 50" | 125,000 full stroke cycles |

Electrical

| | |
|---|---|
| Input Impedance | 1000 Ω ±15% |
| Output Impedance | 0 to 1000 Ω |
| Excitation Voltage | 25 Volts max. AC or DC |

Environmental

| | |
|---|---|
| Operating Temperature | -25°C to 75°C |
| Storage Temperature | -50°C to 80°C |
| Operating Humidity | 95 R.H. max. non-condensing |
| Vibration | 15 G's 0.1 ms max. |
| Shock | 50 G's 0.1 ms max. |
| Ingress Protection | NEMA 1, IP-40 |

**TABLE 1**

| MODEL | RANGE (inch) | RANGE (mm) | NOMINAL OUTPUT (mV/V/in) | NOMINAL OUTPUT (mV/V/mm) | NOMINAL WIRE ROPE TENSION (oz) | NOMINAL WIRE ROPE TENSION (N) |
|---|---|---|---|---|---|---|
| LX-PA-2 | 2 | 50 | 469 | 18.5 | 16 | 4.4 |
| LX-PA-2.8 | 2.8 | 70 | 341 | 13.4 | 14 | 3.9 |
| LX-PA-3.8 | 3.8 | 96 | 258 | 10.1 | 11 | 3.1 |
| LX-PA-4.7 | 4.7 | 120 | 207 | 8.1 | 8 | 2.2 |
| LX-PA-10 | 10 | 250 | 88 | 3.5 | 16 | 4.4 |
| LX-PA-15 | 15 | 380 | 64 | 2.5 | 14 | 3.9 |
| LX-PA-20 | 20 | 500 | 49 | 1.9 | 11 | 3.1 |
| LX-PA-25 | 25 | 625 | 39 | 1.5 | 8 | 2.2 |
| LX-PA-30 | 30 | 750 | 32 | 1.3 | 14 | 3.9 |
| LX-PA-40 | 40 | 1000 | 24 | 1.0 | 11 | 3.1 |
| LX-PA-50 | 50 | 1250 | 20 | 0.8 | 8 | 2.2 |

CIRCUIT DIAGRAM

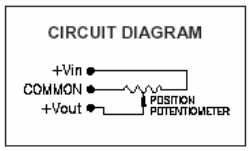


Specifications provided by Unimeasure's website:
http://www.unimeasure.com/obj--pdf/pdf-lx-pa.pdf

# Appendix E: Uniaxial Experimental Data

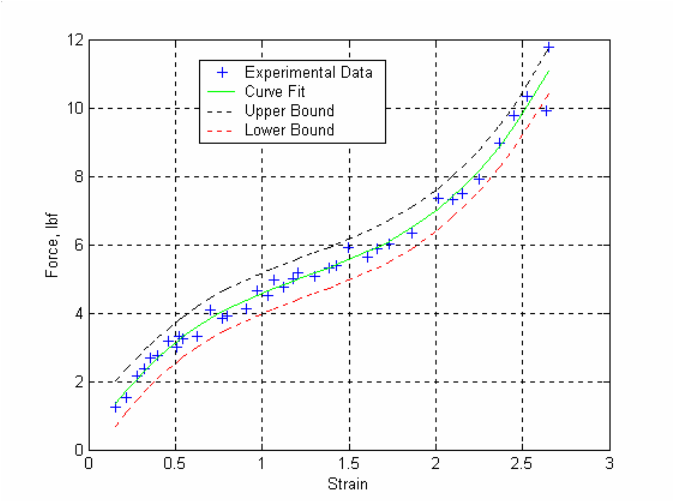


**Figure E-1.** Experimental results of Tecoflex® 80A, experiment 1b.

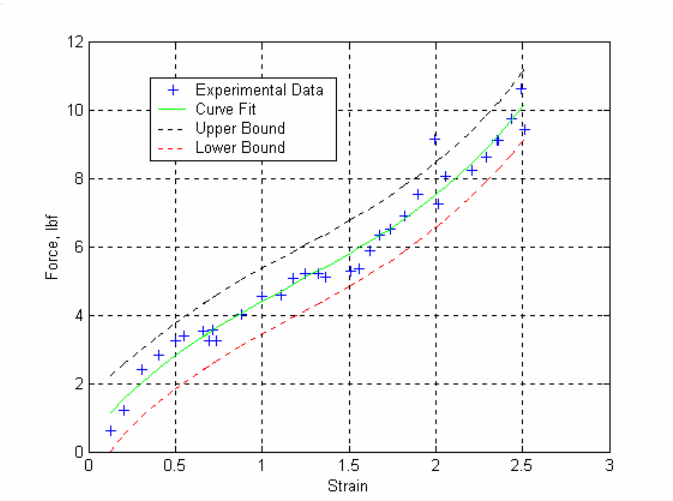


**Figure E-2.** Experimental results of Tecoflex® 80A, experiment 1c.

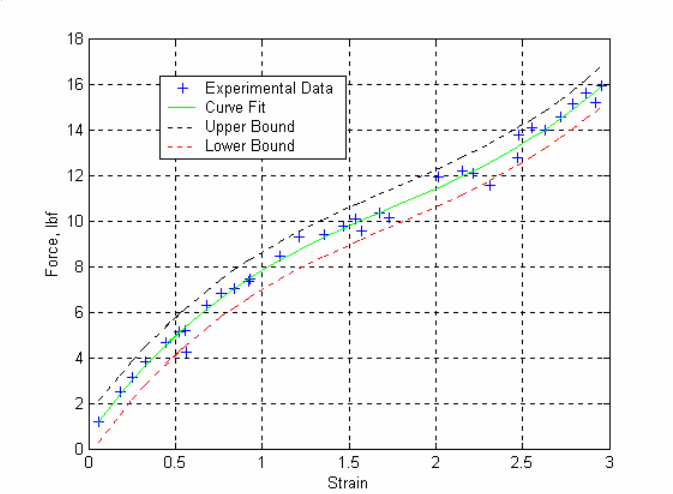


**Figure E-3.** Experimental results of Tecoflex® 80A, experiment 2a.

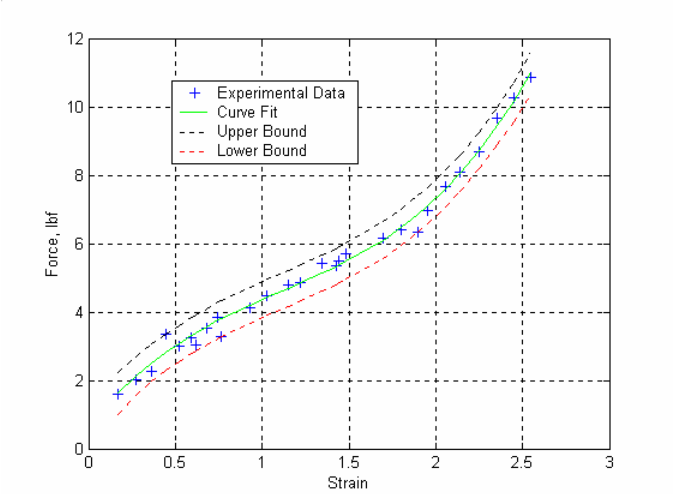


**Figure E-4.** Experimental results of Tecoflex® 80A, experiment 2b.

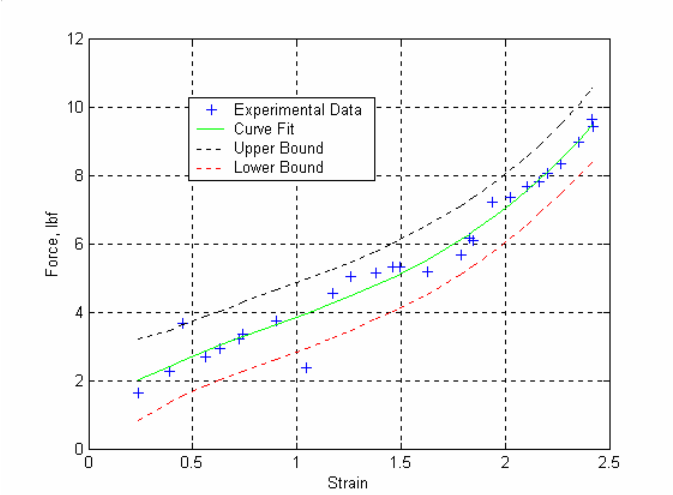


**Figure E-5.** Experimental results of Tecoflex® 80A, experiment 2c.

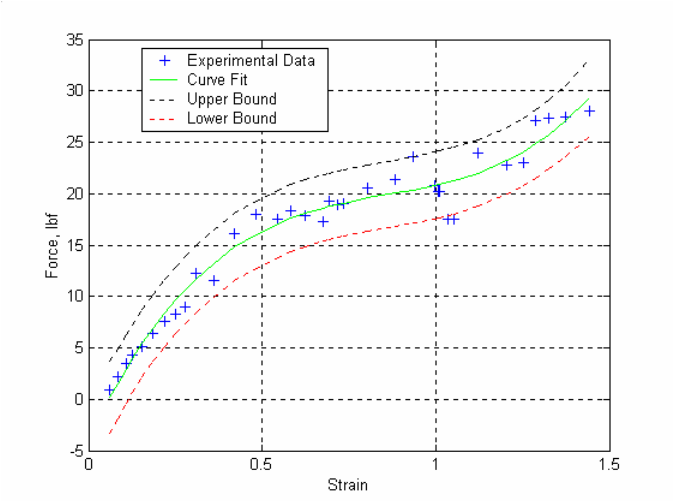


**Figure E-6.** Experimental results of Tecoflex® 100A, experiment 1.

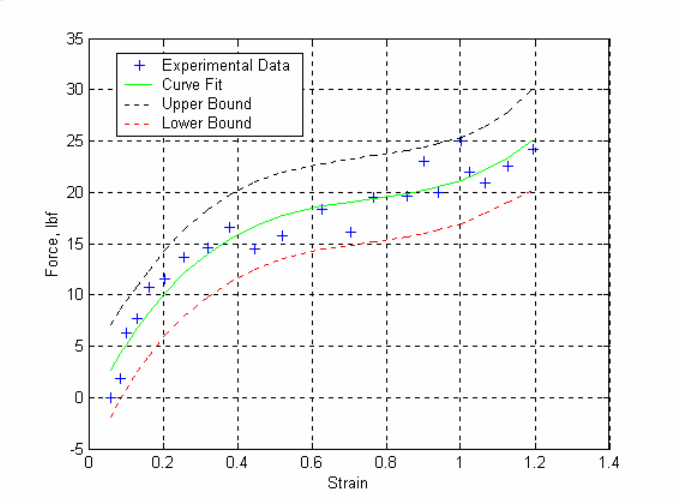


**Figure E-7.** Experimental results of Tecoflex® 100A, experiment 2.

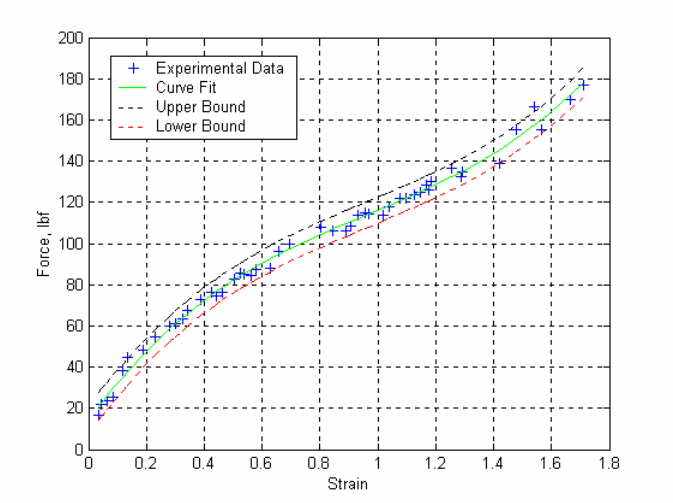


**Figure E-8.** Experimental results of Tecoflex® 93A, experiment 1.

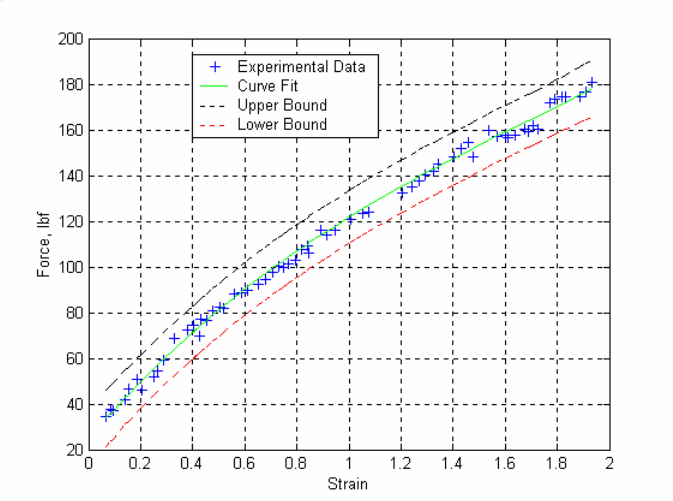


**Figure E-9.** Experimental results of Tecoflex® 93A, experiment 2.

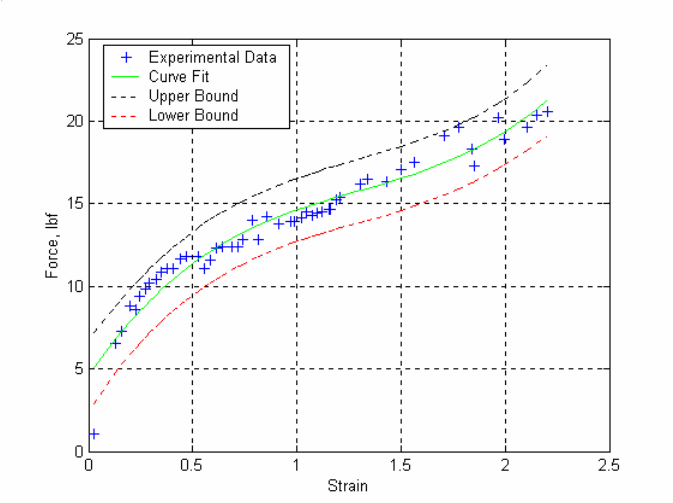


**Figure E-10.** Experimental results of Riteflex® 640, experiment 1.

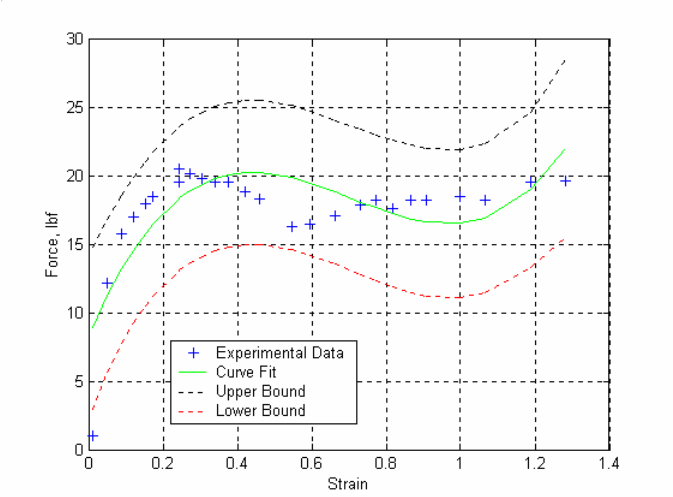


**Figure E-11.** Experimental results of Riteflex® 663, experiment 1.

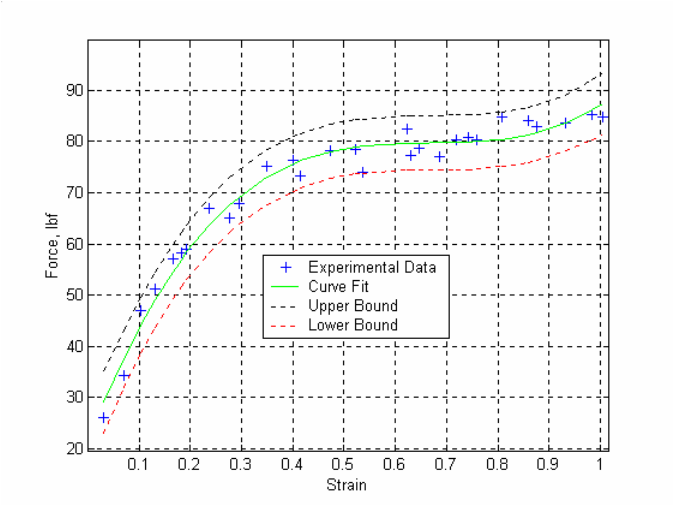


**Figure E-12.** Experimental results of Arnitel®, experiment 1.

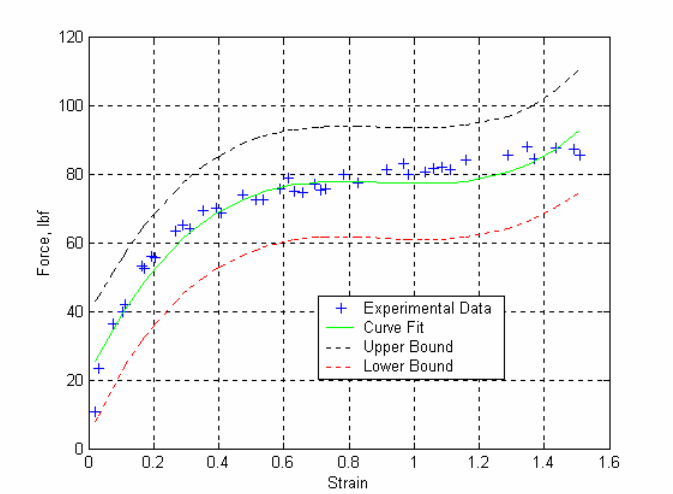


**Figure E-13.** Experimental results of Arnitel®, experiment 2.

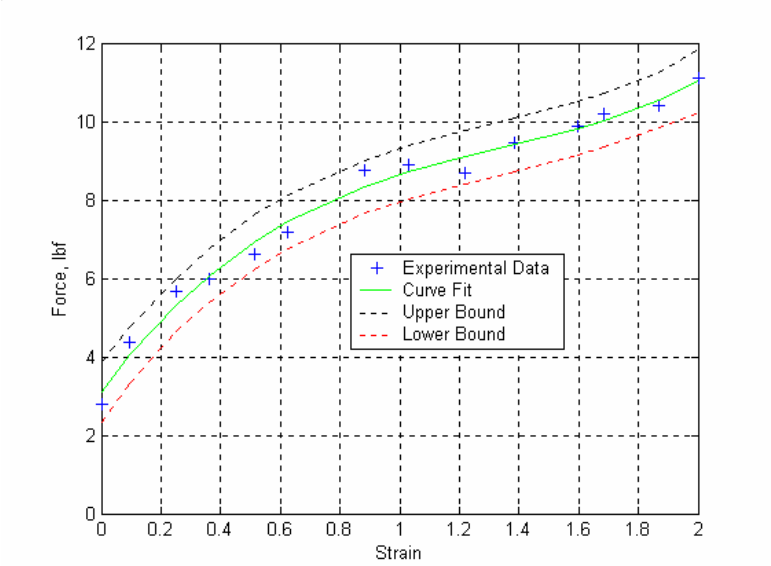


**Figure E-14.** Experimental results of the shape memory polymer, experiment 1.

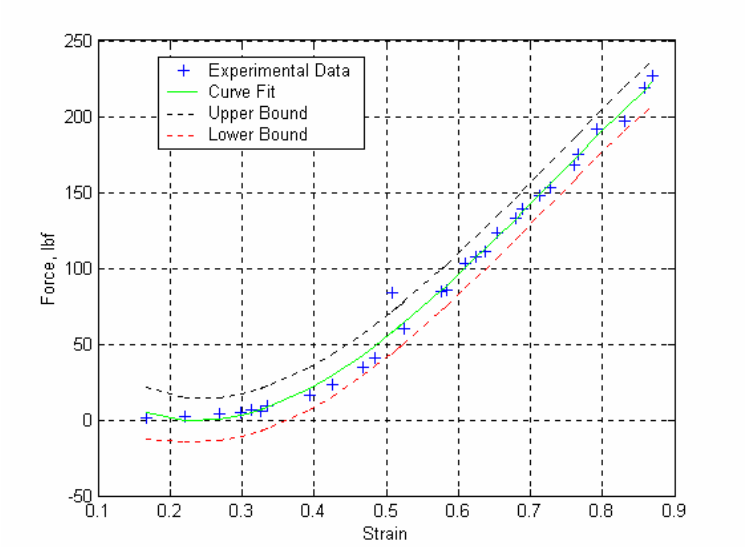


**Figure E-15.** Experimental results of Spadura®, experiment 1a.

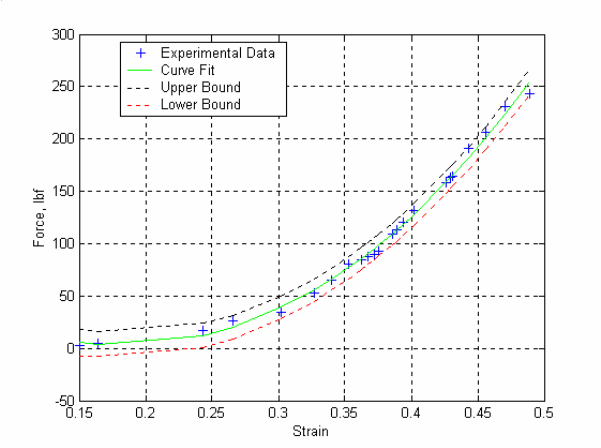


**Figure E-16.** Experimental results of Spadura®, experiment 1b.

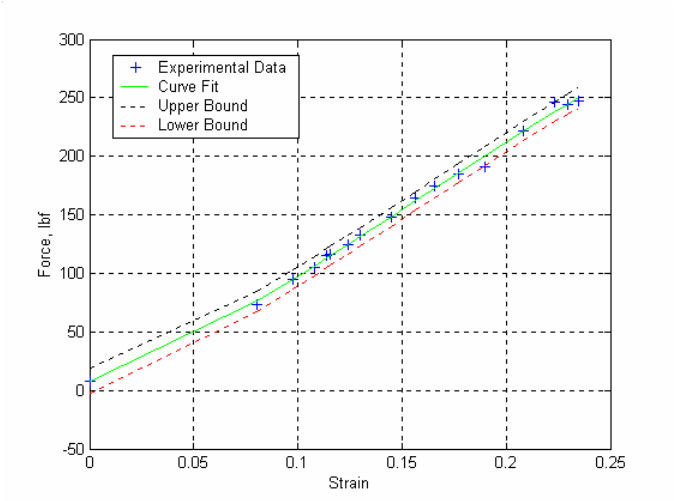


**Figure E-17.** Experimental results of Tru-Stretch®, stiffly woven experiment 1.

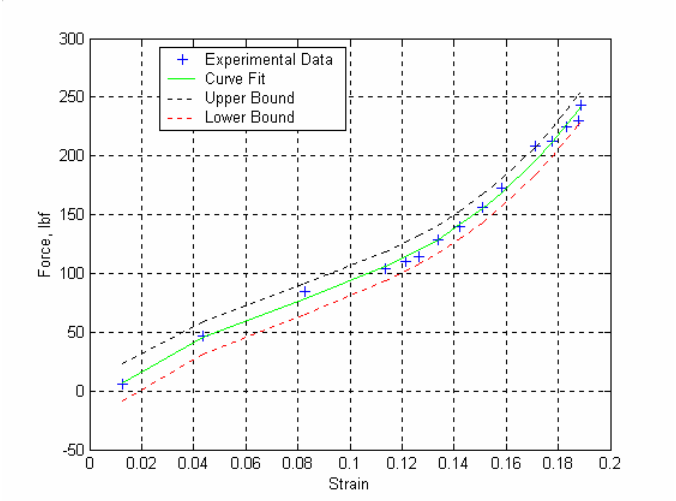


**Figure E-18.** Experimental results of Tru-Stretch®, stiffly woven experiment 2.

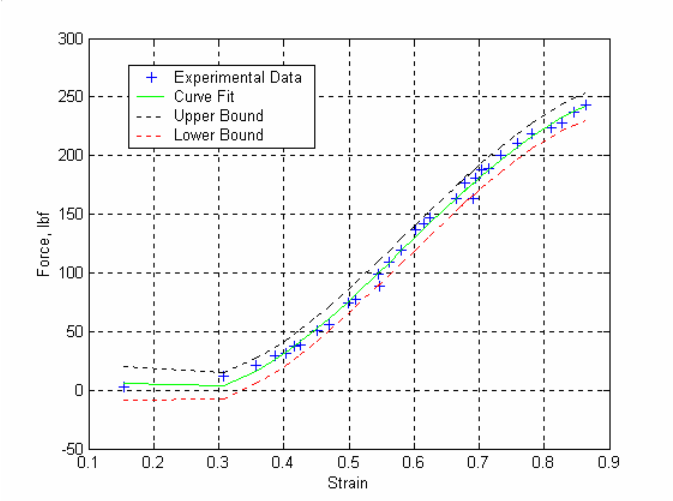


**Figure E-19.** Experimental results of Tru-Stretch®, lightly woven experiment 1.

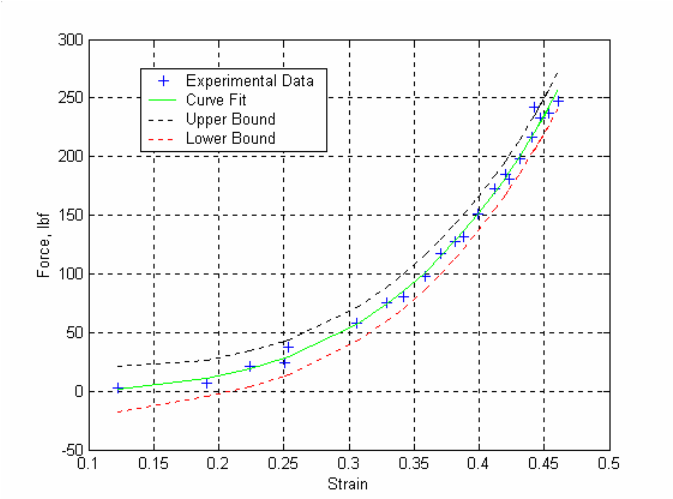


**Figure E-20.** Experimental results of Tru-Stretch®, lightly woven experiment 2.

# Vita

Michael Thomas Kikuta was born on August 9, 1979 at 11:35 a.m. PST in Chula Vista California. Michael attended Herndon High School in Herndon, Virginia from 1994 to 1998. Michael continued his education by attending Virginia Polytechnic Institute and State University (Virginia Tech) where he received his Bachelors of Science degree in mechanical engineering on May 11, 2002. Since Virginia Tech had a strong graduate program, Michael stayed to receive his Masters of Science degree in mechanical engineering in December of 2003.